Shi, Wei

PHOTOINDUCED ELECTRON TRANSFER OF 2,2'-BIPYRIDYL RUTHENIUM (II) ADSORBED ONTO POROUS VYCOR GLASS

City University of New York PH.D. 1986

PHOTOINDUCED ELECTRON TRANSFER OF $RU(BPY)_3^{2+}$ ADSORBED ONTO POROUS VYCOR GLASS

by

WEI SHI

A dissertation submitted to the Graduate Faculty in chemistry in partial fulfillment of the requirements for the degree of Doctor of Philosophy, The City University of New York

1986

This manuscript has been read and accepted for the Graduate Faculty in Chemistry in satisfaction of the dissertation requirement for the degree of Doctor of Philosophy.

6/2/86
date

Harry D. Gafney
Chairman of Examining Committee

5/29/86
date

A. M.
Executive Officer

Thomas C. Strekas

Michael Wiener

Supervisory Committee

The City University of New York

ACKNOWLEDGEMENT

I wish to thank my Thesis Advisor, Dr. Harry D. Gafney for his guidance and assistance in the preparation of this Dissertation, and for his constant concern and encouragement during the entire period of my graduate study at The City University of New York.

I also wish to thank Dr. Thomas C. Strekas, a member of my Thesis Committee, and Dr. Arther D. Baker, both of Queens College, for their generous help in the course of this work.

I am grateful to Proffesor Yingwu Chen,my former collegue and graduate advisor at The Lanzou Institute of Chemical Physics, China, for encouraging me to work in the field of photochemistry.

Finally, I wish to express my deepest gratitute to the members of my family: my parents, who have cared for my education and achievement ever since my first day in the primary school; and my wife, who has been so patient and supportive throughout the years of my stay in the United States as a graduate student.

TABLE OF CONTENTS

LIST OF TABLES

LIST OF FIGURES

INTRODUCTION

The recognition of the unique photo-induced electron transfer properties of the complex tris(2,2'-bipyridyl)Ru(II), $Ru(bpy)_3^{2+}$, preceded the energy crisis by less than two years.[1] This coincidence promoted extensive and far-reaching research into the photo-redox chemistry of this and other transition metal complexes in conjunction with the development of solar energy conversion and storage devices.[2-11] Much research effort in this field has focused on light-induced water-splitting systems where the photoreactive transition metal complexes act as the light energy receiving photosensitizers.[12-21] Despite the large number of metal complexes examined during the last decade, however, $Ru(bpy)_3^{2+}$ remains to be the most widely used sensitizer and the best characterized compound in terms of excited state properties. In part, the long-lasting popularity of this complex arises from the following unique qualities:

(1) the complex ion is easily prepared and relatively stable toward photodecomposition;

(2) the redox active excited state, an MLCT state, is long-lived at room temperature in fluid solution;

(3) the excited state luminesces visiblly at room temperature in fluid solution, which provide a valuable spectral probe for monitoring photochemical processes; and

(4) the excited state undergoes facile energy or electron transfer, in the latter case to give oxidized, $Ru(bpy)_3^{3+}$, and reduced, $Ru(bpy)_3^{+}$, products, which are themslves sufficiently strong oxidant and reductant, respectively,and are able to initiate subsequent reactions.

Earlier studies of the complex's photoredox chemistry were largely confined in homogeneous media. While these have produced a detailed account of its excited state properties in such systems, efficient energy conversion has not been achieved, largely due to the inability to control the exergonic, thermal back reaction that accompanies the photoinduced reactions in fluid solution. To control reversibility, recent research in this field has focused on the photophysical and photochemical properties of the complex in heterogeneous and interfacial systems.[22-25]

The shift from homogeneous to heterogeneous systems not only reflects the need for a more realistic energy conversion scheme, but also opens a field for basic research that is of interest in its own right. Solar energy conversion is accomplished in Nature by photosythesis which takes place in complicated, non-homogeneous biological environment. Compartmentalization of various components in the process is an essential feature of this highly efficient energy conversion apparatus.[26,27] In designing artificial photosynthesis devices, therefore, heterogeneous media capable of organizing the reacting species offer an exciting

promise that can not be achieved in homogeneous solutions where diffusion randomizes all reagents and their possible reactions. The intrinsic complexity of the heterogeneous systems, however, poses a considerable chalenge to the chemist. Since most of the available information on the photoredox chemistry of $Ru(bpy)_3^{2+}$ refers to homogeneous solutions, a detailed understanding of its photoinduced processes in new environments is essential to the development of efficient energy conversion systems. This includes investigating the interactions between the photochemical reagent, e.g. $Ru(bpy)_3^{2+}$, and the surroundings, and the alterations that are caused by such interactions in the chemical properties of the reagents. Studies of photophysical and photochemical phenomena in the solid phase or in interfacial systems, however, requires a combination of techniques from conventional solution photochemistry and from traditional surface and materials sciences.

A. Photophysics and Photochemistry of $Ru(bpy)_3^{2+}$ in Homogeneous solutions

1. Characterization of The Excited State

A variety of experimental and theoretical studies have evolved a detailed description of the excited state of $Ru(bpy)_3^{2+}$ in aqueous and aprotic organic solutions, which can be summarized as follows.[28-44]

In its electronic ground state, $Ru(bpy)_3^{2+}$ can be viewed

as a d^6 metal ion in a octahedral microsymmetry(D_3). A simplified representation of the electronic situation for such a molecule is shown in Figure 1. One electron excitation could lead to four possible orbital types for the excited states: d-d*, d-pi, pi-d and pi - pi*, both singlets and triplets. Transitions such as promotion of an electron from t_2 to e orbitals are essentially confined to the metal and such d d or metal-centered transitions give rise to weak (Laporte forbbiden) absorption bands(ϵ = ca. 100). Excitation of a metal t_2 electron to pi*-antibonding orbitals on the ligand results in d-pi* states. Such transitions involving transfer of electronic charge from the metal to the ligand (or vise versa) are labeled charge transfer (MLCT or LMCT) transitions. These transitions have significant absorption in the visible region (ϵ = 20000-25000). Transitions from the ligand pi-bonding orbitals to the pi-antibonding orbitals, known as pi - pi* or ligand-centered transitions, usually lie at high energies and are substantially ligand in character.

Figure 2 presents the absorption and the emission spectra of the $Ru(bpy)_3^{2+}$ complex in aqueous solution at room temperature. Indicated therein are the current assignments of the various absorption bands.[28,30,34] The absorption and emission properties of the complex are summarized in Table 1. The intense UV band at 285 nm (ϵ = 86000) is easily assigned asa ligand centered pi - pi* transition by comparison with the spectrum of the protonated bipyridine ligand. In the visible region, the absorption is dominated by an intense

Figure 1. A diagram of energy levels of a d^6-metal complex in an octahedral field.

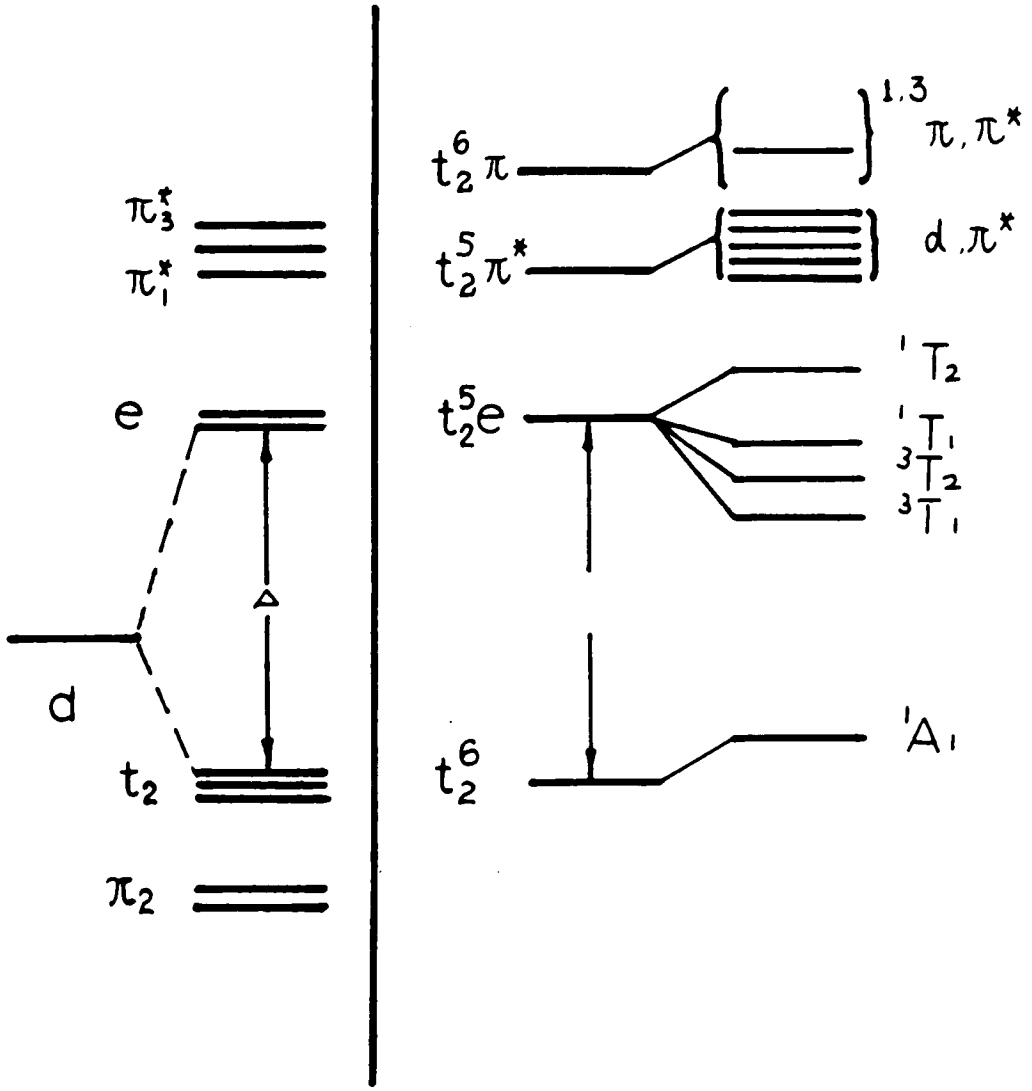

orbitals states

Figure 2. Absorption and emission spectrum of $Ru(bpy)_3^{2+}$ in aqueous solution at room temperature along with assignments for the bands.

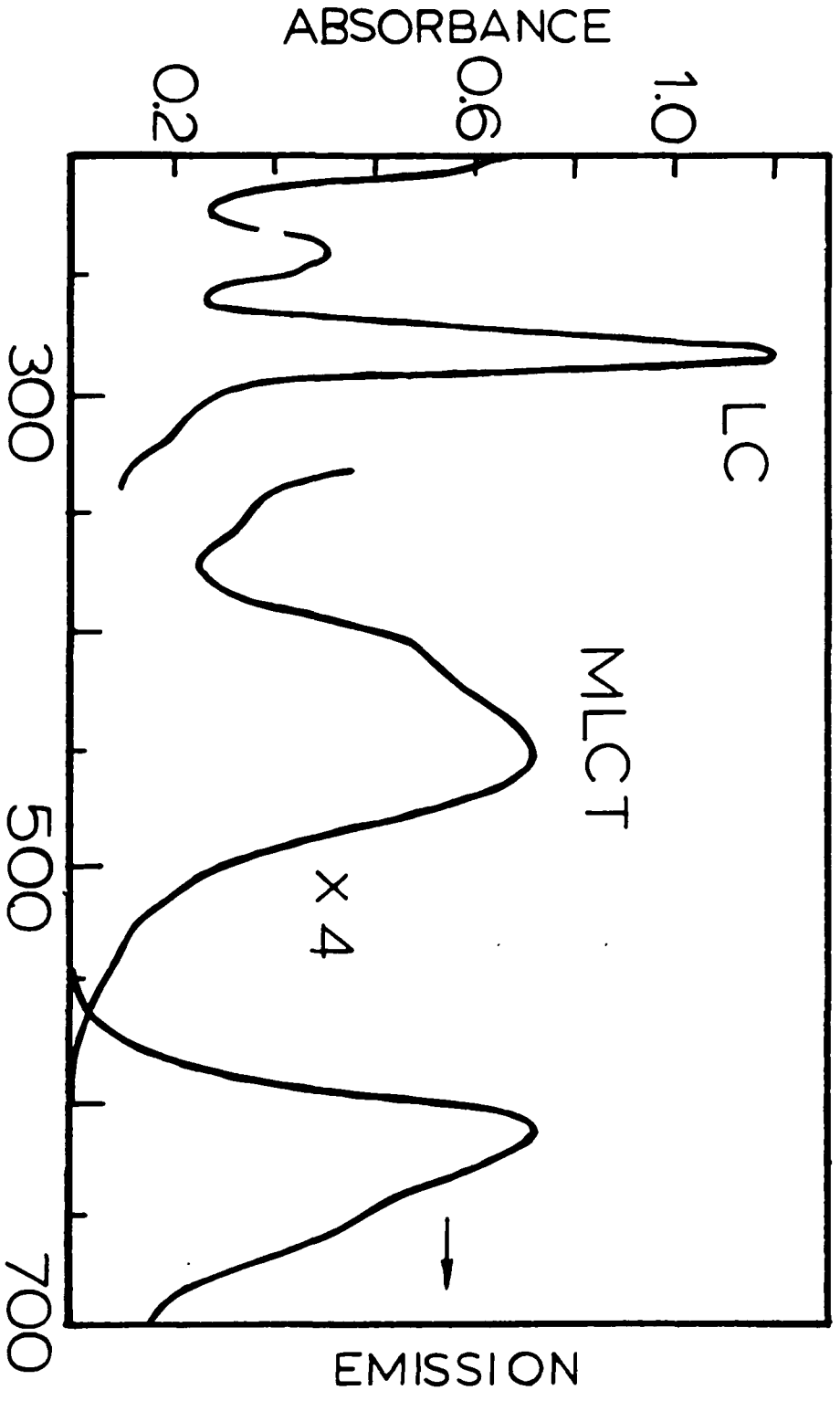
ABSORBANCE
0.2
0.6
1.0
300
500
700
LC
MLCT
X 4
EMISSION

TABLE 1

Absorption and Emission Properties of $Ru(bpy)_3^{2+}$ in water [a]

Room temperature (25 C) absorption			
λ max. (nm)	452,	345,	285
$\epsilon \times 10^{-3}$	14.6,	6.6	87.0
Room temperature emission			
λ max. (nm)	610		
ϕ	0.042		
τ (ns)	600		
77 K Absorption			
λ max.(nm)	456,	286,	244
$\epsilon \times 10^{-3}$	14.6,	79.2,	25.6
77 K emission			
λ max. (nm)	584,	630,	680
ϕ	0.376		
τ (ns)	5300		

τ = lifetime, ϕ = quantum yield

[a] Reference 11.

band with maximum at 452 nm(ϵ = 14000). This is assigned as a metal to ligand charge transfer transition in which an electron is promoted from the metal t_2 orbital to the excited pi* orbital associated with the ligands.

The orbital nature of the emitting state, long a center of controversy, has now been firmly established to be essentially of charge transfer type, spin-forbidden in character.[29,30] $Ru(bpy)_3^{2+}$ shows a broad, structureless orange-yellow emission in solution at 293 K with maximum around 610 nm. In glassy solutions at 77 K, however, the emission band is well resolved with the band origin at 580 nm and a vibrational progression of ca.1350 cm^{-1}.[28] Based on the luminescence quantum yields and decay characteristics in polymethylmethacrylate(PMMA)matrix, Crosby et al. proposed an electron-ion parent coupling model to describe the emitting state.[30-34] According to this model, the luminescent state can be envisioned as a $4d^5$ Ru core and three bpy ligands with one transferred electron in the lowest anti-bonding pi* orbital of the coupled ligands. The emitting state is really a manifold of three closely spaced states(separated by 10 cm^{-1} and 80 cm^{-1}, respectively), whose relative populations are described by a Boltzman distribution throughout the emission process.

In the emissive MLCT state, the transfered electron appears to be localized on one of the three bpy ligands rather than delocalized throughout the ring system. This was

originally proposed by Hipps and by Fujita and Kabayashi to account for the observed emission polarization which far exceeds the possible value for a D_3 symmetry molecule.[38,45-47] Excited state resonance Raman spectroscopy studies later provided the most direct evidence for the localized model, which shows that in the emissive MLCT state the complex is best described as $Ru(bpy)_2(bpy^-)^{2+}$.[48-50] More recent studies, however, suggest that in frozen glass, where molecular motions are curtailed, molecular distortions do not produce a localized trap. Under these conditions, the excited state is best described as a system in which the excited electron is delocalized over the three equivalent bipyridine ligands.[51,52]

In addition to the emissive MLCT excited state, photochemical and photophysical studies reveal a low-energy, metal centered d-d excited state that lies ca.3600 cm^{-1} above the emissive state.[42] This d-d state, which can be populated by thermal activation from the emissive state, accounts for the observed photosubstitutional chemistry of $Ru(bpy)_3^{2+}$ and represents a major deactivation pathway at room temperature and above.[43,44]

In addition to crossing to the d-d state, deactivation of the MLCT states can occur via both radiative(emission) and non-radiative(thermal depopulation) pathways. Since the latter mechanism involves energy transfer(ultimately) to solvent molecules, its rate depends strongly on the efficiency of vibrational coupling of the solvent molecules

to the complex.[42,52-56] This is probably best illustrated by the significant isotope effect of the emission quantum yield and the excited state lifetime. In dearaeted H_2O at room temperature, the emission quantum yield of $Ru(bpy)_3^{2+}$ is 0.042 and the excited state lifetime is ca. 600 ns. In D_2O, the respective values are 0.07 and 1020 ns, indicating a slower non-radiative deactivation (the radiative rate remains essentially constant) due to the relatively inefficient coupling between D_2O and the complex.[42]

The energetics of the various states discussed above is represented in a diagram in Figure 3. The kinetic scheme that has proven useful in explaining the observed excited state dynamics of the complex is shown in Scheme 1, where the superscripts 1 and 3 refer to excited states of the complex largely singlet and triplet in character, respectively.

Scheme 1.

$Ru(bpy)_3^{2+}$ -----> $^1Ru(bpy)_3^{2+}$ (absorption)

$^1Ru(bpy)_3^{2+}$ -----> $^3Ru(bpy)_3^{2+}$ (intersystem crossing)

$^3Ru(bpy)_3^{2+}$ -----> $Ru(bpy)_3^{2+}$ + hv (emission)

$^3Ru(bpy)_3^{2+}$ -----> $Ru(bpy)_3^{2+}$ + heat (radiationless decay)

$^3Ru(bpy)_3^{2+}$ + heat -----> $(d\text{-}d)Ru(bpy)_3^{2+}$
(thermally activated intersystem crossing to d-d state)

$(d\text{-}d)Ru(bpy)_3^{2+}$ -----> $Ru(bpy)_3^{2+}$ or photoproducts
(non-radiative deactivation from d-d state)

Figure 3. Various excited excited states of $Ru(bpy)_3^{2+}$ and excited state deactivation pathways.

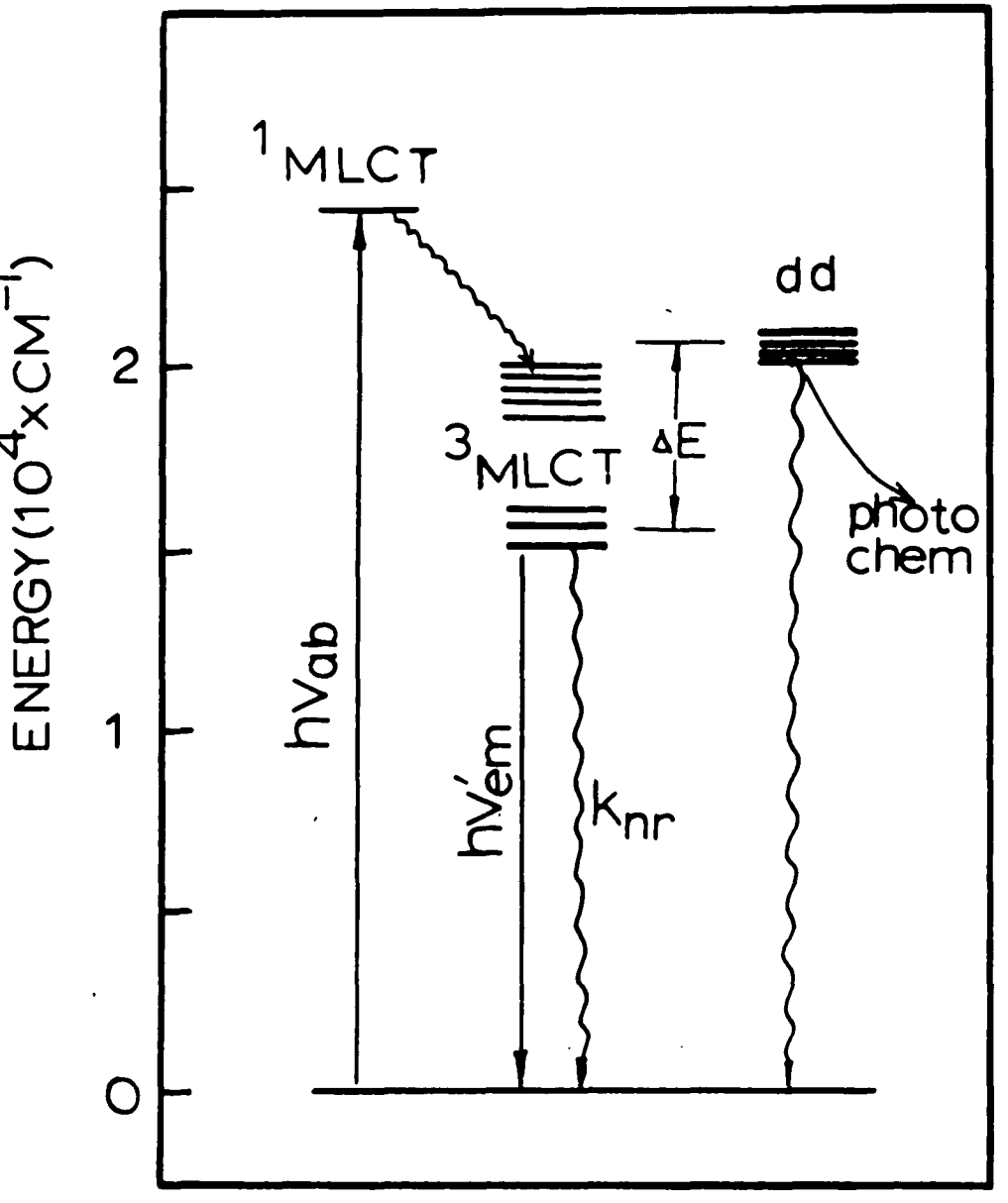
ENERGY(10^4xCM^{-1})
2
1
0
^{1}MLCT
^{3}MLCT
dd
ΔE
photo chem
hνab
hν'em
k_{nr}

2. Redox Properties of the Excited State

Numerous studies during the past decade have established the excited state redox chemistry of $Ru(bpy)_3^{2+}$ in fluid solution.[57-75] As shown in Figure 4, the emitting MLCT state, which is also redox active, lies ca.2.12 eV above the ground state. While the ground state $Ru(bpy)_3^{2+}$ is thermodynamically stable in respect to either oxidation or reduction ($E^{\circ}$for $Ru(bpy)^{3+/2+}$ is 1.26 V, $Ru(bpy)^{2+/1+}$ is 1.24 V), the excited state, being 2.12 eV higher in energy, is both a powerful oxidant and a strong reductant. Thus, absorption in visible, MLCT region transforms the molecule from one with no practical oxidizing or reducing capability into one which is very potent in these aspects. Consequently, a huge number of studies of $Ru(bpy)_3^{2+}$ have involved its use as an excited state redox reagent, as either an oxidant or a reductant.

In addition to its rich photoredox chemistry, $Ru(bpy)_3^{2+}$ sensitizes the formation of triplet excited states of inorganic and organic molecules via the process of energy transfer.[75-77] Thus, whenever the excited state undergoes bimolecular reactions with an external additive, one can envision three possible reactions:

(a) Oxidative quenching in which the excited state acts as a reductant

$$*Ru(bpy)_3^{2+} + Q \text{ -----> } Ru(bpy)_3^{3+} + Q^{-} \qquad (1)$$

Figure 4. The redox active MLCT state of $Ru(bpy)_3^{2+}$ along with various redox potentials.

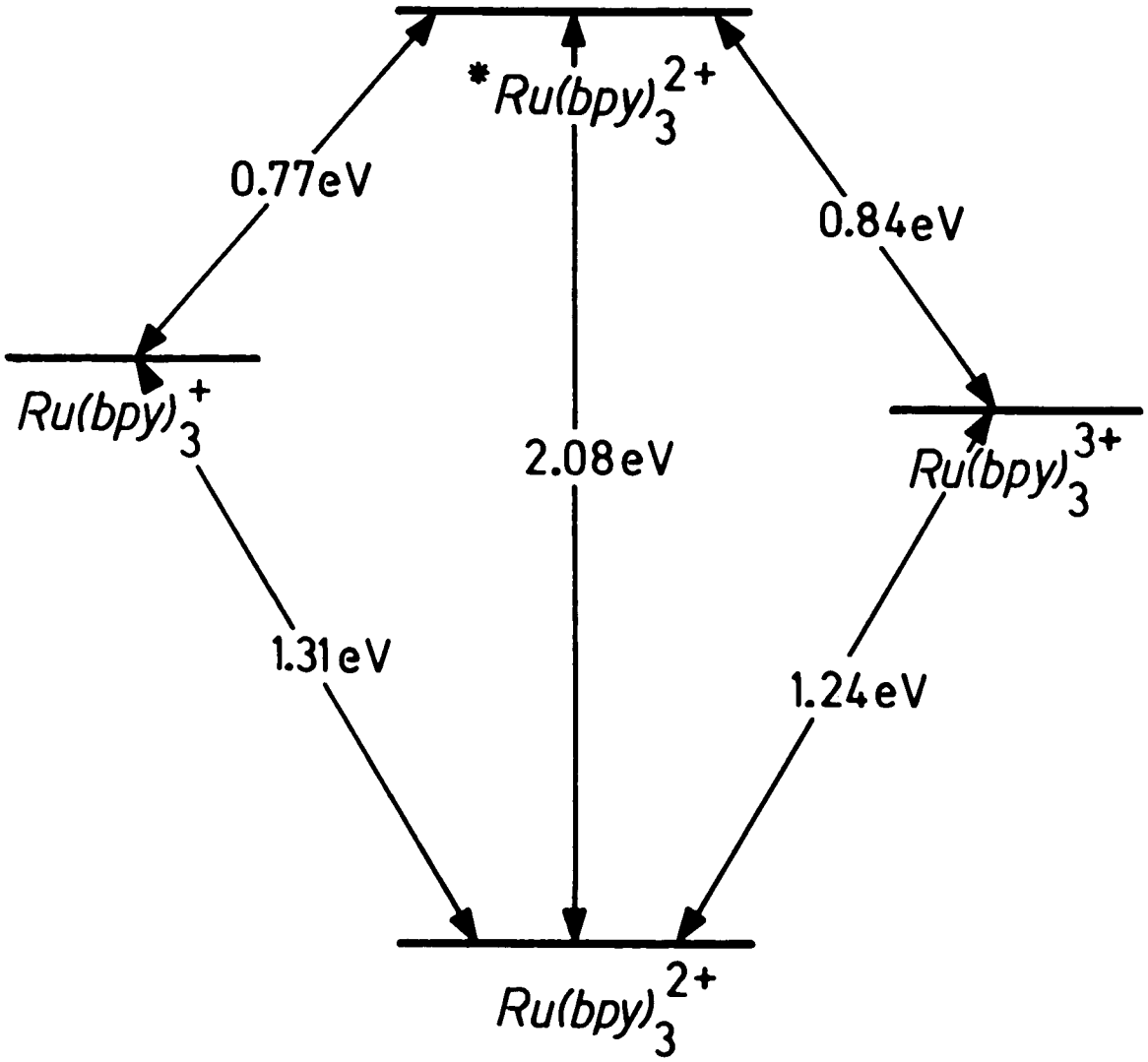
*Ru(bpy)3 2+
0.77eV
0.84eV
Ru(bpy)3 +
2.08eV
Ru(bpy)3 3+
1.31eV
1.24eV
Ru(bpy)3 2+

(b) Reductive quenching in which the excited state acts as an oxidant

$$*Ru(bpy)_3^{2+} + Q \text{ -----> } Ru(bpy)_3^{+} + Q^{+} \qquad (2)$$

(c) Energy transfer quenching in which the excited state acts as an energy donor

$$*Ru(bpy)_3^{2+} + Q \text{ -----> } Ru(bpy)_3^{2+} + *Q \qquad (3)$$

The actual quenching mechanism that is operative for a particular quencher can often be distinguished by thermodynamic considerations. The ability to undergo energy transfer quenching is directly related to the spectroscopic energy levels(spectral overlap) of the donor-acceptor pair, and that of electron transfer quenching to the redox potentials.

Electron transfer quenching of $*Ru(bpy)_3^{2+}$ by various inorganic molecules has been extensively studied. Metal ions such as Fe^{3+},[70-72] Cu^{2+},[73,74] Tl^{3+},[11] quench $*Ru(bpy)_3^{2+}$ oxidatively to yield $Ru(bpy)_3^{3+}$ and corresponding the reduced metal ions as the product. Eu^{2+} and the metal complexes $Fe(CN)_6^{4-}$ and $Mo(CN)_8^{4-}$, on the other hand,quench the excited complex reductively to form $Ru(bpy)_3^{+}$ and the corresponding oxidized quenchers.[77] Cr^{3+} quenches *Ru(bpy) by an energy transfer mechanism, as evidenced by the occurence of emission characteristic of the excited state Cr^{3+}.[67]

Although many organic compounds quench *Ru(bpy)

efficiently. the most thoroughly studied is perhaps N,N'-dimethyl 4,4'-bipyridinium ion, hereafter denoted MV^{2+}.[79-89] This reaction has been studied as the first step in the $*Ru(bpy)_3^{2+}$ sensitized photo-reduction of water to produce molecular hydrogen, in which MV^{2+} acts as an electron relay between $*Ru(bpy)_3^{2+}$ and a reduction catalyst

$$*Ru(bpy)_3^{2+} + MV^{2+} \text{ ------> } Ru(bpy)_3^{3+} + MV^{+} \quad (4)$$

$$MV^{+} + H_2O \xrightarrow{\text{catalyst}} MV^{2+} + H_2 \quad (5)$$

Table 2 summarizes various electron transfer and energy transfer quenching reactions of $*Ru(bpy)_3^{2+}$ in fluid solution along with the kinetic parameters.

Bimolecular quenching in fluid solution, where diffusion is rapid, follows the Stern-Volmer relation

$$I_o/I = 1 + K_{SV}(Q) \quad (6)$$

where I_0 and I are the emission intensities of the unquenched and quenched solutions, respectively, and (Q) is the quencher concentration. The bimolecular rate constant of the reaction is then calculated from

$$k_q = K_{SV} / \text{tau} \quad (7)$$

where tau is the natural (unquenched) emission lifetime of $*Ru(bpy)$.[90]

In fluid solution, bimolecular quenching rates that approach the theoretical diffusion-controlled limit, 2 x

TABLE 2

Rate parameters of quenching of $Ru(bpy)_3^{2+}$ by various compounds in solution [a]

Quencher	Medium	$k_q (M^{-1}s^{-1})$	Mechanism
Fe^{3+}	water	2.7×10^9	Oxidative e^- transfer
Cu^{2+}	water	6.2×10^7	Oxid.
Cr^{3+}	water	1.2×10^7	Energy transfer
Tl^{3+}	water	1.9×10^9	Oxid.
$Fe(CN)_6^{4-}$	water	3.3×10^9	Reductive e^- transfer
$Mo(CN)_8^{4-}$	water	3.4×10^8	Reduc.
MV^{2+}	water	5.6×10^9	Oxidative e^- transfer
	CH_3CN	2.4×10^9	Oxid.

[a] Reference 11

$10^9 M^{-1}s^{-1}$ have been found for many of the photoredox reactions with $Ru(bpy)_3^{2+}$. MV^{2+}, for example, oxidizes $*Ru(bpy)$ with a rate constant $k_q = 1.0 \times 10^9$ in aqueous solution in room temperature.

In low temperature matrices where diffusion is absent, the Stern-Volmer mechanism is not applicable. The rate "constant" k_q becomes a function of the distance between the donor and the quencher according to the Perrin equation[90]

$$I_0/I = k_0 \exp(cV) \qquad (8)$$

where k_0 is a constant, c is the quencher concentration and V the volume of the quenching sphere. According to the Perrin model, only those quenchers that are inside the quenching sphere can quench. More recent studies have shown that for electron transfer processes, V is a function of the redox potential of the reaction.A similar difficulty is encountered with a supported reaction system since it is not immediately obvious as to what the mobilities of the adsorbates are.

3. The Problem of Reversibility

Despite the high efficiency with which many photoredox reactions proceed, few reactions actually result in a net chemical change. Since photoactivation thermally inverts the reaction system, the lack of net chemical change arises from the extremely rapid thermal back reaction that, in the absence of some controling mechanism, follows the

photoinduced electron transfer. The driving force for the reduction of $Ru(bpy)_3^{3+}$ and the oxidation from $Ru(bpy)_3^{+}$ to form the ground state $Ru(bpy)_3^{2+}$ are 1.24 eV and 1.31 eV, respectively (Figure 4), exceeding the corresponding driving forces of the photo-driven electron transfer from the excited state, 0.84 eV and 0.86 eV. Consequently, good quenchers and good reducing agents for water reduction do not necessarily lead to good yield of photoproducts.For example, MV^{2+}, inspite of its high quenching rate constant, and suitable redox potential($MV^{2+/+}$ = - 0.43 V) for reducing water to hydrogen (H_2O/H_2 = - 0.41 V), has not led to H_2 evolution from water in the simple sensitizer/relay/catalyst three component system. The absence of a direct reduction of water is due to the thermodynamically favored back reaction, which for the $Ru(bpy)_3^{3+}$-MV^{+} redox pair has a rate constant, k_b, of 2.4×10^9 $M^{-1}s^{-1}$. To date, hydrogen generation from water has only occured in the presence of a fourth component, an external electron donor that irreversiblly reduces $Ru(bpy)_3^{3+}$ to $Ru(bpy)_3^{2+}$, thereby supressing the back reaction.[11] However, use of such sacrificial component makes cyclic water splitting, at present, economically unfeasible.

Preventing the energy-wasting, thermal back reaction, therefore, has becomes the focal point of solar energy conversion research. Homogeneous solutions based on the simple complex $Ru(bpy)_3^{2+}$ offer little hope in this respect. Consequently, increasing attention in recent years has been paid to two alternative approachs:

First, the synthesis of new, more complicated transition metal complexes, including those with two or more metal centers, which are capable of transfering electrons in a predetermined direction. However, these compounds, also known as "molecular photodiode", suffer from a low thermal and photochemical stability compared to the parent compound $Ru(bpy)_3^{2+}$.[91,92]

Second, the use of certain organized media in which the photosensitizer, the electron donor and acceptor, and other necessary components are assembled in ways that facilitate the photo-driven electron transfer while the thermal back reaction is retarded by physical and/or energetic barriers.[93-95]

The second stratagy is particularly interesting because it more closely resembles analogue compartmentalized, highly efficient natural photosythetic apparatus than homogeneous systems, and studies in this area may both benifit from, and contribute to, our understanding of the natural processes.[96-99]

B. $Ru(bpy)_3^{2+}$ Redox Chemistry in Heterogeneous Media

1. General Remarks

An impressive number of studies have examined the photophysical and photochemical behavior of $Ru(bpy)_3^{2+}$ in a variety of heterogeneous media.[93-140] These materials include

organic, polymeric and inorganic substrates. Typical examples of organic systems include micelles, vesicles, microemulsions, and ion exchange resins. Polymers such as synthetic cellulose, Nafion membranes, and polymethylmethacralate have been studied. Numerous inorganic materials, particularly hydroxylated silicas, layered silicates(clay minerals), zeolites and other metal oxides, have been attracting much recent attention as media for Ru(bpy) based photoredox processes. Semiconductor materials, including TiO_2, SnO_2, and CdS which not only act as supports for $Ru(bpy)_3^{2+}$, but directly participate in the electron transfer processes, have received considerable attention. Table 3 lists some of the heterogeneous systems recently described in the literature.

The differences between homogeneous, fluid solution and a heterogeneous medium include differences in chemical, physical, and geometric constraints imposed by the medium. Therefore, in transposing a photochemical reaction system from solution phase to a solid, or a colloidal support, for example, one may expect changes in reactivity and efficiency at each step in the reaction sequence. These changes may arise from different interactions of the reagent with the immediate environment and from differences in the accesibility of the reacting species to one another. Specifically, the goal of using heterogeneous media is to control the direction of the charge transfer. Whether a particular support or the interfacial phenomena it introduces

TABLE 3

Heterogeneous Media for $Ru(bpy)_3^{2+}$ Photoredox Reactions

Medium	Reactions	Reference
Colloidal SiO_2/H_2O	PVS reduction	128,129
	Quenching by MV^{2+}	110,126
Layered Silicates	Quenching by MV^{2+},Cu^{2+}, etc.	134
	Emission Studies	117
	Quenching by Various compounds	118
	Spectroscopic Studies	119
	Quenching by Fe^{3+}	125,131,133
Cellulose	Quenching by Fe^{3+}, Cu^{2+},	
	Cr^{3+}, MV^{2+},	120-123,140
Ion Exchange Resin	Quenching by Fe^{3+}, Cu^{2+}	115,116
Zeolites	Formation of Ru^{3+}	100,101
Nafion Films	Emission	124
Colloidal TiO_2	Emission	111
	Water reduction	147-151
	Emission Quenching	145
Micelles	Photoredox reactions	97
Vesicles	Electron transfer to MV^{2+}	127,128

can impose such control depends on how the system is modified by the new environment as compared to fluid solution. Fundamental to understanding these heterogeneous systems and, eventually, designing suitable heterogeneous photoredox systems are the following questions:

(1) how do the photophysical and photochemical properties of $Ru(bpy)_3^{2+}$ and other components in the heterogeneous media compare with those in fluid solution;

(2) how do the reagents distribute in the new media since, unlike in homogeneous solutions, a uniform distribution can no longer be automatically assumed; and

(3) how does the mobility of each component in heterogeneous media compare with that in fluid solution.

The first question is related to changes in efficiency that may occur when a reaction is transposed from fluid solution to a support. Both the ground state and the excited state can be sensitive to environmental changes. Solvent effects, for example, influence the photophysical and photochemical pathways of $Ru(bpy)_3^{2+}$.[52-56] On a support, factors that may cause an alteration of thse properties are local polarity, pH, and the type and the strengh of binding between the reagents and the support, which are, in turn, determined by the microstructure of the support.

The second question of reagent distribution is unique to each particular heterogeneous system and has no counterpart

in homogeneous solutions. It is of central importance to solving the problem of reversibility in $Ru(bpy)_3^{2+}$ photoredox chemistry since spatial separation of the primary photoproducts is essential to curbing the thermal back reaction.

The third question, that of the mobility, is crucial to developing efficient photoredox chemical systems because all electron transfer processes are bimolecular. Studies of mobility of the supported species is a prerequisite to controlling it. Adsorbate mobility and, in the absence of mobility,adsorbate distribution are the two most important features that distinguish heterogeneous systems from homogeneous, fluid solutions.They represent not only the greatest advantages of heterogeneous systems, but also their most perplexing problems.

2. Modifications of Spectral and Photophysical properties of $Ru(bpy)_3^{2+}$ on Supports

a) Absorption spectra

In aqueous solution, $Ru(bpy)_3^{2+}$ hows two intense absorption bands in the UV-visible region. The band at 285 nm (ϵ = 84000) is assigned to the bipyridine ligands pi-*pi transition by comparison with the absorption of the free ligand in acidic solution. The peak at 452 nm (ϵ = 14000) is due to the t_2-pi* metal to ligand charge transfer.

Adsorption onto some supports, however, produces significant changes in the absorption spectrum. Van Damme and co-workers find that the 285 nm band splits into two peaks, at 272 nm and 295 nm, and the extinction coefficient of this band decreases by a factor of 2-3, when the $Ru(bpy)_3^{2+}$ complex is intercalated onto various clay colloids.[117,118] On the other hand, Bard and co-workers report a red shift of the visible MLCT band of up to 20 nm, and a 50% increase of its extinction coefficient, for the clay adsorbed complex.[119] These changes, which are beyond what might be attributed to "solvent-like effects", have been attributed to molecular distortions of the bipyridine rings upon intercalation into the clay sheets.

b) Emission spectra

The incorporation of $Ru(bpy)_3^{2+}$ into heterogeneous media changes the emissivity of the complex. The most significant changes occur when the complex is incorporated into a polymerized silica colloid,[110] or when adsorbed onto metal oxide powders, e.g. TiO_2, SnO_2, SiO_2.[111] In the polymerized silica, the emission spectrum of $Ru(bpy)_3^{2+}$ shows two maxima, one at 570 nm and the other at 610 nm. This sharply contrasts with the spectrum in fluid solution where only the 610 nm peak is observed at room temperature. The emission quantum yield and the excited state lifetime also increase considerably upon incorporation, ϕ from 0.042 to ca.2.0, and tau from 600 ns to ca.2.0 μs. These observations are interpreted on the basis of the rigid environment in the

silica, which effectively prevents the full relaxation of the excited state.[110]

When $Ru(bpy)_3^{2+}$ is adsorbed on powders of TiO_2, and several other metal oxides, the emission spectrum shows a maximum at 570 nm and a shoulder around 610 nm. Furthermore, the decay of the excited state of the supported complex does not follow the first order kinetics found in homogeneous solution. The non-exponential decay curve of the adsorbed complex can be resolved into two or three exponential components, each corresponding to a different lifetime, ranging from 3 ns to 3500 ns. The faster decay is associated with the emission peak at 570 nm, whereas the longer lived component is due to the 610 nm emission. The very fast decay (ca.3 - 30 ns) of $Ru(bpy)_3^{2+}$ on the surface of the semiconductors,such as TiO_2 and SnO_2, can be attributed to the effective electron transfer quenching in which the MLCT state transfer an electron to the semiconducors' conduction band. In the case of the SiO_2 powders, which is not a semiconductor and can not act as an oxidative quencher, possible explanation of the multi-component decay includes self-quenching by ground state $Ru(bpy)_3^{2+}$. The latter, present in very high local concentrations, may enhance coupling with the ground state, thereby leading to a faster decay of the excited state. Tight binding between the complex and the support is thought to be responsible for the slower decay since the rigid environment curtails the vibrational distortions necessary for relaxation of the excited state.

3. Distribution of $Ru(bpy)_3^{2+}$ on the Supports

The non-exponential decays described above are a common observation in the study of various heterogeneous photoredox systems involving $Ru(bpy)_3^{2+}$. In the absence of external quenchers, the non-exponential decay is attributed to either concentration quenching,[112] where ground state $Ru(bpy)_3^{2+}$ quenches the fraction of the complex that has been excited, or to excited state anihilation where the excited complex molecules react with each other to form the ground state molecules.[113] Since the calculated concentrations of $Ru(bpy)_3^{2+}$ in these heterogeneous systems are usually quite low, the above phenomena can only result from non-homogeneous distribution of the complex where very high concentrations in certain regions of the support are possible. The non-exponential decay of $*Ru(bpy)_3^{2+}$ in the presence of external quencher is more difficult to explain, however. Several factors may have involved: first, non-uniform distributions of both quencher and excited complex. Second, the absence of diffusion of the reacting species at rates comparable to the rate of excited state relaxation. Finally, the shielding effect of the support, which, by physically separating the quencher from the complex, retards the quenching process.

Considering the complexity of a heterogeneous system, a study of reagent distribution may offer some insights into

the following specific aspects:

1). The location of the reagents on the support, i.e.,to what part of the support does the reagent bind?

2). Whether the adsorbed molecules aggregate or are uniformly distributed within the area they reside.

3). Whether different compounds on the support are mixed or segregated if two or more compounds are present.

The question of reagent location has attracted much attention in studies of $Ru(bpy)_3^{2+}$ photochemistry in micellar solutions. The regular micelles, formed by the dispersion of a surfactant such as sodiumdodecyl sulphate in water, consists of agrregates where the polar ends of the surfactants are exposed to the bulk solvent while the nonpolar tails are bundled together. $Ru(bpy)_3^{2+}$ and other polar species, e.g., MV^{2+}, adsorb onto the outer, polar surfaces of the suspended aggregates. In a reversed micellar system, the surfactants are placed in a nonpolar medium with small amount of water.[93] Under these conditions the aggregation is reversed with the polar ends toward the interior and the hydrophobic tails exposed to the bulk solvent. Such reversed micelles incorporate the water molecules into their polar regions forming " micro pools " dispersed throughout the organic phase. These "pools" in turn dissolve water soluble ionic compounds. In this case, $Ru(bpy)_3^{2+}$ be found inside the micelles. These effects have been extensively used to compartmentalize units in many

photochemical processes.[97]

Whether or not the supported $Ru(bpy)_3^{2+}$ aggregates in the area it distributes affects the excited state decay pathway. In the micellar systems, $Ru(bpy)_3^{2+}$ aggregation is considered to be the reason for the observed non-exponential decay of the excited state.[113] On the other hand, uniform distributions are found for $Ru(bpy)_3^{2+}$ adsorbed onto colloidal silicates and cation exchange resins dispersed in water.[114,115,126] Earlier reports on adsorption of $Ru(bpy)_3^{2+}$ in clay minerals assumed uniform distribution of the complex between the silicate sheets.[117,118] Recently, however, there has been evidence that $Ru(bpy)_3^{2+}$ tends to completely fill in one layer before distributing into another.[119] The decay of $*Ru(bpy)_3^{2+}$ in these clay minerals, which is non-exponential even without added quenchers, can be intepreted as concentration quenching rather than the original suspected "impurity effect" in view of this preferential distribution and and the consequent high local concentrations.[119]

When other reagents are present in the heterogeneous system, the reaction between these species and $Ru(bpy)_3^{2+}$ will largely depend on their relative position. In general, one can envision three possible situations. First, both $Ru(bpy)_3^{2+}$ and the other component, e.g. a quencher, are randomly distributed on the support and are well mixed. This is the case for such supports as polymer films and silica gels when both the complex and the quencher are polar

molecules.[120-124] Second, both compounds adsorbed on the support, but are spatially separated into different zones. One important example of this arrangement is found in vesicles in which one of the components is incorporated into the interior of the large aggregates while the other remains adsorbed on the outer surface.[127,128] Third, one of the reactants is adsorbed on the surface of the support while the other, for various reasons, remains in the bulk solution phase. In this case, charge transfer proceeds across the interfacial barrier.[129,130]

4. Electron Transfer of $Ru(bpy)_3^{2+}$ in Heterogeneous Media

The changes in the physical and chemical properties of adsorbed $Ru(bpy)_3^{2+}$, as well as the changes in the spatial distributions of the reacting molecules in heterogeneous media, as discussed in the preceding sections, are bound to affect the outcomes of the electron transfer processes. A number of photoredox reactions of $Ru(bpy)_3^{2+}$, which had been extensively studied in fluid solutions, have been re-examined in various heterogeneous systems. These results, some of which is briefly outlined below, demonstrate the importance of the environmental effect on the reaction systems, and the possibility of using these media to control the photo-induced reactions.

a. Silica Surfaces

One of the most succesful examples of using surface

phenomena, introduced by a heterogeneous medium, to control $Ru(bpy)_3^{2+}$ photoredox chemistry was demonstrated by Calvin and Willner and their co-workers.[129,130] These authors studied the electron transfer between $Ru(bpy)_3^{2+}$ and a zwitterionic viologen, propyl viologen sulfate (PVS), equation 9, in colloidal silica suspensions.

$$Ru(bpy)_3^{2+} + PVS \text{ ----> } Ru(bpy)_3^{3+} + PVS^- \qquad (9)$$

In aqueous solution, the SiO_2 particles develop a negative surface charge of -170 mV. The cationic $Ru(bpy)_3^{2+}$ is strongly adsorbed on the surface by electrostatic attraction, whereas the neutral PVS remains in the solution phase. The photoinduced electron transfer between the adsorbed complex and PVS in the solvent occurs with a diffusion controled rate constant, ca. 10^9. The thermal back reaction between the oxidized complex and the reduced viologen, however, is substantially retarded by the repulsion of the negatively charged redox product, PVS^- , and the anionic SiO_2 surface. This repulsion significantly reduces the bimolecular rate constant for the back electron transfer. The rate constant of the back reaction is $7 \times 10^9 M^{-1}s^{-1}$ in water, but only 5×10^7 $M^{-1}s^{-1}$ with the silica support.

Retardation of back electron transfer has also been observed by Thomas and co-workers using MV^{2+} as electron acceptor in a polymerized silica colloid.[110] In this system, $Ru(bpy)_3^{2+}$ is incorporated into the interior of the particles, and photoinduced electron transfer between the

complex and MV^{2+}, which adsorbs on the outer surface of the particles, occurs by an electron tunneling mechanism. The net yield of the reduced viologen is substantially higher than in either homogeneous solution or with non-polymerized silica. Apparently, the physical barrier, in this case the SiO_2 wall between the Ru complex and the quencher, plays an essential role in preventing the otherwise efficient back reaction.

b. Clay Minerals

Van Damme et al. and Bard et al. have examined $Ru(bpy)_3^{2+}$ photoredox chemistry in clay membranes of the Smectite and Hectorite type.[117,118,119,122] These are layer lattice silicates of very high surface area and are known to show excellent catalytic properties. $Ru(bpy)_3^{2+}$ and other reagents cation exchange onto the clay and intercalate between the layers. Two types of quenching of the excited $Ru(bpy)_3^{2+}$ can take place in the clay: quenching by the lattice Fe^{3+} ions , and by the exchangable ions adsorbed on the clay sheets.

Intensity quenching of $Ru(bpy)_3^{2+}$ luminescence by Fe^{3+} ions fixed in the clay lattice is of the Perrin type, where quenching rate depends exponentially on the distance between the electron transfer partners (eq. 8). [131] This is a definitive evidence that $Ru(bpy)_3^{2+}$ on the clay surface is immobilized. The time resolved decay of the excited state, however, is more complicated. Van Damme and coworkers have found that the non-exponential component of the decay curve

depends on the amount of lattice Fe , and have developed a model based on the random distribution of the ions and the excited state complex.[135] On the other hand, Bard and co-workers have recently noticed that even in the absence of Fe ion the decay is still non-exponential. These authors, therefore, have attributed the observed decay to a concentration quenching caused by the non-uniform distribution of the $Ru(bpy)_3^{2+}$ complex.[132]

The most significant difference between the lattice ions and the adsorbed ions is that the latter are relatively free to move about within the clay layer, and the electron transfer quenching by these ions, shows different kinetics from that of the fixed Fe. Thomas and co-workers find linear Stern-Volmer type plots for Cu^{2+} and Eu^{3+} ions at low concentrations, but leveling off at higher concentrations.[134] This is attributed to the limited adsorption of the quencher ions between the silicate layers. Contrary to these observations, Bard and coworkers find that quenching of the $Ru(bpy)_3^{2+}$ emission by MV^{2+} in the clays is inefficient, $k \leq 2 \times 10^6$. Unlike what had been previously assumed,they suggest that the distribution of both the complex and the MV^{2+} ions are not uniform. Rather, they tend to partition into different layers separated by the silicate sheets.[131]

As in the case of lattice ion quenching, the time resolved decay of $*Ru(bpy)_3^{2+}$ in the presence of adsorbed quencher is also non-exponential, despite the mobility of the quencher ions. At present, an explanation of the deviations

is not available, since assumption such as multi-component decay have met only with limited succes. Very recently, a theoretical model has been suggested by Darwent and coworkers which interprets the non-exponential kinetics found in various heterogeneous systems in terms of particle size distribution of the supports.[139]

c) Cellulose Films

In a cellulose film, the $Ru(bpy)_3^{2+}$ ions and the quenchers are both immobilized and the quenching follows the Perrin mechanism.[120,123,140,141] The most striking result of the cellulose systems is that the reduced MV^{2+} in the cellulose is unusually stable against oxidation by oxygen. This has been explained on the basis of the shielding effect of the cellulose which prevented the oxygen molecules from reaching the incorporated $Ru(bpy)_3^{2+}$. In this system the use of a sacrificial agent is necessary to provide the electrons.[140,141] In another study, however, Thomas and co-workers report that small amount of MV^+ can be formed in the cellulose without using any sacrificial electron donor. Apparently, unlike most other supports, the cellulose is actively involved in the reaction, perhaps acting scavenger of the oxdized Ru complex prior to the back reaction.[123]

d) Semiconductors

A variety of metal oxide semiconductors, including TiO_2, SnO_2 , Fe_2O_3, and WO_3, have been used as electron transfer media for $Ru(bpy)_3^{2+}$ photoredox chemistry.[142-150] Unlike the

SiO_2, whose band gap energy, 6.9 eV, far exceeds the MLCT energy 2.2 eV, these metal oxides have band gap energies and redox potentials suitable for direct participation of the electron transfer processes. The most popular system in this category is the TiO_2 colloid suspension. When $Ru(bpy)_3^{2+}$ is introduced into the solution visible light irradiation leads to electron transfer from the complex to the conduction band of the semiconductor particles, directly, or via an electron relay such as MV^{2+}. The electron trapped in the particle can then be "tunneled" to a catalyst doped on the particle, which in turn reduces water to molecular hydrogen.[144-150] A schematic explanation of the process is shown in Fig.5. In this case, the separation of the photoproducts is achieved by the potential barrier at the water/semiconductor interface.

Despite the great effort that has been devoted to the studies of semiconductor mediated electron transfer, several crucial questions remain answered. The first question corncerns the adsorption of various reagents on the semiconductor particles. Although electron transfer between TiO_2 and MV^{2+} has been studied in great detail, whether or not MV^{2+} adsorbs on the particle remains controversial.[143] Very recently it has been shown that cations adsorb onto only crystaline TiO_2, whereas neutral and anionic species adsorb onto amorphous TiO_2 particles.[144]

Another problem facing the optimization of the semiconductor based systems is the particle size dependence

Figure 5. A schematic representation of photoelectron transfer from $Ru(bpy)_3^{2+}$ to a semiconductor particle's conduction band. *S is the excited photosensitizer. The electron is tunneled to a catalyst which facilitates water reduction.

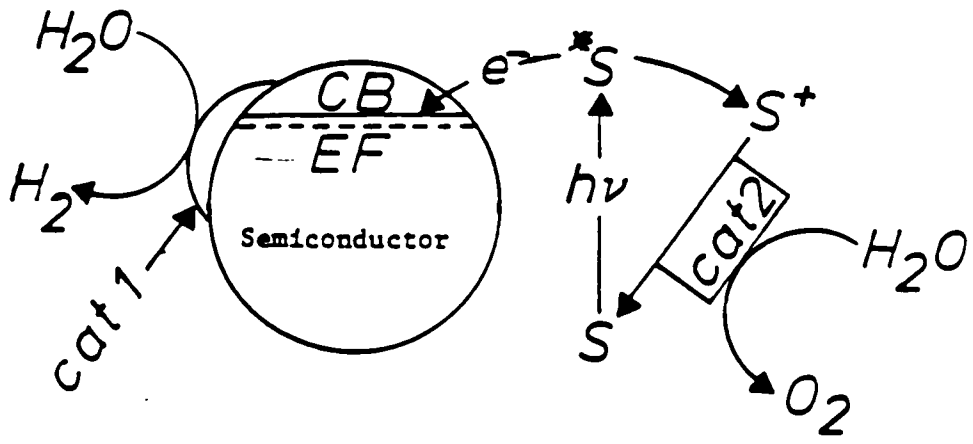

Figure

of many electron transfer processes, and the difficulties in reproducing particles of the desired sizes.[93] Preparation of the colloids and deposition of the reagent, such as catalyst, onto these colloids is more art than science. Furthermore, the poor stability of most preparations toward aggregation requires the use of certain protecting agents such as polyvinyl alcohol(PVA). These protecting reagents, however, interfere with the electron transfer processes. For instance, PVA coated onto TiO_2 acts as an ultimate electron donor in the reduction of MV^{2+} by the TiO_2 colloids.[152]

Some of these difficulties may be overcome by incorporating the semiconductors into polymer films,[154] micelles,[155] and clay membranes.[156] Efficient photosensitized electron transfer and charge separation in vesicle entrapped CdS illustrates these principles.[153] Recently, the spectroscopic properties of CdS incoporated into porous Vycor glass also have been reported.[151]

In part, the inability to resolve the questions raised above arises from the inability to spectroscopically probe the adsorbed reagents due to support opacity. The fact that the majority of heterogeneous systems examined to date are various colloidal suspensions reflects the need for spectroscopic accessibility of the medium. The colloidal systems, while optically transparent, suffer from their intrinsic instability. To circumvent these difficulties, this laboratory has examined the use of Corning's code 7930 porous Vycor glass as a support.

C. Porous Vycor Glass as a Medium for Photoredox Processes

1. General Description of Porous Vycor Glass

A desired medium in which to study the photophysics and photochemistry of a supported metal complex such as $Ru(bpy)_3^{2+}$, is one that is transparent to visible and near UV light. The support should allow ready access of various reagents to the adsorbed complex so that bimolecular reactions can be invesgated. Inaddition, the support should be chemically stable and possess sufficient mechanical strength to permit experiments under varied conditions.

Corning's code 7930 porous Vycor glass, hereafter denoted PVG, satisfies all of the above criteria. Its unique combination of optical transparency($\geq$ 250 nm), large surface area(200 m^2/g), and large pore volume(28% of total volume)makes it an attractive support material for the studies of $Ru(bpy)_3^{2+}$ photoredox chemistry. PVG is prepared by acid leaching a borosilicate glass, resulting in an open pore structure of 70 Å cavities randomly connected in a three dimentional array throughout the entire glass. The chemical composition of the glass is similar to that of regular silica gels, with 96% of hydroxylated SiO_2, 3% of B_2O_3, and 1% other metal oxides. The surface silanol groups are slightly acidic and are randomly distributed on the surface, and cation exchange with ions in fluid solution occurs readily. A summary of the characteristics of PVG is presented in Table

4.

While the similarities between PVG and silica gels are obvious, significant differences exist in their physical and geometric properties. PVG can be monitored spectroscopically either in solution or in the "dry" form without solvent. Silica gels, on the other hand, can only be studied when they are dispersed in solutions. Another extremely important distinction between these two media is that of the surface geometry. As will be discussed in more detail later, most commercially available silica gels have a very high fractal dimention, 3.0. In contrast, PVG has one of the lowest fractal dimentions of all the surface materials. Because of these differences, it is not surprising that photoredox chemistry of $Ru(bpy)_3^{2+}$ adsorbed on PVG departs, sometimes radically, from that of the silica bound complex.

2. Results of Previous Studies of the System

Earlier studies in this laboratory have established that $Ru(bpy)_3^{2+}$ cation exchanges onto PVG by binding to anionic silanol sites on the surface. The visible spectrum of the asorbed complex closely resembles that of the complex in aqueous solution in both the band position and extinction coefficient. The resonance Raman spectrum shows that adsorption does not change the positions of the seven bipyridine vibration modes resonant with the electron transition. The spectral similarity with the solution spectra establishes that $Ru(bpy)_3^{2+}$ retains its primary

TABLE 4

Properties of Porous Vycor Glass

Composition	SiO_2	96 %
	B_2O_3	3 %
Density		1.5 g/cm^3
Void Space (% Total Volume)		28 %
Average Pore Size		70 A
Internal Surface Area		140 m^2/g
Transparency		250 nm

coordination sphere upon adsorption.[157,158]

Despite the apparent similarities in some properties between the adsorbed complex and the complex in fluid solution, striking differences in the photoinduced electron transfer processes are observed. These results, which not only differ from those of the fluid solution, but also from those observed in other heterogeneous systems, demonstrate the effect of environment on the reaction system and the need for further exploration. A brief description of some of these changesis presented below.

a) Photo-induced Disproportionation of $Ru(bpy)_3^{2+}$ on PVG

Photoinduced disproportionation of $Ru(bpy)_3^{2+}$ in PVG, like that in aqueous solution,[159] proceeds via a mechanism that involves a biphotonic ionization of $Ru(bpy)_3^{2+}$. The photodetached electron then reduces another $Ru(bpy)_3^{2+}$, i.e.,[160]

$$Ru(bpy)_3^{2+} \text{ -------> } Ru(bpy)_3^{3+} + e^- \qquad (10)$$

$$e^- + Ru(bpy)_3^{2+} \text{ ------> } Ru(bpy)_3^{+} \qquad (11)$$

$$2\ Ru(bpy)_3^{2+} \text{ -------> } Ru(bpy)_3^{3+} + Ru(bpy)_3^{+} \qquad (12)$$

Although the reaction mechanism in these two media are similar, the stability of the photoproducts are surprisingly different. The reduced complex, $Ru(bpy)_3^{+}$, generated by radiolysis or UV photolysis in aqueous solution has lifetimes from 2 ms - 3 s.[159,161] In contrast, $Ru(bpy)_3^{+}$ generated in PVG is indefinitely stable in the absence of air. The result

is even more significant if one considers the tremendous driving force of the back electron transfer between $Ru(bpy)_3^+$ and $Ru(bpy)_3^{3+}$ (2.5 eV). EPR and flash photolysis studies and concentration dependence of quantum yield of the photoproducts suggest that, unlike in fluid solutions, the photodriven electron transfer occurs between a fixed array of adsorbed reactants. The electron from the excited $Ru(bpy)_3^{2+}$ molecule can , when mediated by the PVG surface, migrate over a distance of 50 Å to reduce another $Ru(bpy)_3^{2+}$. On the other hand, the thermally activated back electron transfer can only take place when the distance between the reacting molecules is < 13 Å. The unusual stability of the photoproducts in PVG seems to arise from two critical conditions that can be met in the glass but not in fluid solutions: a) the Ru complex must be immobilized on the surface and b) the distance between the complex molecules must be beyond that of the thermal electron transfer (13 Å),[160] but within that of the photodriven electron transfer (50Å).

b) Quenching of Excited State $Ru(bpy)_3^{2+}$ by Gaseous molecules

Quenching of $*Ru(bpy)_3^{2+}$ adsorbed onto PVG by the gases N_2O, SO_2,and O_2 have been examined.[158] The quenching pattern involves static or dynamic quenching, which process dominates depends on whether the quencher adsorbs strongly or weakly on the PVG surface. The weakly adsorbed N_2O quenches the emission by almost an pure dynamic process. Conversely, the more strongly adsorbed SO_2 and O_2 show mostly static

quenching. These results, like those from the disproportionation reactions, indicate that rapid diffusion of the surface adsorbed $Ru(bpy)_3^{2+}$ complex is not present.

3. Objectives of This Study

Despite the considerable amount of information gathered by the previous work on the photoredox chemistry of $Ru(bpy)_3^{2+}$ on PVG surface, many questions that are crucial to a better understanding of the observed phenomena remain to be answered. These questions are also the more specific versions of the general problems raised in Section B of this Introduction. In the present study, attempts are made to address and answer the questions outlined below:

a) The changes of the excited state properties of $Ru(bpy)_3^{2+}$ upon adsorption to PVG. Previous studies have largely focused on the ground state properties such as absorption spectra, band positions of resonance Raman scattering. Since the excited state is so radically different from the ground state for this complex, and since the photoredox chemistry is essentially an excited state event, it is necessary to characterize the excited state of the adsorbed complex in more detail. Studies of emission under various conditions will provide valuable information in this area.

b) The mobility of the adsorbed complex. As shown in the

previous work, the diffusion, or the lack of it,of the adsorbates on the surface, plays a vital role in determining the electron transfer processes. Direct experimental evidence on the mobility of the Ru complex on PVG will not only verify the proposed mechanism for the results of disproportionation, but will provide a basis for designing other photochemical reaction systems using PVG as a medium.

c) The distribution of reagents on PVG. This study, although extremely important in view of the low mobility of the adsorbates on the glass surface and the nature of the electron transfer processes, was not possible in the previously examined systems (quenching by gaseous molecules). Quenching of $Ru(bpy)_3^{2+}$ emission by adsorbed ions, coupled with optical spectroscopic techniques, on the other hand, can provide unambiguious information on the whereabouts of the adsorbates on the PVG surfaces.

d) The effects of semiconducting materials on the electron transfer on PVG. Incorporation of TiO_2, and other semiconductors onto PVG provides a viable means of controling the particle size and enhancing the stability of these particles. Studies of electron transfer between $Ru(bpy)_3^{2+}$ and the semiconductors on the PVG surface will be of interest since it can provide an alternative for the colloidal systems which suffer from the poor stability of the suspentions and the difficulties in producing suitable particle sizes.

EXPERIMENTAL

A. Materials

$[Ru(bpy)_3]Cl_2 \cdot 3H_2O$ was prepared according to the procedure of Palmer and Piper,[162] and the UV-VIS absorption spectrum of the twice recrystallized complex agrees with the published spectra.[163] The other metal complexes, i.e., $Fe(bpy)_3^{2+}$, $Os(bpy)_3^{3+}$, and $Cr(bpy)_3^{3+}$ were also prepared according to the procedures in literature.[167]

Reagent grade $FeCl_3 \cdot 6H_2O$, $CrCl_3 \cdot 6H_2O$, and $CuCl_2 \cdot 6H_2O$ were purchased from Fischer Scientific Company and J.T. Baker Chemical Company, and used without further purification. Methyl viologen was purchased from Aldrich Chemical Company as a chloride salt. Titannium tetrachloride, $TiCl_4$, and titanium tetraisopropoxide, $Ti(i\text{-}OC_3H_7)_4$, $SbCl_3$ and $SnCl_4$ were obtained from Aldrich.

All gases were from the Linde Corporation and with the exception of argon, were used as received since the purity levels of each exceeds 99 %. Argon was dried by passage through a 6"x 1" column of either $CaSO_4$ or $Mg(ClO_4)_2$. O_2 was removed from argon by scrubbing the gas with a solutionof Cr^{2+}.

95 % aqueous ethanol (reagent grade) required no further purification. Reagent grade isopropanol and methanol were dried by reflux over Linde 4A molecular sieves and were

subsequentkly distilled, immediately prior to use. H_2O was distilled in a Corning distillation apparatusand stored in polyethylene. All remaining chemicals were reagent grade and used as received.

Porous Vycor glass, code no. 7930, was received from the Corning Glass Works in the form of 300 mm x 300 mm x 4.5 mm sheets. Samples of the glass for impregnation with reagents were obtained and preteated in the following manner. The glass sheet was immersed in water to saturate the pore volume, and then cut into 25 mm x 25 mm sections with a water/oil cooled tungsten carbide saw. The cutting oil was rinsed from the cut glass by Soxhlet extraction for $\geq$ 6 hours with hot distilled water, after which the glass was heated to 40 C under reduced presure to remove bulk water. When the glass became completely transparent, an indication that the bulk water is no longer present, it was placed in a muffle furnace. The furnace temperature was increased from 25 C to 550 C at a rate of ca. 100 °C/hour. Moderately increasing the temperature prevents cracking of the glass induced by rapid release of adsorbed water molecules. As the glass is heated, it begins to char, eventually becoming transparent, indicative of the burning of carbonaceous impurities which were adsorbed to the glass. The glass was maintained at 550 °C until immediately prior to its impregnation with reagent.

B. Impregnation of PVG

1. General Procedures for Adsorption from Solutions

Impregnation of porous Vycor glass with compounds that are low vapor presure solids at room temperature involves adsorption of a solution of the compound. Typically, one to three clean PVG samples were weighed and mounted upright in an Eastman Kodak Chromagram Developing Jar containing 50 ml of the adsorbate solution. The impregnating time ranged from 12 to 48 hours. The sample was then removed from the solution and rinsed with the solvent to prevent a layering of the adsorbate on the glass surface. The solvent was then removed from the impregnated sample by pumping under vacuum.

To determine the amount of the compound adsorbed on the PVG sample, the absorbance of the solution was recorded before and after impregnation, correcting for the absorbance for the change in solution volume owing to pore penetration by the solvent. The number of moles of the comp[ound adsorbed, n_{ads}, is given by

$$(OD_i - OD_f/OD_i) \times n_i \qquad (13)$$

where OD is the volume corrected optical density at the monitoring wavelength, the subscripts i and f denoting initial and final values. n_i is the number of moles of adsorbate in the solution prior to impregnation. Dividing n_{ads} by the total weight of the clean glass gives the number of moles adsorbed per gram of PVG. The typical samples used weighed 1.5 to 4.5 gram, and loading levels ranged from 10^{-7} to 10^{-4} moles of adsorbate /gram of PVG.

2. Impregnation of Cationic Reagents

$Ru(bpy)_3^{2+}$. PVG samples impregnated with $Ru(bpy)_3^{2+}$ were prepared according to the above procedure. Aqueous solutions of $[Ru(bpy)_3]Cl_2 \cdot 6H_2O$, 1 x 10^{-4} M to 1 x 10^{-3} M, were used. The absorption at 452 nm was monitored for concentration determination. With a few exceptions, the impregnation level of the complex was purposely limited to allow measurements of absorption spectra of the adsorbed complex.

Fe^{3+}, Cr^{3+}, Cu^{2+}, and MV^{2+}. All the metal ions were adsorbed from aqueous solutions of the respective hexaquo chloride. To prevent hydrolysis of Fe^{3+} and Cr^{3+}, however, acidic solutions were used. The acidity was usually adjusted to pH < 3 with HCl. Since the adsorption rate is pH dependent, the solutions of Cu^{2+} and MV^{2+} were also adjusted to this low same pH for comparison, though hydrolysis in these cases were negligible at higher pH. Optical absorption was monitored at 256 nm for MV^{2+}, 440 nm for Cr^{3+}, and 810 nm for Cu^{2+}. Fe^{3+} does not absorb in the visible and near UV region, and, to determine the solution concentration, the ferric ion was converted to the complex FeSCN by addition of NH_4SCN to the solution containing Fe^{3+} according to the procedure described by Vogel.[165] The intensely red-colored FeSCN has a characteristic absorption at 485 nm (ϵ = 3500), which was used to determine the content of the ferric ion in the impregnation.

3. Deposition of Semiconductors onto PVG

Titanium Dioxide. Porous Vycor glass was impregnated with TiO_2 by equilibration of the glass with an acidic $Ti(i\text{-}OC_3H_7)_4$ solution. The latter was prepared by dissolving either $TiCl_4$ or $Ti(i\text{-}OC_3H_7)_4$ in isopropanol.[147] The amount of Ti adsorbed on the glass was calculated via the spectroscopic methode described above. Howevr, since the titanium compound has no absorption maximum in either the visible or the UV region, but has a rising absorbance in the UV, the absorbances at various wavelenghs between 300 nm and 400 nm were measured and the OD_i and OD_f in these wavelenghs were averaged to minimize errors. After impregnation, the solvent was removed from the sample, which was then heated in air to 600 C in a three zone Lindberg Heavy-Duty furnace (Model 9744), raising the temperature of all 3 zones simultaneously at a rate of ca. 100 C/hour. The UV-VIS spectra of the impregnated sample were recorded before and after heating. This procedure yielded transparent glass samples (λ > 350 nm) containing from 10^{-7} to 10^{-5} moles of TiO_2/g PVG.

SnO_2/1% Sb. A spray pyrolysis technique, similar to those previously described,[164] was used to deposit transparent, conducting, thin films of SnO_2 doped with 1 % Sb on one 25 mm x 25 mm face of PVG samples. An acidic methanol solution of Sn^{4+} and the dopant, Sb, was prepared by dissolving one part $SbCl_3$ and 199 parts anhydrous $SnCl_4$, by weight, in methanol.

The Sn^{4+} concentration in these solutions was typically ca.1 M. The solution was placed in a glass bottle equipped witha a screw top consisting of a pump handle and a fine nozzle. Squeezing the handle produces a fine mist of the Sn^{4+}/Sb^{3+} solution which was directed at a clean PVG sample situated face up in a beaker within a furnace at 600 C. This method yielded optically transparent ($\lambda \geq 350$ nm), conducting, thin films of SnO_2 doped with Sb.

4. Mounting of Impregnated Samples in Cells

An impregnated PVG sample was rigidly mounted in an upright position with a Teflon holder in a 3 cm x 4 cm x 1 cm quartz cell such that the 25 mm x 25 mm face of the sample was parallel to the 3 cm x 4 cm windows of the cell.The cells were equipped with a 2" diameter O-ring joint for mating to an upper section which has a high-vacuum stopcock and 10/30 joint. The latter joint was used to attach the cell to a vacuum line for evacuation and introduction of gases. The lower and upper sections of the cell were fastened by 2" diameter aluminum rings held together with three screws and nuts.

B. Instrumentation and Physical Measurements

1. Electronic Absorption Spectra

Electronic absorption spectra were recorded on a Cary 14 spectrophotometer. To obtain spectra of the impregnate PVG samples, the glass was placed in the cell and the latter

placed into a rectangular cell holder within the sample compartment such that the 25 mm x 25 mm face of the sample was perpendicular to the path of the spectrophotometer source beam. A clean piece of PVG was rigidly mounted in the reference compartment to compesate for absorption and scattering by the glass itself. Prior to impregnation, the absorption spectrum of the PVG sample was recorded versus the reference piece in order to obtain a baseline. Following impregnation and evaporation of the solvent, the absorption spectrum of the impregnated sample was taken, and the difference between this spectrum and the baseline gave the net absorption spectrum of the adsorbate.

2. Steady State emission spectra

Room temperature emission intensities and emission spectra of $Ru(bpy)_3^{2+}$ were recorded on a Perkin-Elmer Hitachi MPF-2A emission spectrophotometer equipped with a red-sensitive photomultiplier tube. To measure the emission from the adsorbed complex, the cell holder was adapted to rigidly hold the rectangular cell and the PVG sample within at an angle of 50^0 relative to the exciting light. The emission was monitored at an angle of 90^0 to the excitation.

Emission at various temperatures between -20°C and 100°C were measured with the sample cell mounted in a thermostated cell holder, and the temperature was adjusted with a Haake Model FK-2 temperature control bath. For emission at 77 K, a

water-glycerol solution (1:1) of $Ru(bpy)_3^{2+}$ was placed in a quartz tube (diameter 2 mm) which was then immersed in a Dewar filled with liquid N_2. A separate cell holder was used to hold the Dewar in the sample compartment of the emission spectrophotometer. The emission of adsorbed $Ru(bpy)_3^{2+}$ was also measured at 77 K. A 2-mm diameter PVG rod was impregnated with the complex, and then placed directly in the Dewar filled with liquid N_2.

3. Emission Decay Measurements

Emission decays of $Ru(bpy)_3^{2+}$ in solution or adsorbed on PVG were monitored using the apparatus described below. The quartz cell containing the sample was mounted in a cell holder within a sample compartment made of aluminum. The sample was excited perpendicular to the 25 mm x 25 mm face by a 5 ns FWHM light pulse from an Ortec Model 9352 nanosecond light pulser operated at 20 kHz with a contineous flow of purified N_2 gas. The pulses consist predominately of 337 nm and 358 nm light, the most intense lines in the N_2 emission spectrum. An Ortec Model 9290 high-voltage power supply charged the hot electrode to 8 kV. The emitted light of $Ru(bpy)_3^{2+}$ at 90^0 relative to the excitation (from the 25mm x 25 mm face of the glass sample) was passed through a Bausch and Lomb Model 33-86-76 grating monochromator set at 610 nm, or through two red-transparent glass filters ,and was detected by an RCA Model C31034A photomultiplier tube. The latter was charged to - 1800 V by a Tennelec Model TC941

negative high-voltage power supply. The photomultiplier was mounted in a Pacific Precision Instruments Model 3470 AD/6 thermoelectrically cooled housing where its output was fed directly into a 100-fold amplifier/discriminator. The latter was set at a triggering threshold of 350 mV to maximize signal/noise ratio. The 25 mV discriminator output pulses were fed into a PAR Model 115 wideband preamplifier to provide a 10-fold amplification prior to being fed into a PAR Model 164 gated integrator modul/Model 162 boxcar averager. The time-resolved emission intensity was generated by triggering the boxcar averager scan across a 2 usec time base via the negative output of the light pulser. Scanning was accomplished by sweeping a 5 ns conducting aperture across the time base by means of a voltage ramp.The latter increases the delay between the trigger and the opening of the aperture on succesive triggers.This process was repeated until the aperture had moved completely across the time base. Since the first aperture opening can occur no sooner than 75 ns after the first trigger, the signal input to the gated integrator was delayed in order to monitor the rise of the emission. Sixty feet of RG 58/AU 50 ohm coaxial cable originating at the discriminator output and terminating at the preamplifier input served as the delay line.

The time-resolved emission intesity was displayed on a Hewlett-Packard Model 7044B X-Y recorder at the scanning rate by feeding the voltage output of the boxcar averager to the Y-input of the recorder and utilizing the 0-1 VDC scan ramp

of the boxcar to generate the time (X) axis.

4. Resonance Raman Spectra

Resonance Raman spectra of $Ru(bpy)_3^{2+}$ were recorded with a Spex Raman Spectrometer. The excitation source was the 457.9 nm line from a Spectra Physics Model 164-88 CW argon ion laser. The scanning range was 1000 cm^{-1} to 1700 cm^{-1}., with a resolution of ca. 1 cm^{-1}.

C. Studies of Impregnated PVG

1. Distributions of Adsorbates

The cross sectional distribution of $Ru(bpy)_3^{2+}$ and other adsorbate, e.g., Cu^{2+}, Fe^{3+}, were examined spectroscopically for glass samples containg these adsorbates from 10^{-7} to 10^{-5} moles of adsorbate/ g of PVG, by mapping the absorbance of the adsorbate at its respective absorption maximum as a function of sample thickness. Variable sample thicknesses were obtained by grinding the glass surface using 220 grit carborundum paper. The sample thickness was measured at various stages of grindingwith a vernier caliper, after which the absorbance of the remaining adsorbed compound was recorded. Since grinding the PVG surface results in an immediate loss of transparency to visible light due to scattering, prior to each spectral measurement the glass was immersed in chlorobenzene, whose refractive index, 1.53, is very close to that of the glass, 1.50. When the ground glass

is saturated with chlorobezene it is completely transparent to visible light. The absorbance measured after each grinding, where ca. 0.05 to 0.1 mm of the glass was ground off, was plotted as a function of the sample thickness.

2. Emission Quatum Yield of $Ru(bpy)_3^{2+}$ on PVG

To calculate the emission quantum yield of the adsorbed complex, a series of PVG samples containing 10^{-7} to 10^{-5} moles of $Ru(bpy)_3^{2+}$ /g were prepared. For each sample the absorbance at 452 nm was recorded. The emission, excited at 452 nm, was then monitored at 610 nm. For glass samples where the absorbance at 450 nm was ≥ 4, it was assumed that all of the exciting light was adsorbed on the immediate surface of the sample nearest to the source. The emission intensity of the adsorbed complex was then compared to that of a high optical density, deaerated aqueous solution of the complex, according to the "optical dense method". This was to insure that all of the exciting light was absorbed within a very narrow path of the samples (glass and solution) so as to monimize the possible difference in the sample geometry and positioning, which are known to greatly affect the detected emission intensity. The reference solutions were contained in a 1 mm cell which was then placed in the rectangular cell at the same position as with the PVG sample. The rectangular cell was mounted in the cell holder within the sample compartment of the emission spectrophotometer, a· emission intensities were recorded.

The emission intensities from glass samples with 452 nm absorbance ranging from 0.37 to 49 were measured. The recored intensity was the average of three readings for each sample.

3. Emission Polarization Measurements

In the emission polarization measurements, the samples, glass and solution, were oriented so that the front face of the sample was perpendicular to the incident exciting light. The emitted light was monitored at 90^0 to the exciting beam. Polarized exciting light was generated by placing a Polaroid polarizer between the source and the sample. Another polarizer was placed between the sample and the detector. The second polarizer was rotated about the emitted light beam from 0 to 90^0 relative to the first polarizer. For a sample with zero polarization ratio, the detected emission intensity is independent of the rotation. This fact was used to calibrate the instrumental bias due to the preferential sensitivity of the gratings toward light polarized at certain directions. The aqueous solution of $Ru(bpy)_3^{2+}$ at room tenperature has a polarization ratio of < 0.001, therefore providing a fairly good calibration reference. The instrumental factor thus determined (see RESULTS) was used to calculate the polarization ratios of the complex in other media.

4. Quenching of Emission of $Ru(bpy)_3^{2+}$

Quenching in Solutions. Intensity quenching of $Ru(bpy)_3^{2+}$ emission in aqueous solutions were measured using the afore mentioned emission spectrophotometer. The solution containing the complex and the quencher was placed in a 1 cm covette, equalibrated with air. The emission was excited at 450 nm and monitored at 610 nm. No corrections were necessary for quenching by MV^{2+} and Fe^{3+}, since both have negligible absoption at the above wavelenghs. Cu^{2+} has a small absorption at at > 600 nm. Under the concentrations used for solution quenching, however, the sample absorbance at 610 nm was < 0.05 and no corrections were made. Cr^{3+}, on the other hand, has an absorption spectrum with two maxima, at 435 nm (ϵ = 226) and 630 nm (ϵ = 210). Because of the relatively high concentrations of Cr^{3+} used, corrections were made for the absorption at the excitation wavelengh, 450 nm, according to the following equation

$$(I_0/I)_{corr} = (I_0/I)([1 - 10^{-Ad - Aq}]/[1 - 10^{-Aq}])Ad/[Ad + Aq]$$

where I_0 and I are the emission intensities of the unquenched and the quenched solutions, respectively, Ad is the absorbance of $Ru(bpy)_3^{2+}$ and Aq is the absorbance of the quencher, Cr^{3+}. To correct for the quencher absorption at the emission wavelengh, 610 nm, a pathlengh of 0.5 cm was assumed and the percentage absorption of Cr^{3+} at 610 nm was determined for each concentration with the Cary 14 spectrophotometer. Lifetime quenching in solution was measured with the lifetime apparatus described above. The

samples containing both the complex and the quencher were deaerated by bubbling Ar for at least 10 minuts prior to each measurement.

Quenching on PVG. Steady state intensity quenching of the $Ru(bpy)_3^{2+}$ emission on PVG by coadsorbed quencher was measured with the sample in vacuo ($< 10^{-3}$ torr). As in the solution quenching studies, no corrections were necessary for quenching by MV^{2+} and Fe^{3+}. Because of the low impregnation level of Cr^{3+}, the absorption by the ion at both 450 nm and 610 nm was negligible, $A < 0.02$, and corrections were no longer necessary. With Cu^{2+} as quencher, the emission was monitored at 590 nm instead of 610nm, in order to minimize the error introduced by Cu^{2+} absorption in this region. At 590 nm, the maximum absorbance of Cu^{2+} under the experimental conditions was < 0.03.

5. Continuous Photolysis

The apparatus for measuring the quantum yield of $Ru(bpy)_3^{+}$ is shown in Figure 6. The deaerated PVG samples impregnated with $Ru(bpy)_3^{2+}$ were mounted in a temperature variable sample compartment taken from the emission spectrophtometer and then irradiated with the 457.9 nm line from the Spectra Physics Model 164-08 CW Ar ion laser. The white light output from a 100 W high pressure Xe lamp serving as a single beam CW spectrophtometer source was directed at an angle of ca. 10^0 relative to the incident laser beam and

Figure 6. A block diagram of the apparatus used in steady state photolysis of impregnated PVG samles.

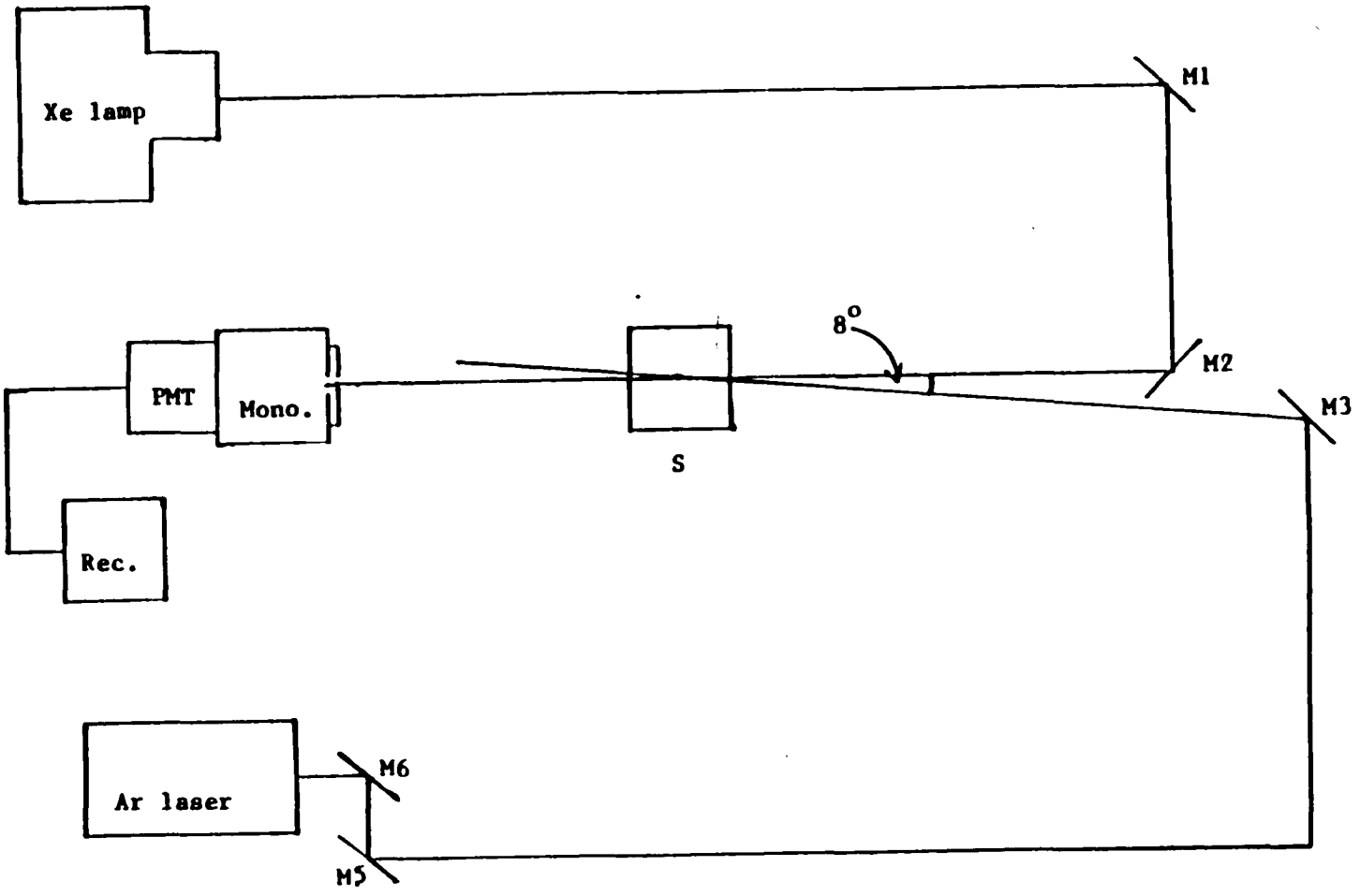

Figure

perpendicular to the sample. The transmitted light was passed through a Bausch-Lomb Model 33-86-76 grating monochromator, and the exiting 510 nm light was detected by a Hamamatsu Model 928 red-sensitive photomultiplier tube, charged with 1 kV by a Pacific Precision Instruments Model 203 high-voltage DC power supply. The photomultiplier output as a function of photolysis time was displayed on a Honeywell Electronik 19 strip chart recorder. The rate of appearence of $Ru(bpy)_3^+$ was monitored via the increase in absorbance at 510 nm, using the equation,

$$abs = \log(1/T) \qquad (15)$$

where T is the ratio of the amount of light transmitted by the photolyzed sample to that by the unphotolyzed sample.

The temperature was controled by a Haake Model FK-2 Temperature control bath with a precision of $\pm$ 0.5^{0}C.

A similar apparatus was used in the photolysis of PVG samples containing $Ru(bpy)_3^{2+}$ and MV^{2+} in studies of MV^+ formation. Here, however, the monitoring wavelengh was 610nm, the absorption maximum of the reduced viologen.

RESULTS

A. Adsorption and Distribution of Reagents

1.Rates of Adsorption of Cationic Reagents

The porous Vycor glass used in these experiments were of the sizes 25 mm x 25 mm x 4.5 mm, or 25 mm x 8 mm x 4.5 mm, cut from large sheets received from Corning Glass Works. The glass contains a random array of interconnected 70 $\pm$ 21 A cavities throughout the entire volume. When pulverized and dispersed in distilled water, porous Vycor glass develops a zeta potential of -26 mV, indicative of an anionic surface, and causes a decrease in the pH of the aqueous phase.[166] Adsorption of various colorimetric, acid-base indicators onto PVG indicates a surface pH of ca.4-5. These results suggest proton dissociation from the silanol groups, i.e.

$$SiOH \text{ -----> } SiO^- + H^+ \qquad (16)$$

and that PVG is capable of cation exchange. Adsorption of $Ru(bpy)_3^{2+}$ and various cationic compounds confirms the cation exchange character of PVG. Placing the glass into an aqueous solution of $[Ru(bpy)_3]Cl_2$ results in adsorption of the dicationic metal complex without a concurrent adsorption of the Cl^- counterion(Figure 7).However, cation exchange is not the sole mechanism of adsorption on PVG from aqueous solution since neutral complexes such as $Ru(bpy)_2(CN)_2$ are also easily adsorbed.

Figure 7. Adsorption of the cationic $Ru(bpy)_3^{2+}$ without concurrent adsorption of the Cl^- couterion. The Cl^- concentration in solution was measured with an ion selective electrode.

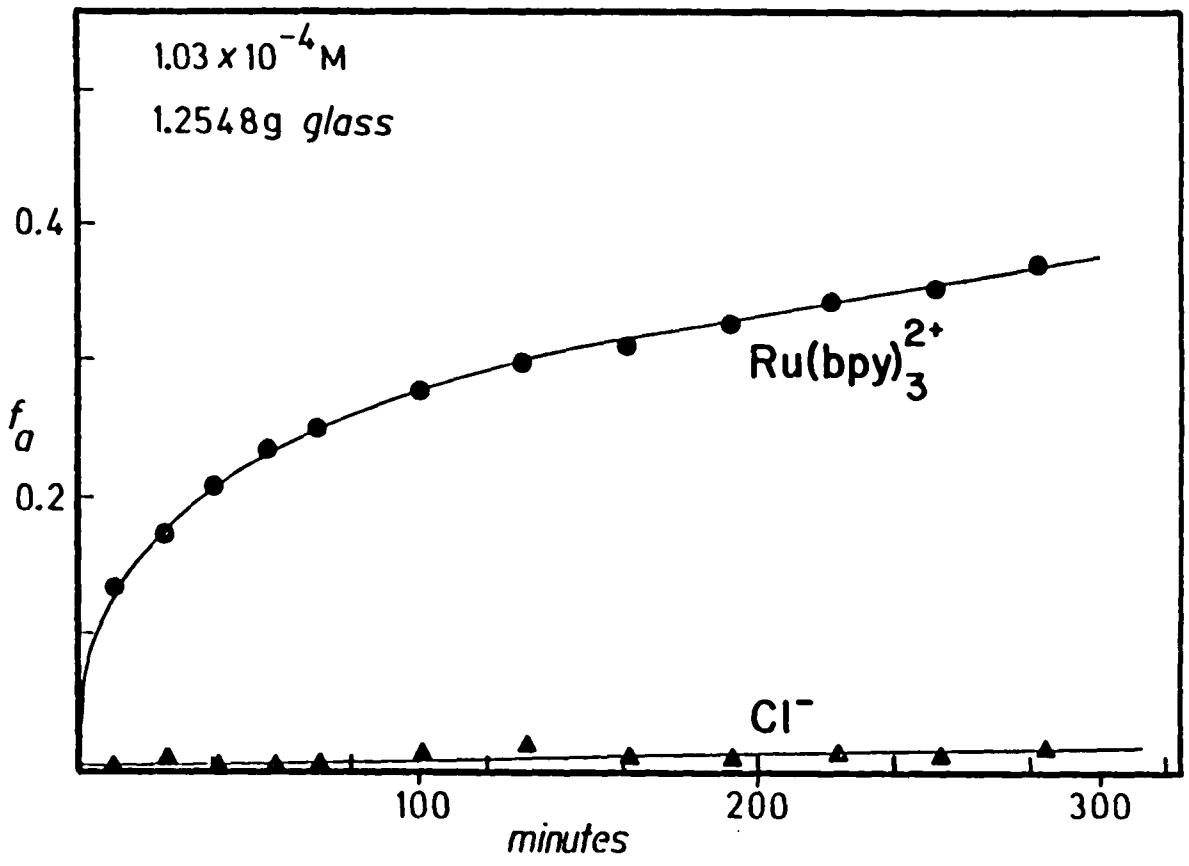
1.03 x 10⁻⁴ M
1.2548g glass
0.4
0.2
f_a
Ru(bpy)$_3^{2+}$
Cl⁻
100
200
300
minutes

a) Adsorption of Individual Compounds

The rate of adsorption of a particular compound depends on a number of factors, including the affinity of the compound toward the surface, the concentration of the solution and the solution pH. A comparison of relative adsorption rates was made for the three cationic compounds, $Ru(bpy)_3^{2+}$, Cr^{3+}, and MV^{2+}. A PVG sample (weight 4.5 g, surface area 140 m^2/g) was placed in a 50 ml, 1.0×10^{-4} M solution (pH 7) of each of the above compounds. The rates of adsorption were calculated from the decline in optical absorption of the impregnation solutions at wavelengths 450 nm(ϵ = 14600), 630 nm(ϵ = 220), and 256 nm(ϵ =20700), respectively. Figure8 is representative of the time dependence of adsorption. For each of the three compounds, the time dependence of the adsorption rate shows a relatively rapid initial rate rise, followed by gradual leveling off. However, these compounds differ sharply in their rates of adsorption as well as the total amount adsorbed during the time the PVG samples are in contact with the solutions, with $MV^{2+} > Ru(bpy)_3^{2+} > Cr^{3+}$ in both the rate and the adsorbed amount.

b) Competitive Adsorption of $Ru(bpy)_3^{2+}$ and MV^{2+}

Figure 9 shows the rates of adsorption of $Ru(bpy)_3^{2+}$ and methyl viologen onto a same piece of PVG. The 25 mm x 25 mm x 4.5 mm PVG sample was placed in a 50 ml solution containing 1.0×10^{-4} M each in $Ru(bpy)_3^{2+}$ and MV^{2+}. The solution

Figure 8. Adsorption of cationic reagents as a function of time. f_a is the fraction of the ion that is adsorbed from aqueous solution to PVG. Concentration of each solution is 1.0×10^{-4}M.

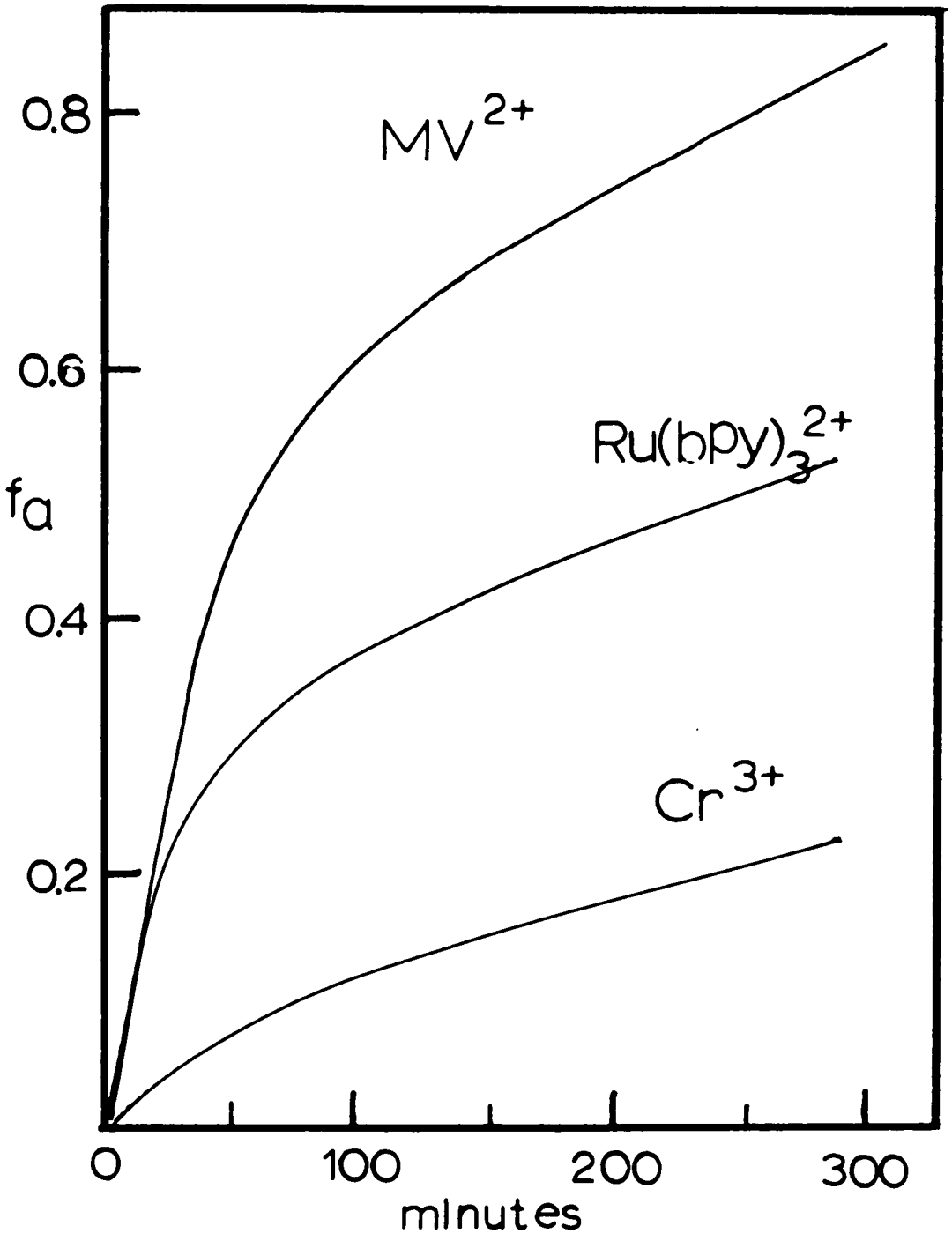
0.8
0.6
0.4
0.2
fa
MV2+
Ru(bpy)32+
Cr3+
0
100
200
300
minutes

Figure 9. Competitive adsorption of $Ru(bpy)_3^{2+}$ with MV^{2+}. The solution contains 1 x 10^{-4} M each of these two compounds. Note that the rate of adsorption for $Ru(bpy)_3^{2+}$ is supressed by MV^{2+} but that of MV^{2+} is not affected by the presence of $Ru(bpy)_3^{2+}$.

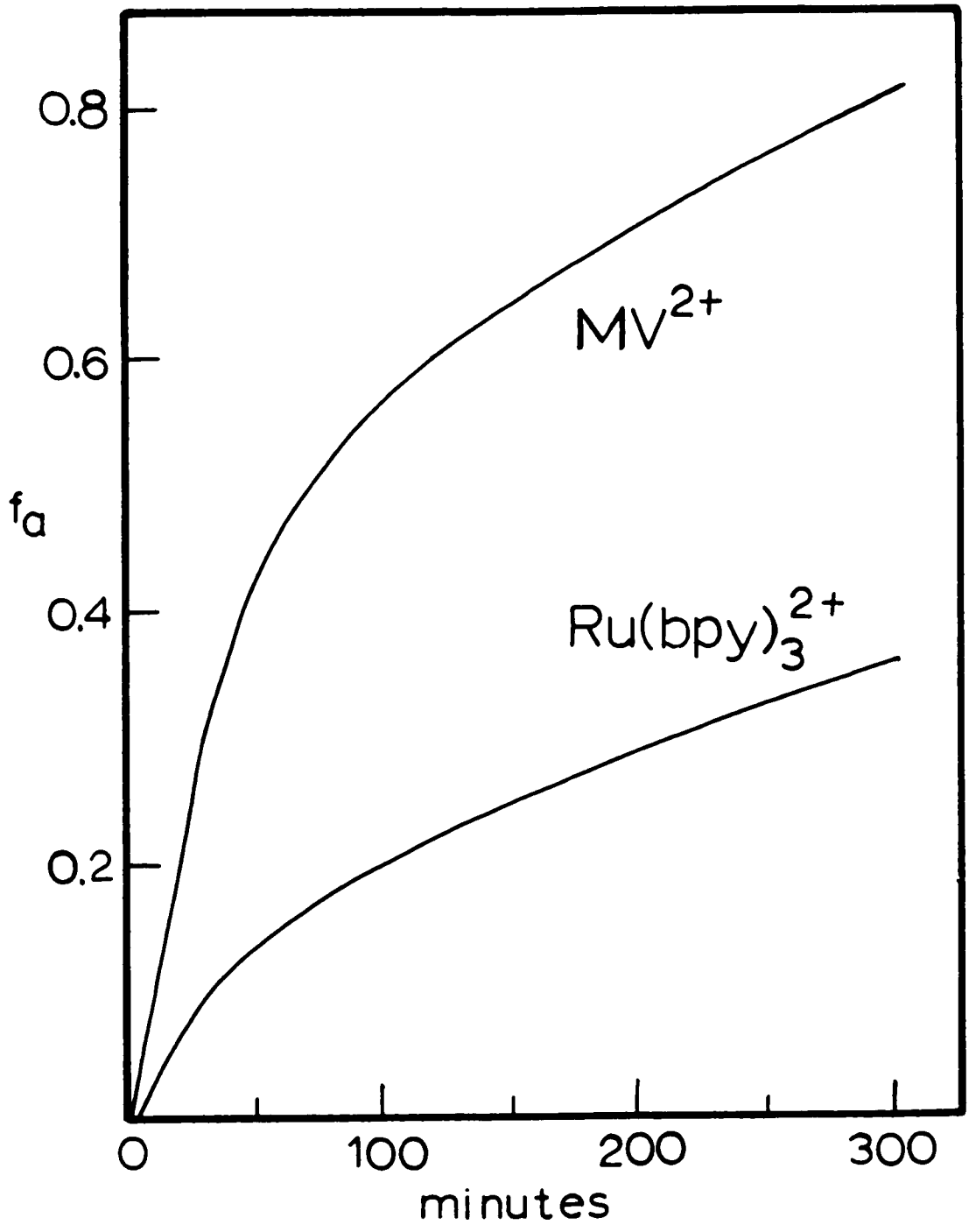
0.8
0.6
0.4
0.2
f_a
MV^{2+}
$Ru(bpy)_3^{2+}$
0
100
200
300
minutes

concentrations were determined from absorbance measurements at 452 nm and 256 nm for thew complex and MV^{2+}, respectively. MV^{2+} has negligible absorption at 452 nm and hence measurement at 452 nm in mixed solution provides the concentration of $Ru(bpy)_3^{2+}$ through its known extinction coefficient(see above). The absorbance at 256 nm was then corrected for that of $Ru(bpy)_3^{2+}$ and the residual absorbance used to calculate the concentration of MV^{2+} in the mixed solution. When compared with the adsorption of individual components (Figure 8), a sharp decrease in the adsorption rate of the Ru complex is observed. For example, at t = 100 min., the amount of $Ru(bpy)_3^{2+}$ adsorbed from the mixture is only ca. 50% of the amount adsorbed from a solution containing only the complex. In contrast, the rate of MV^{2+} adsorption in the presence of the metal complex does not change significantly from that of the pure solution.

c) pH Dependence of Adsorption Rates

The pH dependence of adsorption rates of $Ru(bpy)_3^{2+}$ and MV^{2+} have been examined at PH = 5, 9, and 11. The PVG samples(25 mm x 25 mm x 4.5 mm, 4.5 g) were placed in 50 ml solutions of each of the two compounds.The pH was adjusted with acetate buffer for pH 5 and and with KOH for pH 9 and pH 11. As shown in Figure 10, for solutions 1×10^{-4} in $Ru(bpy)_3^{2+}$ and in MV^{2+}, the rates of adsorption of both compounds increase with increasing pH. Although no attempt was made to saturate the samples, it is most likely that

Figure 10. pH dependence of rate of adorption onto PVG. The concentration of the impregnating solution is 1.0×10^{-4} M. Both MV^{2+} and $Ru(bpy)_3^{2+}$ show similar pH dependence.

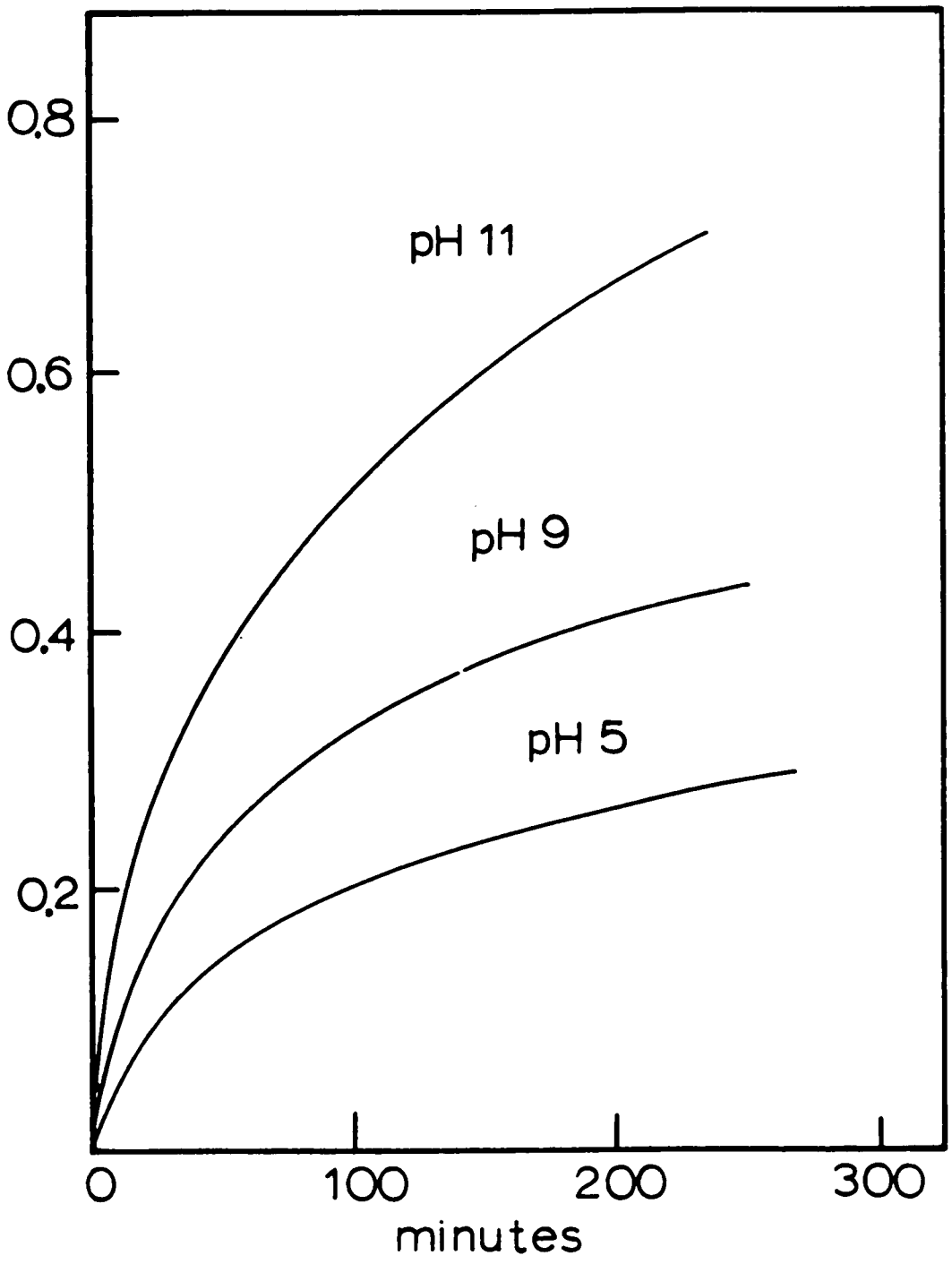
0.8
0.6
0.4
0.2
pH 11
pH 9
pH 5
0
100
200
300
minutes

higher pH will lead to larger amounts of each cation adsorbed on PVG. The pH dependence of adsorption is consistent with the cation exchange nature of the glass. In a basic solution, proton dissociation from the silanol groups on the surface is favored (eq. 13). This increases the surface charge which in turn accelelerates the flow of cations from the solution phase to the surface. However, even at low pH, adsorption of cations can still occur. Fe^{3+} and Cr^{3+} were adsorbed onto PVG from acidic aqueous solutions, pH < 3, to prevent hydrolysis of these metal ions.

2. Distributions of Adsorbates on the PVG Surface

a) Distribution of $Ru(bpy)_3^{2+}$

Despite the open pore structure of the glass, distribution of various compounds on PVG are not always uniform and differ from one compound to another. Consistent with earlier work in this laboratory, $Ru(bpy)_3^{2+}$ is found to distribute preferentially on the outer surface of the glass sample. The penetration depth depends on the concentration of the solution and the length of impregnation time. Under the usual conditions in these experiments, where the 25 mm x 25 mm x 4.5 mm glass samples were placed in 1×10^{-4} M to 1×10^{-3} M $Ru(bpy)_3^{2+}$ solutions for times ranging from 12 to 48 hours, the complex penetrates 0.4 ± 0.1 mm into the glass from each side. Since the thickness of the glass is 4.5 mm, the volume of PVG impregnated with the complex constitutes ca. 18% of the total sample volume. Increasing the contact

time increases the penetration depth and, with sufficient time(on the order of weeks at room temperature, 22 ± 1°C), eventully impregnates the entire piece(Figure 11). However, once adsorbed onto the outer layer of the glass, no redistribution of the complex is detected even if the impregnated sample is placed in pure water for several months.

Figure 12 shows the cross-sectional distribution of the Ru complex on PVG. The sample originally contained 10^{-6} moles of $Ru(bpy)_3^{2+}$ /g PVG. As the sample thickness is reduced by gradually grinding off one side of the surface, the optical density monitored at 450 nm decreases linearly until ca. 0.4 mm of the 4.5 mm thick sample has been ground off over the entire 25 mm x 8 mm side. At this point, the optical density at 450 nm has been reduced to 50% of the initial value, indicating a symmetrical distribution of the complex on the two sides. Futhermore, the linearity of the decreasing optical density with the thickness shows a relatively uniform distribution of the adsorbed complex within this region. The horizontal line in the middle of the piece confirms that no $Ru(bpy)_3^{2+}$ adsorbed in the interior.

Unlike the cross-sectional distribution, adsorption of $Ru(bpy)_3^{2+}$ along the 25 mm x 25 mm surfaces of the glass sample is uniform, as shown by measurements of the optical absorption of the impregnated PVG sample at various points along the surface. The 450 nm absorbance at these points was

Figure 11. The cross sectional distribution of $Ru(bpy)_3^{2+}$ on a PVG sample after several months in contact with impregnating solution.

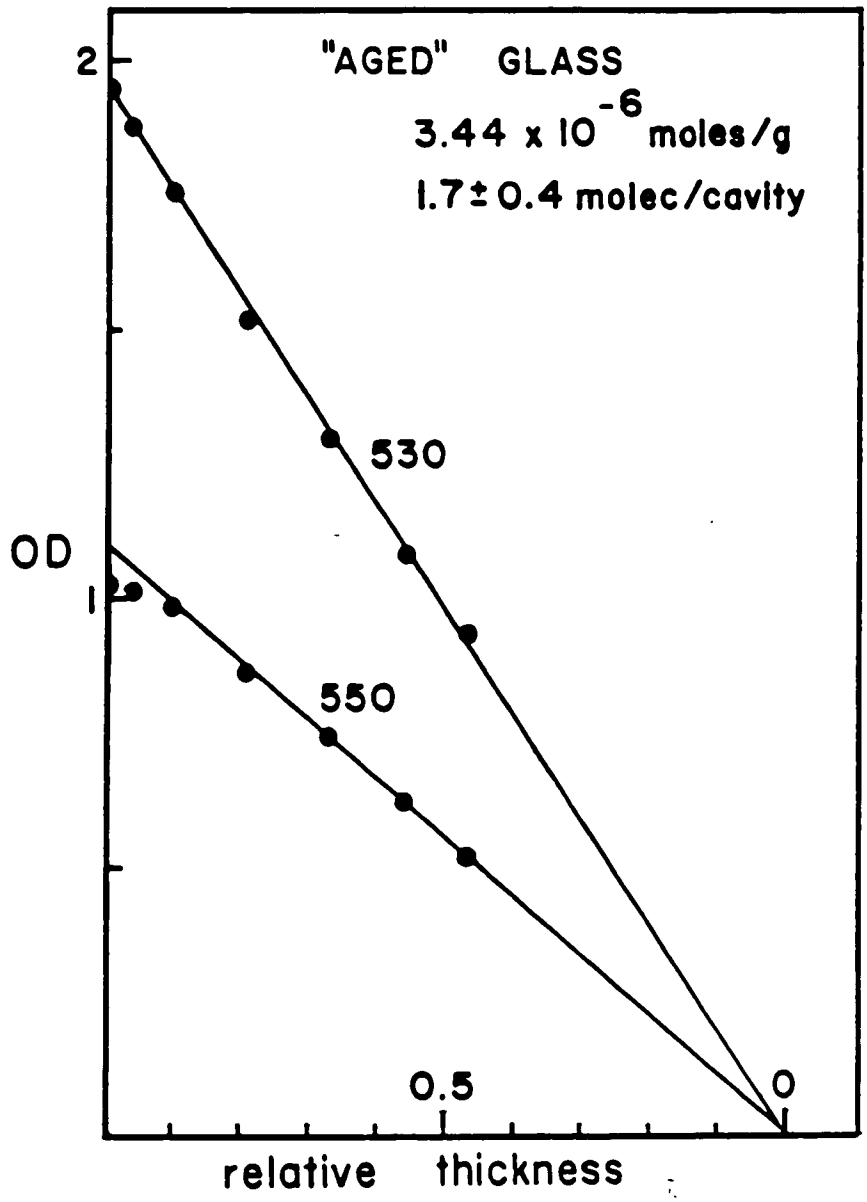
"AGED" GLASS
3.44 x 10^-6 moles/g
1.7 ± 0.4 molec/cavity
2
OD
1
530
550
0.5
0
relative thickness

Figure 12. The cross sectional distribution of $Ru(bpy)_3^{2+}$ on PVG. The sample is prepared by the normal impregnation procedures: solution concentration 1 x 10^{-4} to 1 x 10^{-3} M, impregnation time 24 to 72 hours. The complex penetrates $\leq$ 0.5 mm into the PVG sample.

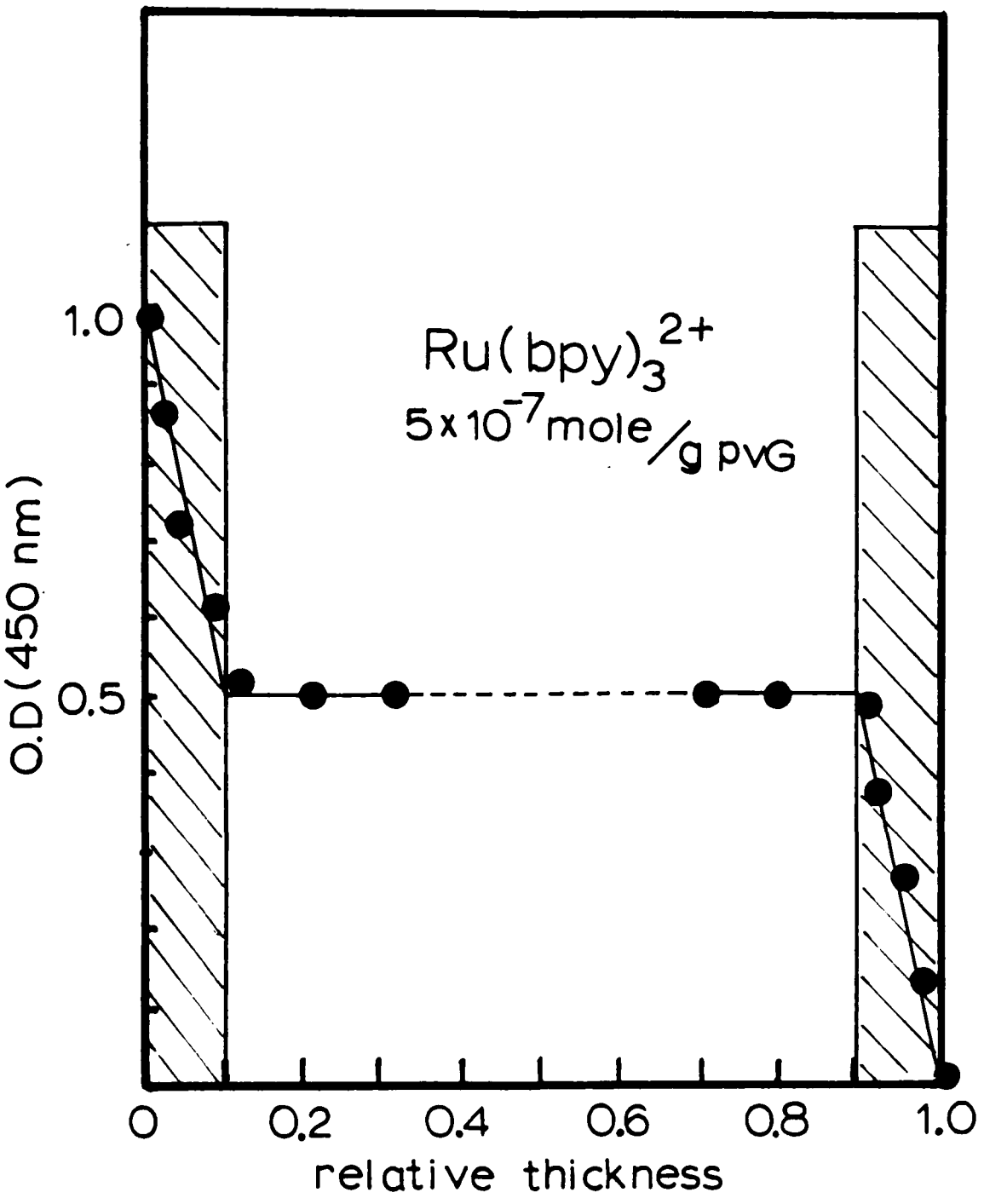
Ru(bpy)$_3^{2+}$
5×10^{-7} mole/g pvG
O.D (450 nm)
1.0
0.5
0
0.2
0.4
0.6
0.8
1.0
relative thickness

constant within experimental error(±5 %), indicating a uniform distribution of the adsorbed complex on each side of the sample.

b) Distribution of Other Compounds

The distributions of other metal complexes, metal ions, and organic compounds were examined. Since previous studies on distribution had been limited to $Ru(bpy)_3^{2+}$ and a few other similar metal complexes, which have similar distribution pattern,[167] the distribution profile shown in Fig. 12 was assumed to be universal for all adsorbates. The unexpected results from $Ru(bpy)_3^{2+}$ emission quenching, however, led to re-examination of the distribution properties of various molecules, e.g., MV^{2+}, Cu^{2+}, Cr^{3+}, and Fe^{3+} by the grinding techniques described above (see Section C). Results from these studies show that, indeed, the cross-sectional distributions of these compounds vary considerably from one another and, according to the penetration depth into PVG, can be classified as the following types.

Type I. Adsorption onto the outermost surface of the PVG sample, where the penetration depth is limited to < 0.1 mm. Cr^{3+} belongs to this class. This extremely limited adsorption appears to be responsible for the difficulties in impregnating PVG with Cr^{3+}. In a typical impregnation experiment, a 1.0×10^{-3} M Cr^{3+} solution was prepared by dissolving appropriate amount of $CrCl_3 \cdot 6H_2O$ into distilled water. The pH of the solution was adjusted to 3.0 to prevent

hydrolysis of the Cr^{3+} ion. A PVG sample(25 mm x 25 mm x 4.5 mm, 4.5 g)was then placed into this solution. After 24 hr., the sample was taken out of the solution and the solvent removed under reduced presure. This dried sample was again placed into a fresh solution of Cr^{3+}. Repeating this soak-and-dry cycles for over two weeks resulted adsorption of $\leq 6 \times 10^{-6}$ moles/g PVG .

Type II. Adsorption onto outer volumes of PVG where the penetration depth is 0.5 $\pm$ 0.1 mm. This is the case for $Ru(bpy)_3^{2+}$ as well as a number of similar metal complexes, including bipyridyl complexes of Cr^{2+}, Fe^{3+}, Os^{2+}. The metal ion Fe^{3+} also falls within this class since, on exposure to 1×10^{-4} M solution of $FeCl_3 6H_2O$, similar volume of PVG are impregnated with Fe^{3+}.

Type III. Adsorption throughout the entire volume of PVG sample. This has been found for two very different compounds, Cu^{2+} and MV^{2+}. When adsorbed individually, these molecules distribute uniformly across the 4.5 mm thick sample. Figure 13 shows a distribution profile for Cu^{2+} obtained by previously described grinding techniques. Only qualitative results are available for MV^{2+}, since its absorption maximum is in the UV region (256 nm) where the intense absorption by the glass makes reliable measurements difficult. However, the presence of MV^{2+} in the interior of the glass can be easily detected by chemically reducing it to the blue colored free radical MV^{+} after grinding off half the sample. A 0.10 M basic solution (pH 12, adjusted with KOH) of the reducing

Figure 13. The cross sectional distribution of Cu^{2+} on PVG. The profile is obtained by grinding the sample and recording the Cu^{2+} absorption at 820 nm.

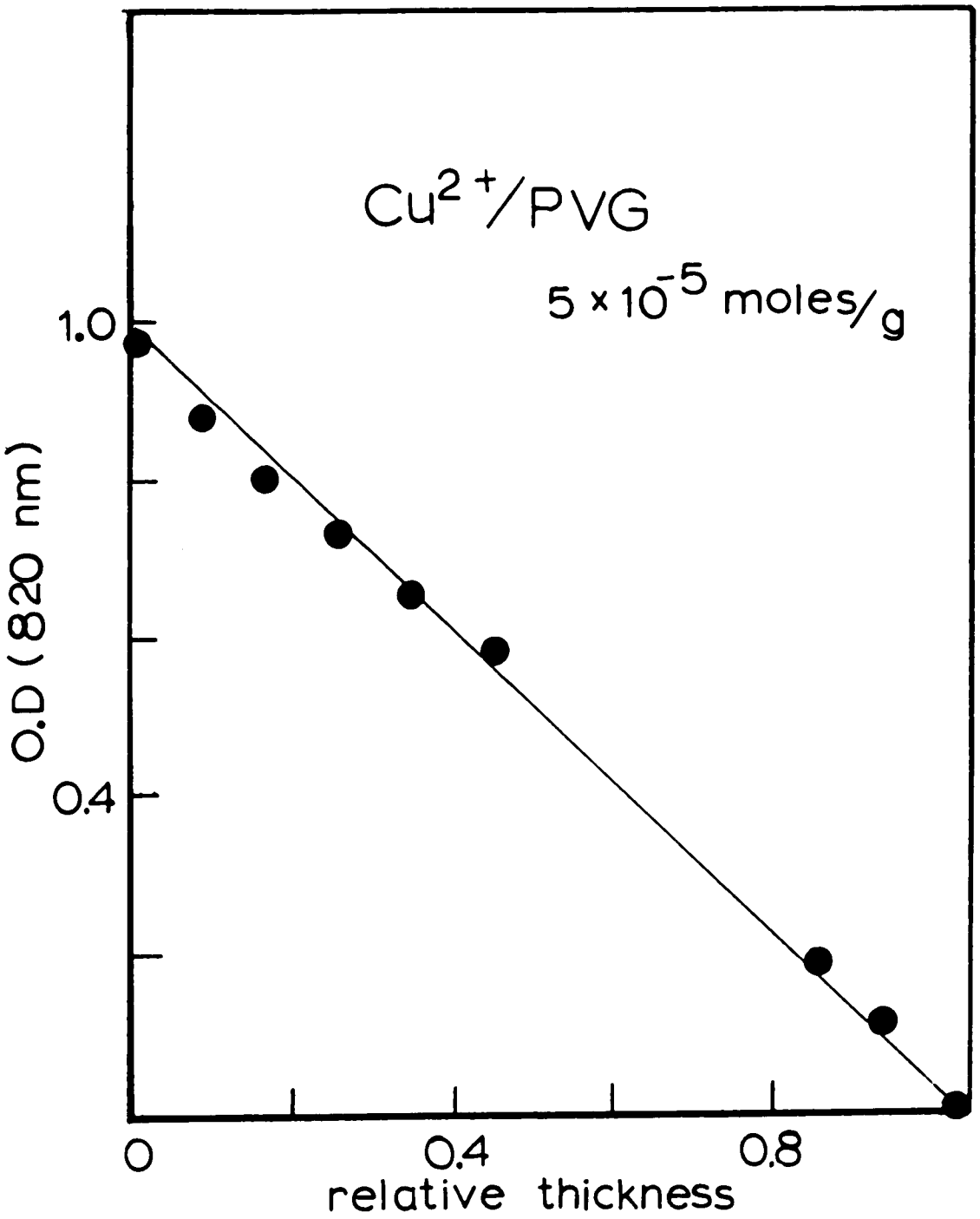
Cu2+/PVG
5 x 10-5 moles/g
1.0
0.4
O.D (820 nm)
0
0.4
0.8
relative thickness

agent, NaS_2O_4, was prepared. A PVG sample impregnated with MV^{2+}, 1.0 x 10^{-5} moles/g, was ground along the 25 mm x 25 mm face. After each 0.1 mm layer was grinded off, theremaining piece was sprayed with the dithionite solution, and the reduced viologen radical, MV^{+}, was observed either by direct inspection of the intense blue color or by measuring its absorption at 605 nm with a spectrometer. This procedure was repeated until half of the PVG sample was grined off, and the blue color of the reduced viologen was observed thoughout. The distribution of methyl viologen over the entire PVG sample can also explain, at least partially, the observed higher rate of adsorption and the amount adsorbed compared to, for example, $Ru(bpy)_3^{2+}$, which adsorbs onto only 18 % of the sample volume.

c) Distribution of Coadsorbed Compounds

Because of the difference in the cross-sectional distributions of different compounds, a totally random mixing of $Ru(bpy)_3^{2+}$ and another component on the PVG surface can not, of course, be assumed. However, the low loading level of the complex within its impregnated region, e.g. the 0.4 mm thick frame on the outer surface of the glass, means that it is possible that within this volume the complex can mix with the co-adsorbate molecules. Typically, the apparent concentration of $Ru(bpy)_3^{2+}$ on the glass is 5 x 10^{-7} moles/g PVG. Since it occupies only 18% of the total volume, the actual concentration of the complex in the impregnated region is ca. 2.6 x 10^{-6} moles/g. Taking 7.5 Å as the radius of the

complex, and the surface area of PVG 140 m^2/g, the above concentration represents a surface coverage of $\leq$ 2%. In view of this small value, one would expect that the presence of the adsorbed complex would not significantly bias the adsorption of the other component within this region. Surprisingly, however, this is not the case found for Cu^{2+} and for MV^{2+}.

The distribution of Cu^{2+} on the glass is uniform throughout the bulk of PVG in the absence of $Ru(bpy)_3^{2+}$. In the presence of the complex, however, the copper distribution in the $Ru(bpy)_3^{2+}$ impregnated region is altered and shows a strong dependence on the total amount adsorbed. Figure 14 shows the cross-sectional profile of Cu^{2+} and $Ru(bpy)_3^{2+}$ distribution in a PVG sample containing 5×10^{-7} M/g of the complex and 3×10^{-5} M/g of Cu^{2+}. The optical absorptions indicative of the two ions as a function of the relative thickness of the sample was monitored at 450 nm and 800 nm, respectively. When the first 0.4 mm of the surface is ground off, the 450 nm peak decreased 50%, indicating that half of the adsorbed $Ru(bpy)_3^{2+}$ on the glass, or all of it on that side of the sample had been lost. However, the peak at 800 nm, characteristic of Cu^{2+}, hardly changed beyond experimental error. If Cu^{2+} was randomly distributed on the entire piece of the sample, the grinding, which reduces the sample volume by 9 %, would require an ca. 9% decrease in the Cu^{2+} absorption. The fact that the 800 nm peak begins to decline only after the 0.4 mm layer has been removed

Figure 14. A) The grinding experiment of a PVG sample containing 4×10^{-7} moles of $Ru(bpy)_3^{2+}$ /g and 2×10^{-5} moles of Cu^{2+}/g. After ca. 0.4 mm of the glass is grinded off, the 450 nm absorption is reduced to 50 % of the original value, but the 810 nm absorption remains essentially unchanged.

B) The cross sectional distribution of Cu^{2+} in the presence of 5×10^{-7} moles of $Ru(bpy)_3^{2+}$ /g. Cu^{2+} preferentially distributed in the interior of the glass while $Ru(bpy)_3^{2+}$ adsorbs on the outer surfaces.

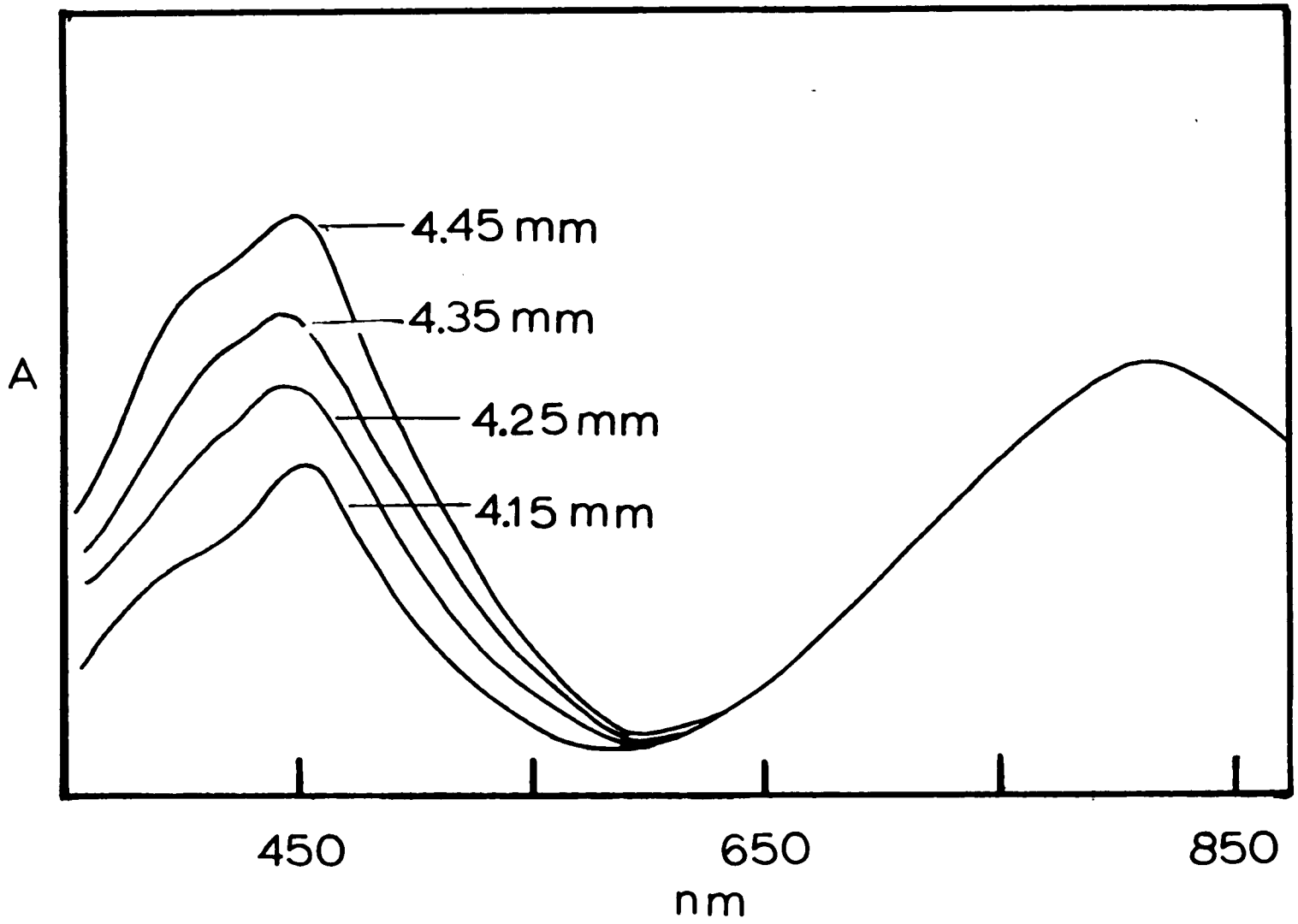
4.45 mm
4.35 mm
4.25 mm
4.15 mm
A
450
650
850
nm

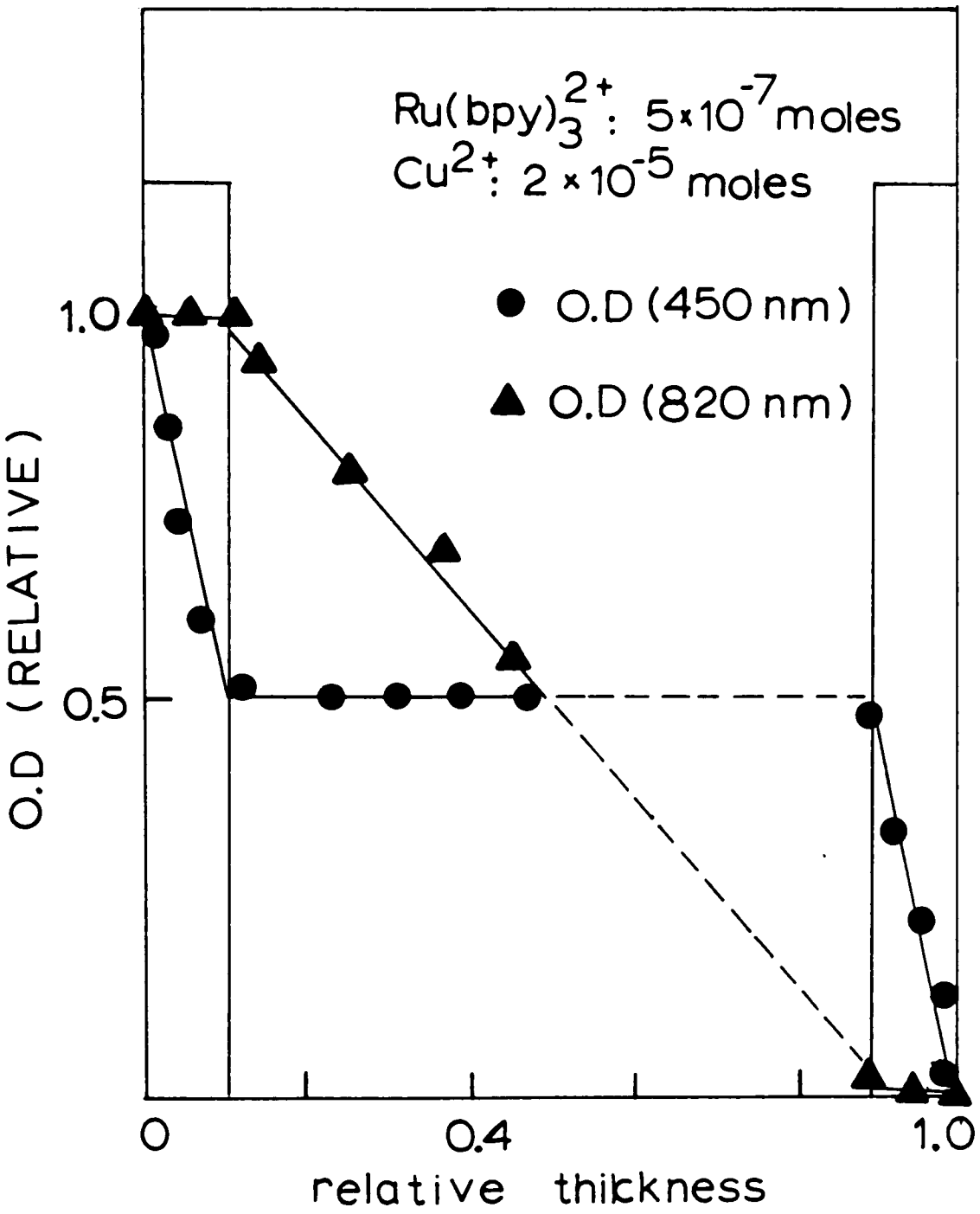
$Ru(bpy)_3^{2+}$: 5×10^{-7} moles
Cu^{2+}: 2×10^{-5} moles
O.D (450 nm)
O.D (820 nm)
1.0
0.5
O.D (RELATIVE)
0
0.4
1.0
relative thickness

indicates that, at this impregnation level, little Cu^{2+} is adsorbed in the volume of the sample impregnated with $Ru(bpy)_3^{2+}$.

At higher Cu^{2+} impregnation levels, however, a different distribution results. In a similar grinding experiment with a PVG sample containing 5×10^{-7} moles/g of $Ru(bpy)_3^{2+}$ and 3×10^{-4} moles/g of Cu^{2+}, a nearly linear decline of the 800 nm absorption is observed throughout the cross section (Figure 15), indicating a uniform distribution of the copper ion in both the outer surface and the interior of the glass. These results are independent of the order in which the two compounds are adsorbed onto the glass.

A similar distribution is also found when MV^{2+} is co-adsorbed with $Ru(bpy)_3^{2+}$, although the results in this case are qualitative rather than quantitative due to the difficulties in monitoring the UV absorption of MV^{2+}(see above). The presence of MV^{2+} in the glass is detected by chemically reducing it to the intensely blue colored MV^{+}. After each grinding(0.05 - 0.1 mm) the remaining piece was treated with the reductant sodium dithionite. The appearance of the blue color on the outer surface was relatively slow, presumably because the dithionite solution has to penetrate into the interior to react with the adsorbed MV^{2+}. As the outer layer was ground off, the color develops instantly when the dithionite solution was dripped on to the glass surface. The grinding and reducing process is repeated until half of the glass is ground, and the blue color is observed even at

Figure 15. The cross sectional distribution of Cu^{2+} at high Cu^{2+} concentration, i.e., 2 x 10^{-4} moles of Cu^{2+}/g. The distribution is nearly uniform across the entire 4.5 mm thickness.

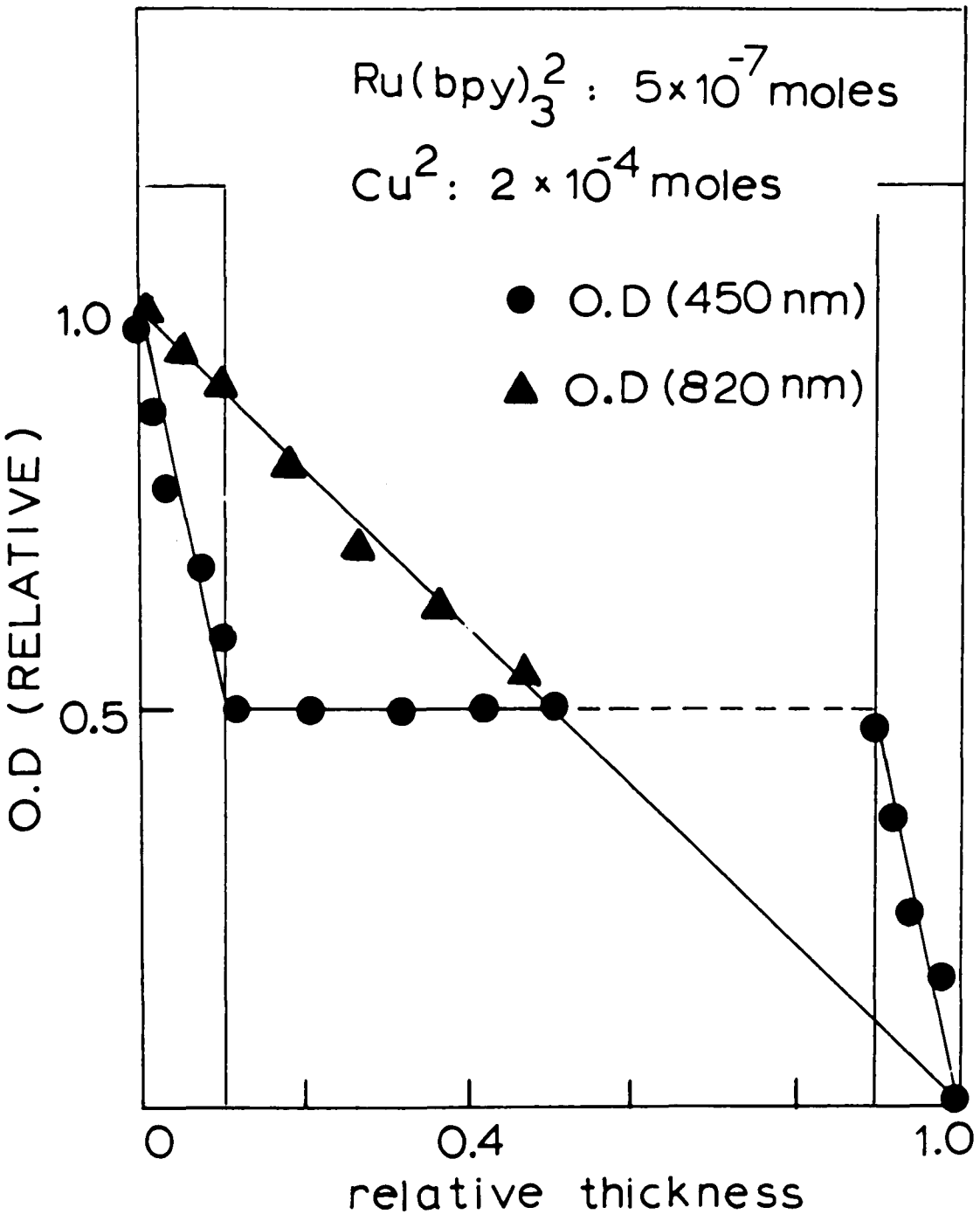
$Ru(bpy)_3^{2}$: 5×10^{-7} moles
Cu^{2}: 2×10^{-4} moles
O.D (450 nm)
O.D (820 nm)
1.0
0.5
O.D (RELATIVE)
0
0.4
1.0
relative thickness

the middle of the sample.

In contrast to these observations, the distributions of Fe^{3+} and Cr^{3+} on PVG are not significantly altered by the presence of $Ru(bpy)_3^{2+}$. However, their rates of adsorption from aqueous solutionsare reduced by the presence of the complex in the PVG sample.

3. Deposition of Semiconductors

a) Titanium Dioxide

TiO_2 can be deposited onto PVG from isopropanol solutions of either $TiCl_4$, or titanium tetraisopropoxide, $Ti(i\text{-}OC_3H_7)_4$. The impregnating solutions using $TiCl_4$ were prepared by slowly adding previously weighed portions of the liquid $TiCl_4$ into HCl acidified isopropanol (pH < 2.0). A weighed piece of PVG sample (4.5 g) was then placed into a 50 ml ca.1.0 x 10^{-3} M solution. Since the titanium compound shows no absorption maximum in either the visible or UV region, the impregnation level was determined by the solution absorbance at ca.350 nm. The experimental error in this case was relatively large due to the steepness of the cutoff near this wavelength. A UV-visible spectrum of the supported semiconductor is shown in Figure 16. Similar to the solution spectrum, the adsorbed compound exhibits no absorption in the visible region. A very sharp rise in absorbance , however, is observed at < 360 nm, the onset of thelatter depends on the level of impregnation. This sharp spectral cutoff is

Figure 16. An absorption spectrum of TiO_2 deposited on PVG. Note that at lower loading levels, the absorption is blue shifted.

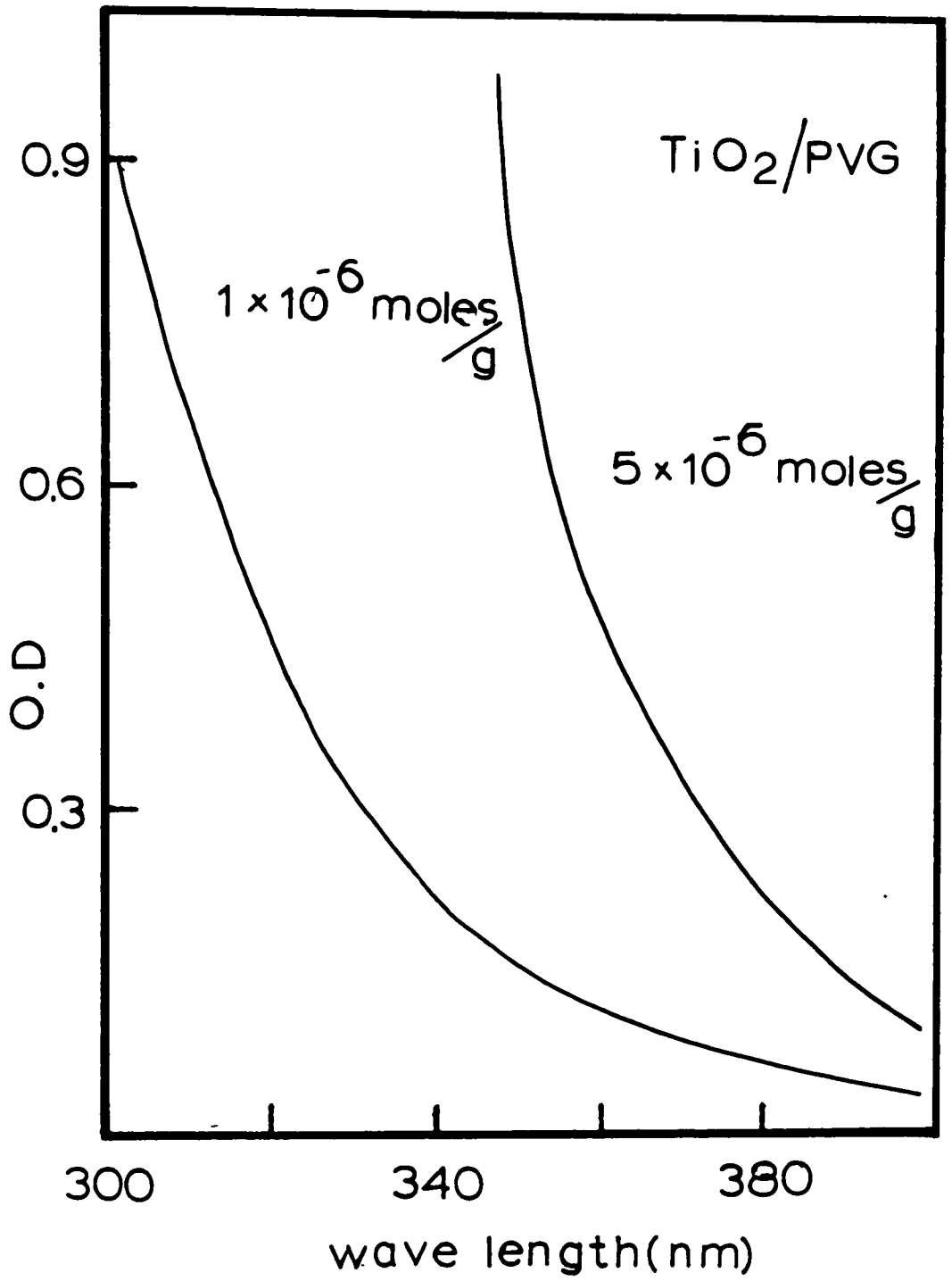
0.9
0.6
0.3
O.D
TiO2/PVG
1 x 10-6 moles/g
5 x 10-6 moles/g
300
340
380
wave length(nm)

characteristic of a semiconductor and,in this case, the spectrum is reminecent of the spectra of the colloidal dispersions of TiO_2 in water.[147] However, the PVG incoporated TiO_2, even at the highest level of impregnation, ca. 10^{-5} M/g, exhibits much less scattering than the colloids in water. This is an indication that the dimension of the semiconductor on the glass is smaller than the presently available ultrafine particles. Heating of the Ti impregnated PVG sample after removing the solvent(isopropanol) to 550 C for 48 hr does not change the absorption spectrum to any significant extent, indicating that the formation of the oxide has been completed during or before the evaporation of the solvent.

The relation between the optical absorption and the light frequency near the band gapof a semiconductor is given by the following equation

$$\nu = A(h\nu - E_g)^{n/2} / h\nu \qquad (17)$$

where n = 4 for TiO_2, A is a constant, nue is the light frequency, is the absorption coefficient near the band edge, and E_g is the band gap energy. When $\nu > E_g$, > 0. The band gap for TiO_2 deposited on PVG is calculated by taking 360 nm as the onset point of the band gap excitation. This corresponds to a band gap energy of ca. 3.5 eV. This energy is somewhat higher than the 3.2 eV and 3.0 eV band gaps reported for anatase and rutile TiO_2, respectively.

Grinding experiments similar to those discussed above

show that TiO_2 does not penetrate deep into the glass, the thickness of the impregnated region is $\leqslant$ 0.2 mm. Consequently the amount of TiO_2 that can be deposited is limited to $\leqslant 10^{-5}$ moles/g of PVG.

b) Sb-doped SnO_2

A thin film of SnO_2 doped with 1% Sb was deposited onto the PVG surface by a spray pyrolysis technique. A UV-visible absorption spectrum of a PVG sample coated with such a film, in Figure 17, reveals that the doped semiconductor film is optically transparent(λ > 350 nm). The extinction coefficient near the band edge obeys eq. 17, where n = 4 for SnO_2,[142] and the band gap energy, E_g = 3.5 eV is in good agreement with E_g for a SnO_2 electrode in a pH 1 aqueous electrolyte.[142] Figure 18 shows the electrical resistance measured with a digital ohmmeter, on the surface of a SnO_2 coated PVG sample as a function of distance between the meter electrodes. PVG itself is an insulator and, in the absence of the coating, shows an infinite resistance. The measurements of a finite resistance ($\leqslant$ 10 M ohms) between points along the glass surface situated up to 2 cm apart establish that the Sb doped SnO_2 is indeed conductive.

c) α-Fe_2O_3

When Fe^{3+} ions adsorb onto PVG from aqueous solution of $[Fe(H_2O)_6]Cl_3$, the actual form of the ion is no longer the hexa aquo, which is known to exist only in $HClO_4$. Even in

Figure 17. An absorption spectrum of Sb-doped SnO_2 deposited on PVG.

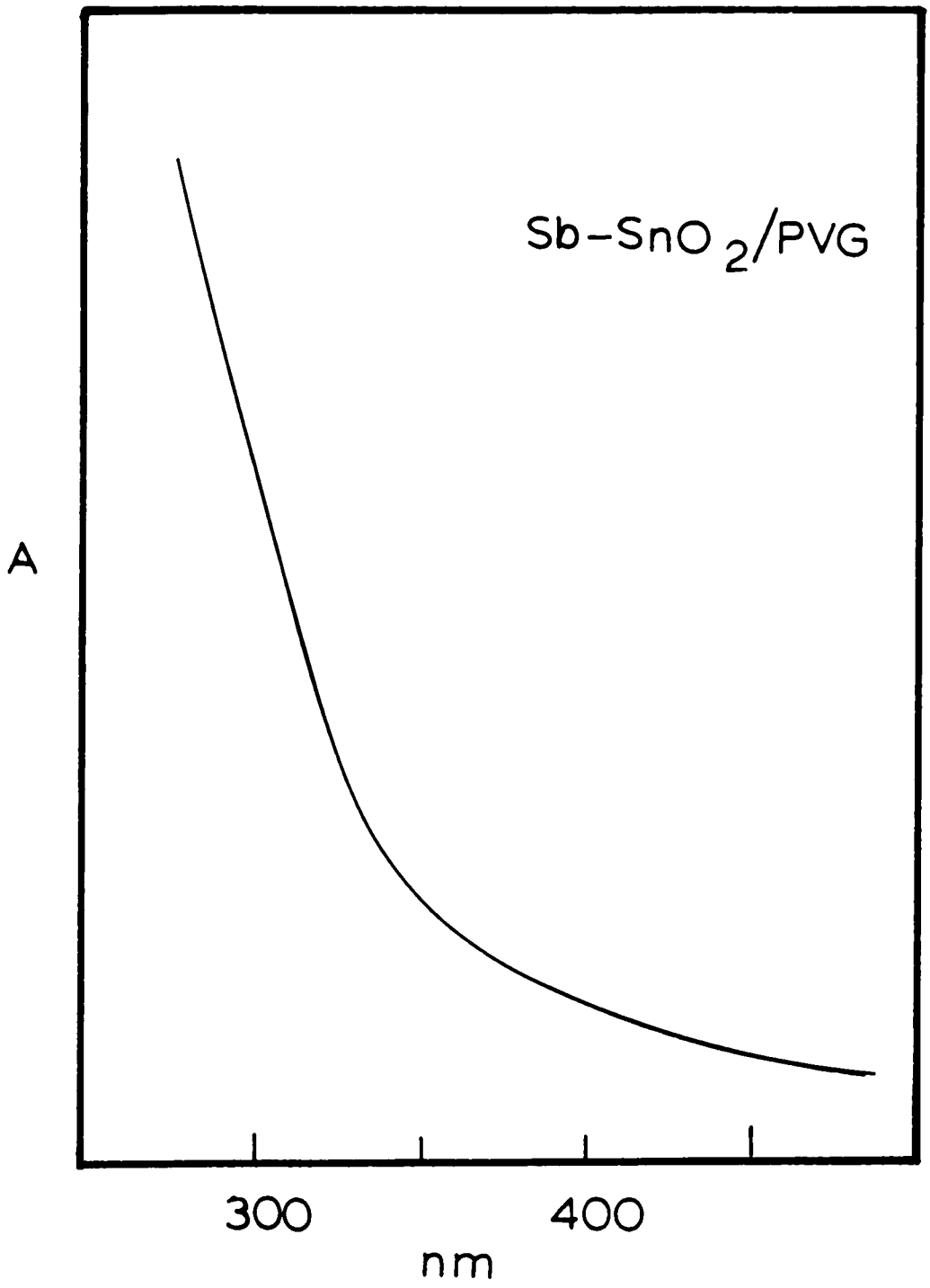
Sb-SnO 2/PVG
A
300
400
nm

Figure 18. The electrical conductivity of the Sb-doped SnO_2 film on the PVG surface. Resistance is ploted as a function of distance between the electrodes of the ohm meter.

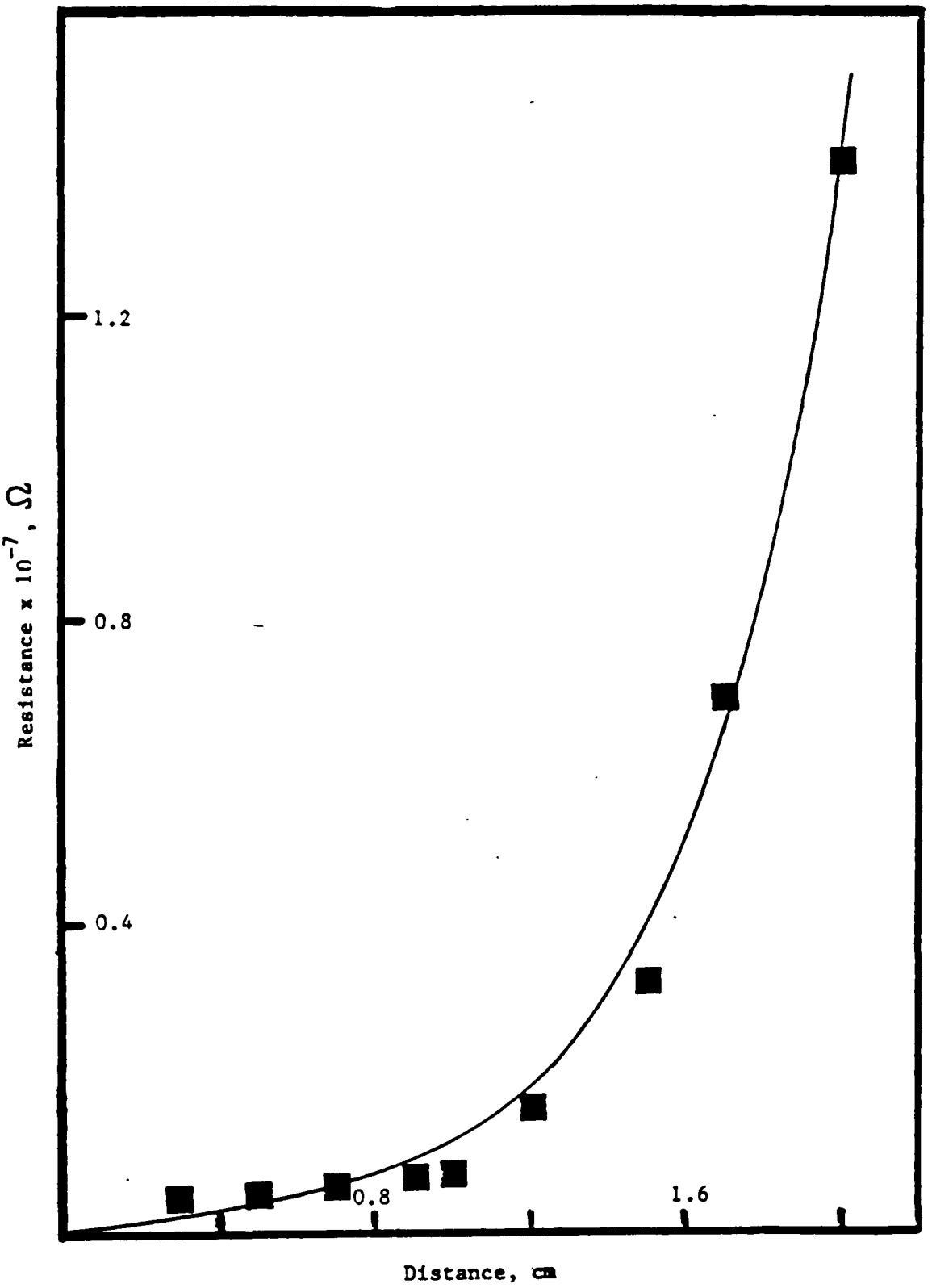
1.2
0.8
0.4
Resistance x 10^{-7}, Ω
0.8
1.6
Distance, cm

solution, which was usually acidified by adding HCl to prevent hydrolysis in these experiments, the ferric ion is probably in the form of $FeCl_4^-$. The absorption spectrum of the PVG supported Fe^{3+} shows no maximum in the visible and near UV region(> 300 nm). Rather, as shown in Figure 19, the absorbance continues to rise in the UV region where the onset of the rising depends on the impregnation level. The appearance of the impregnated glass is lightly brown after removing the acidic solvent, similar to the color of the hydrous ferric oxide, FeO(OH). Indeed, since the PVG surface is only slightly acidic, pH 4, hydrolysis of the ferric ion is likely to occur. When the sample containing the hydrous oxide is saturated with pure water for several hours, the brown color darkens after removing the water, probably due to the complete hydrolysis of the remaining ions in the less acidic water. Heating the hydrolyzed sample at 500^0 C for 24 hrs results in the intense red-brown color characteristic of alpha-Fe_2O_3. The visible absorption spectrum of the final product, shown in Figure 20 is identical to that of the colloidal Fe_2O_3 dispersion in water.[168] The cutoff appears at ca. 550 nm, corresponding to a band gap energy of 2.2 eV.

B. Spectroscopic Properties of $Ru(bpy)_3^{2+}$ on PVG

1. UV-Visible Spectra

As shown in Figure 21, the absorption spectrum of $Ru(bpy)_3^{2+}$ adsorbed on PVG closely resembles the spectrum of the complex in aqueous solution. In the visible region, the

Figure 19. The absorption spectrum of Fe^{3+} adsorbed onto PVG from acidic $FeCl_3 6H_2O$ solution.

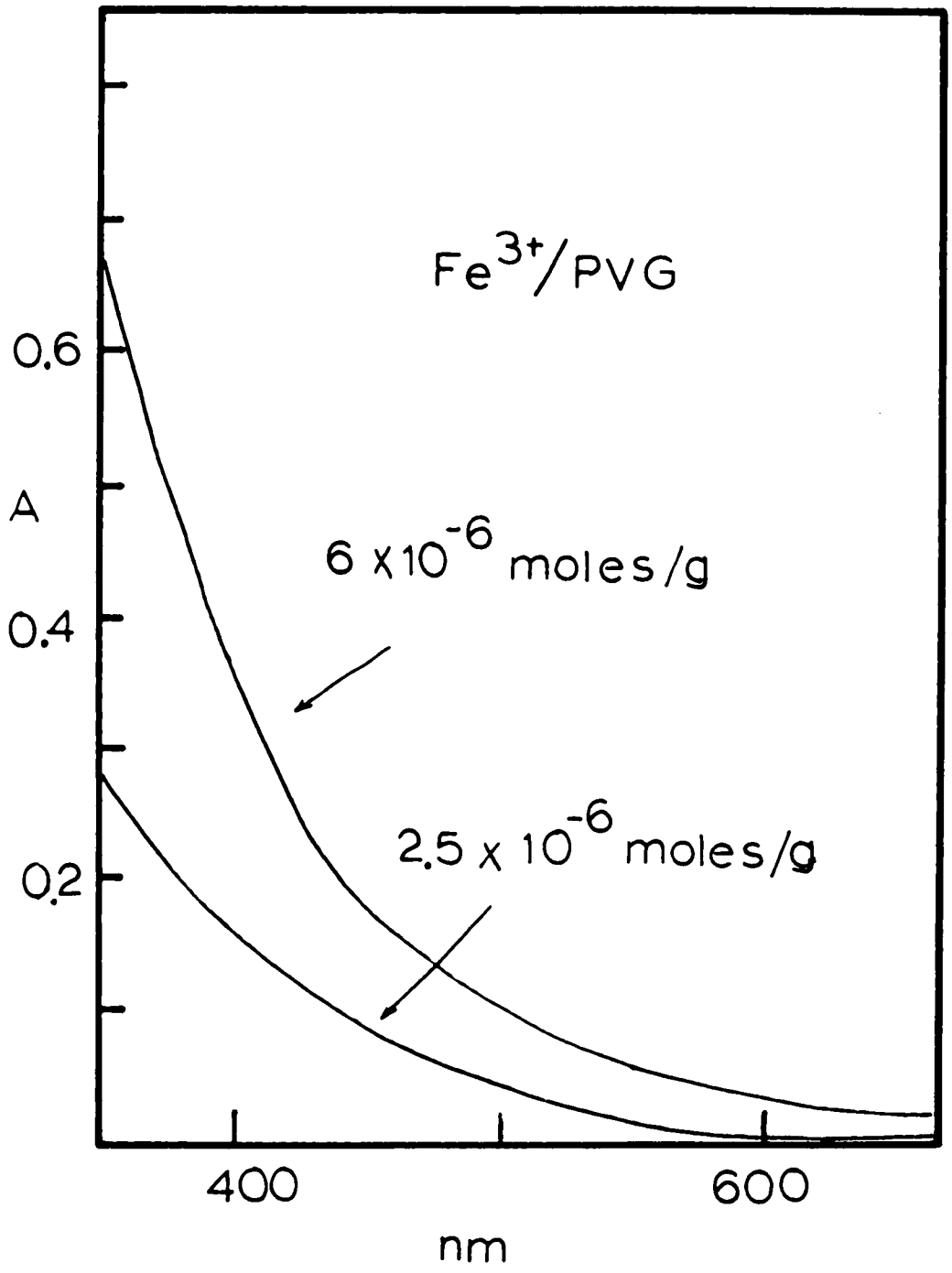
Fe3+/PVG
0.6
A
0.4
0.2
6 X10-6 moles/g
2.5 X 10-6 moles/g
400
600
nm

Figure 20. The absorption spectrum of Fe_2O_3 on PVG. The sample was prepared by heating the Fe^{3+} impregnated PVG at 550 C. The spectrumagrees well with that of the colloidal Fe_2O_3 suspended in water.

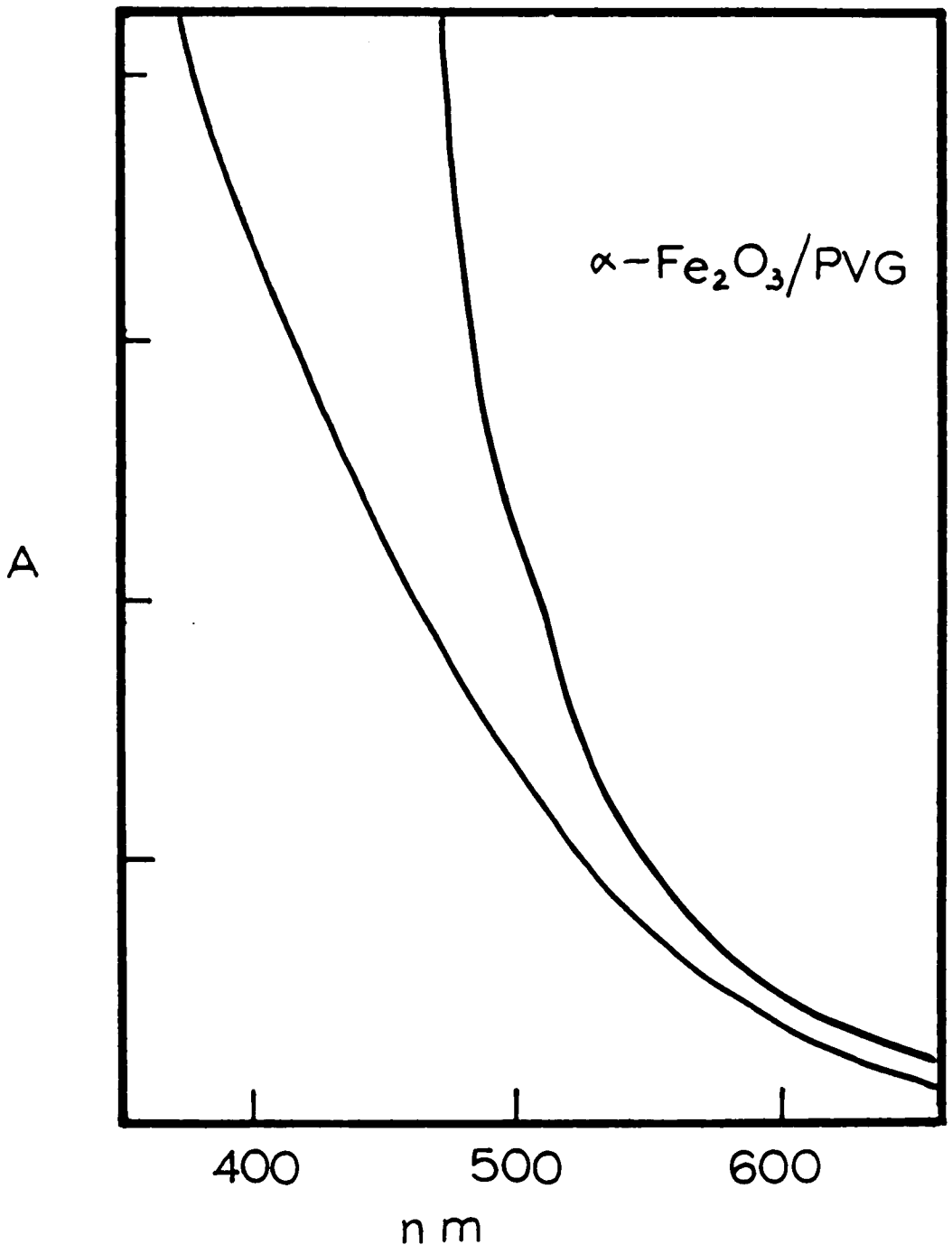
α-Fe2O3/PVG
A
400
500
600
n m

Figure 21. Absorption and emission spectrum of $Ru(bpy)_3^{2+}$ adsorbed onto PVG. Both the absorption and the emission spectra resemble those in aqueous solution.

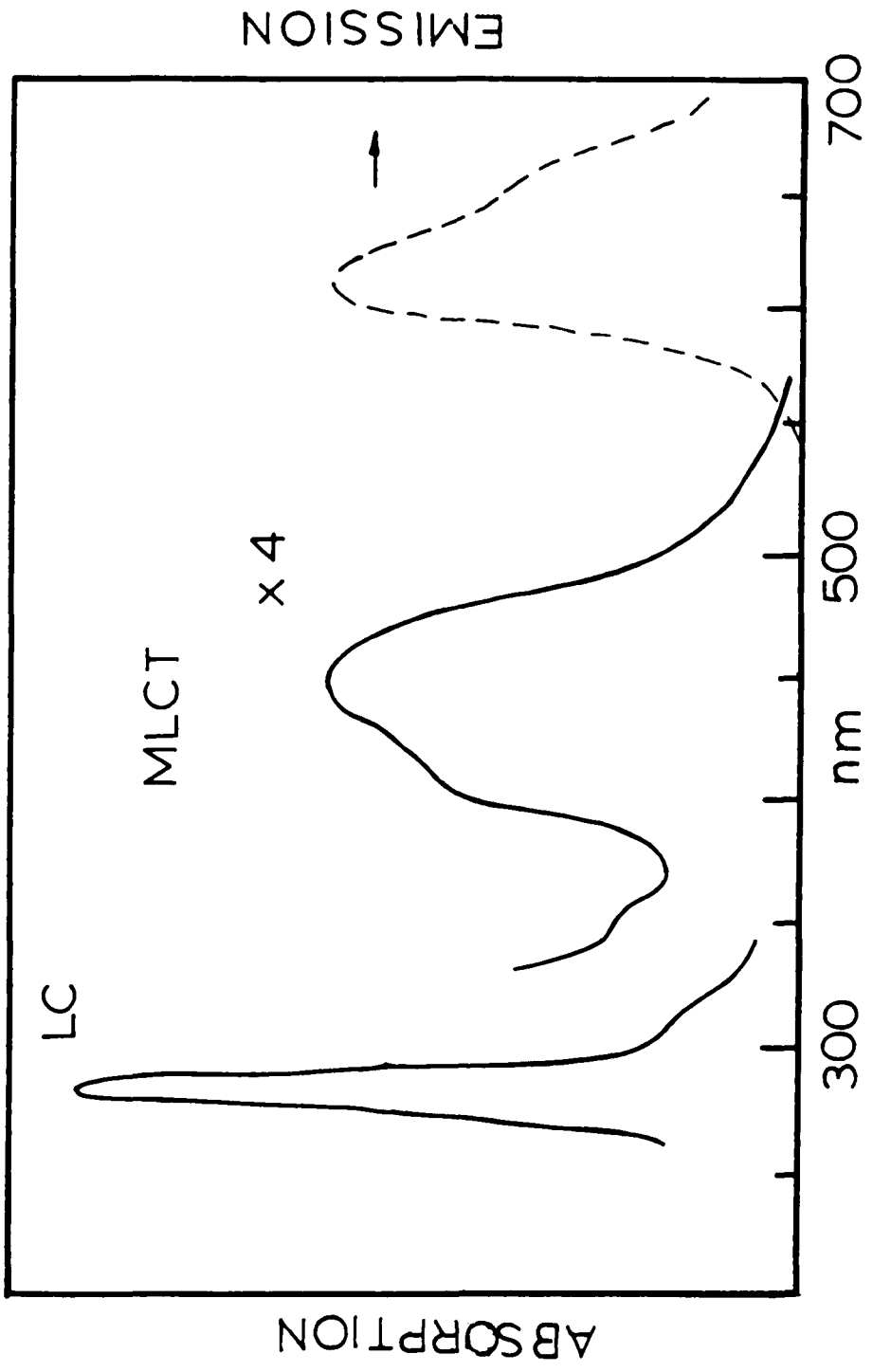
EMISSION
700
500
nm
300
x 4
MLCT
LC
ABSORPTION

spectrum is dominated by an intense MLCT band with a maximum at 450 ± 3 nm and a half width of 70 nm. In aqueous solution the extinction coefficient of the 452 nm peak is 14600 $M^{-1}cm^{-1}$. The extinction coefficient of the adsorbed complex was calculated by assuming that the optical pathlength of the adsorbed complex is equivalent to the penetration depth, 0.4 ± 0.1 mm on each side of the PVG sample. The total pathlength, 0.8 ± 0.2 mm, was then used in the equation

$$E = A/bc \qquad (18)$$

to calculate the extinction coefficient of the adsorbed complex. The value obtained, 15000 $M^{-1}cm^{-1}$, is within experimental error that of the aqueous solution.

In the UV region the intense peak at 285 nm has been assigned to the bipyridine ligand's *pi-pi transition. Because of the intense absorption by PVG in this region (absorbance $\geqslant$ 1.5), accurate measurements of this absorption band were achieved by balancing of the impregnated PVG sample relative to an unimpregnated sample to eliminate the background absorption. Better results were obtained by using pieces of PVG cut from the same sheet and preteated in the same group of samples. The extinction coefficient of the 285 nm absorption of the adsorbed complex was estimated relative to the extinction coefficient of the 452 nm band. The ratio of aborption intensity of the 285 nm band to that of the 452 nm band, after corrected for the PVG absorption, 6.1 :1, is identical to the ratio found in aqueous

solution.[11] Thus the extinction coefficient of the 285 nm absorption for the adsorbed complex is ca. 91000 $M^{-1}cm^{-1}$.

2. Resonance Raman Spectra

The resonance Raman spectrum of the adsorbed complex, in the region between 1000 cm^{-1} and 1700 cm^{-1}, shows seven vibrational bands resonant with the 452 nm MLCT transition. As shown in Figure 22, the band maxima are within experimental error of those found in aqueous solution.[48] There is, however, a significant change in the relative intensity of a specific vibration. It was not possible to measure absolute intensities since the conventional standard, SO_4^{2-}, being anionic, does not adsorb onto PVG, but Figure 22 illustrates the relative change. While the relative intensies of the other six bands are within experimental error in both media, that of the 1492 cm^{-1} band is significantly reduced. When the intensity of this band is compared to, for example, that of the 1609 cm^{-1}, a ratio of 4.4 is obtained for the complex in aqueous solution. However, the ratio reduces to 2.5 for that adsorbed on PVG. Resonance Raman spectra of the complex in several other solvents, e.g., D_2O, ethanol, and methanol, are within experimental error of the aqueous solution.

3. Emission Spectroscopy

a) Emission Spectrum and Excited State Lifetime

Figure 22. Resonance Raman spectrum of $Ru(bpy)_3^{2+}$ a) in aqueous solution and b) adsorbed onto PVG. The positions of the seven bands are within experimental error in both media. However, the relative intensities of the bands are significantly different, particularly that of the most intense band at 1492 cm^{-1}.

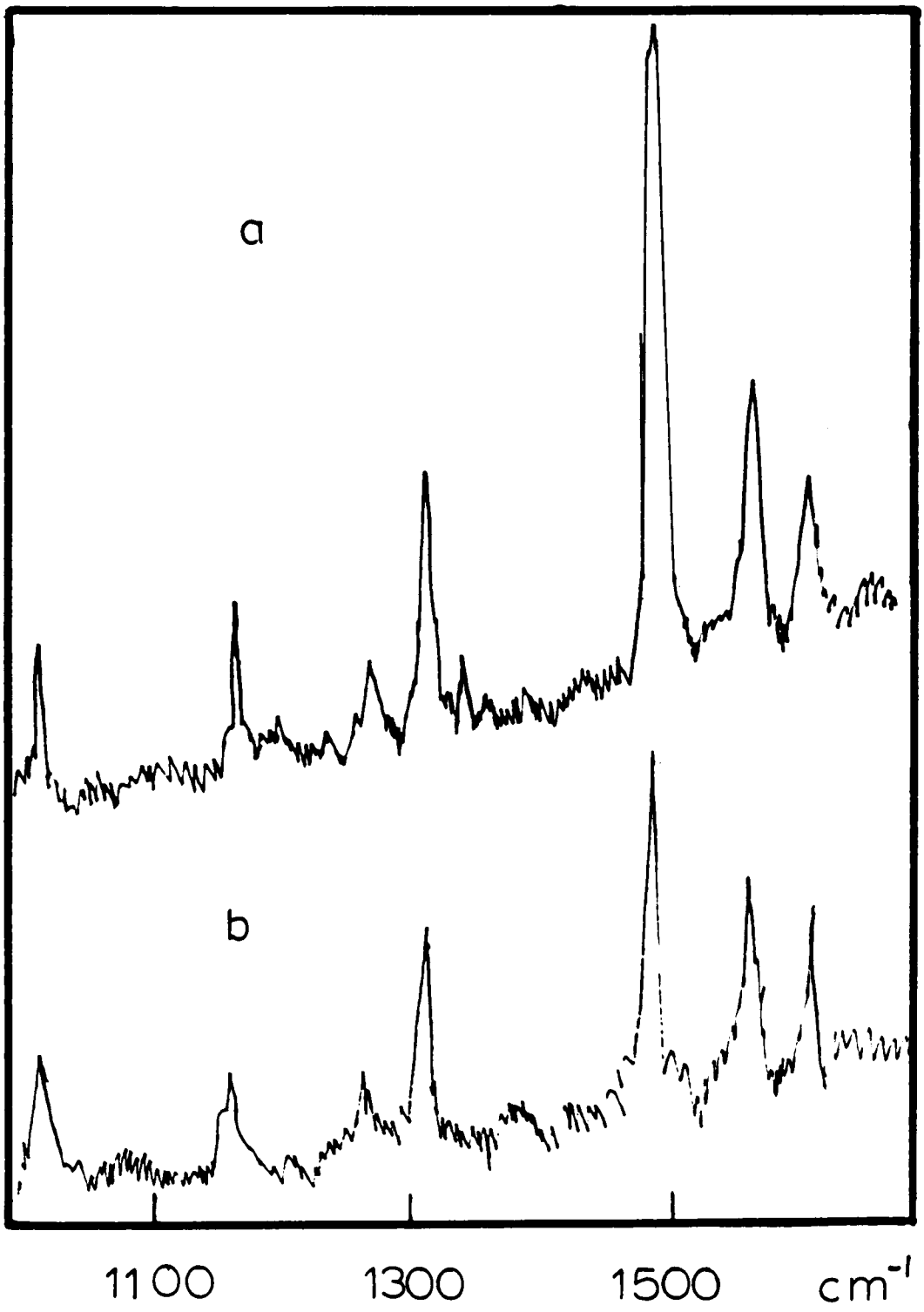
a
b
1100
1300
1500
cm⁻¹

When excited with low intensity light from conventional sources such as arc lamps, $Ru(bpy)_3^{2+}$ adsorbed on PVG shows an emission spectrum with a maximum at 610 nm similar to that obtained with aqueous solution (Figure 22). However, a clearly visible shoulder at ca.660 nm appears in the spectrum of the adsorbed complex, which is less pronounced in the solution spectrum. The excited state lifetime tau, defined as the time required for the population of the excited state to decrease to 1/e of its maximum value (emission intensity immediately following excitation), is measured by monitoring the emission intensity as a function of time. In deaerated water, the $Ru(bpy)_3^{2+}$ emission decays exponentially with a lifetime of 580 ns (Figure 24 A). When adsorbed onto PVG, however, the emission decay curve measured in vacuum is not strictly single-exponential. An initial fast decay (within ca. 200 ns after excitation pulse) is followed by a relatively slow, exponential one with a lifetime of ca. 780 ns(Figure 24 B) . Since this was not observed in the aqueous solution, several possible causes of this non-exponential component may have been involved. First, it could be the result of concentration quenching, due to possible non-uniform distribution of the complex. This is, however, inconsistent with the emission quantum yield measurements which shows higher emission quantum yield for the adsorbed complex than for aqueous solution (see below). Furthermore, in a concentration quenching process, the relative intensity of the fast component will increase with increasing concentration. The intensity of the observed non-exponential

Figure 24. Emission decay of $Ru(bpy)_3^{2+}$ a) inaqueous solution and b) adsorbed onto PVG. The small non-exponential component in the PVG sample is due to scattered excitation light.

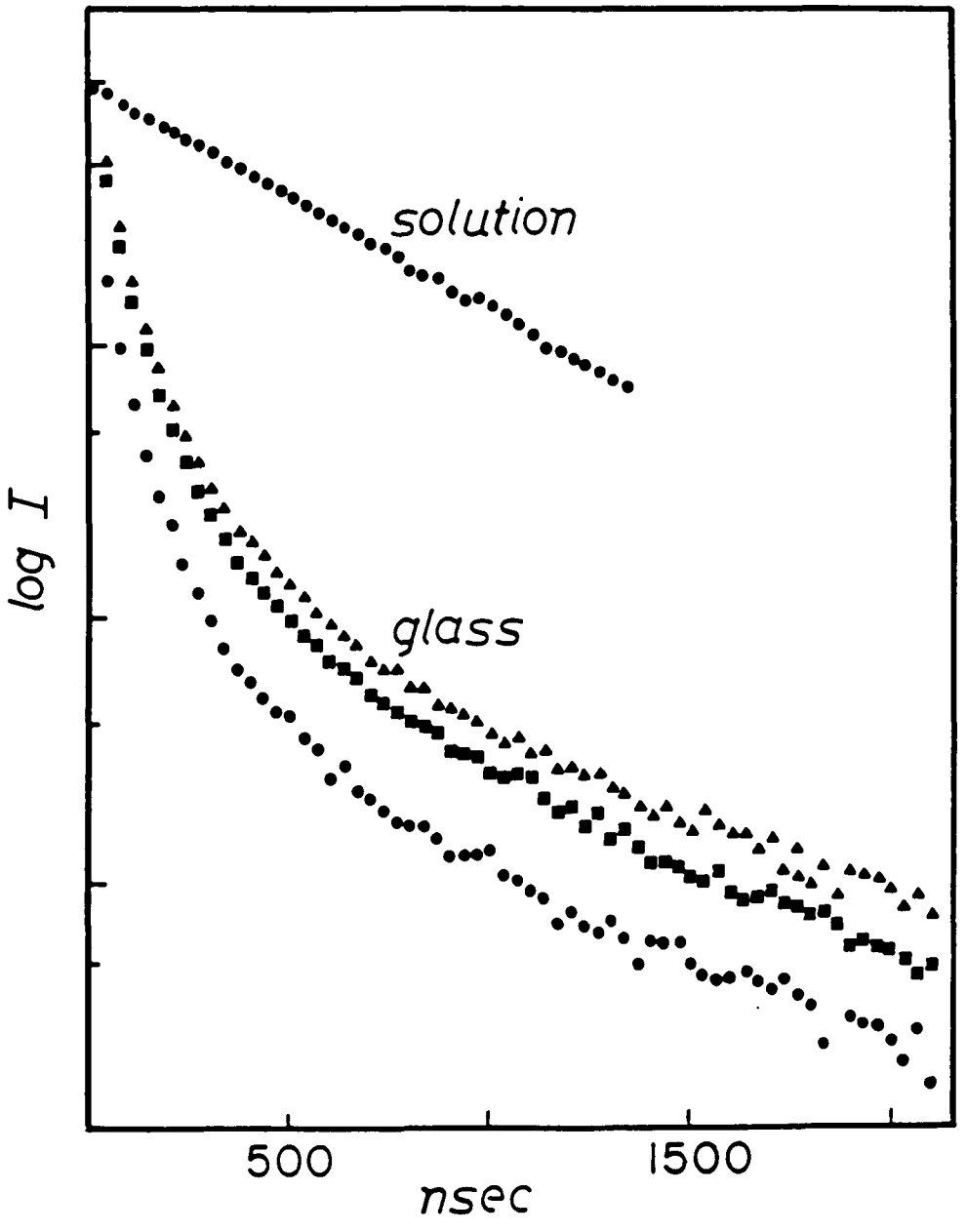
solution
glass
log I
500
1500
nsec

component, however, is independent of the impregnation level of $Ru(bpy)_3^{2+}$ on PVG. Thus, the possibility of concentration quenching under these experimental conditions can be ruled out.

Another possible source of the non-exponential component is the tail of the excitation pulse. The duration of the pulse, ca.5 ns, is considerably shorter than the observed fast component. However, oscillascopic traces showed that, compared to the emission, the excitation pulse was almost infinitely more intense. Consequently, even at times far longer than the excitation pulse duration, the residual intensity of the excitation pulse could still be comparable to that of the emission. Since light scattering from the glass is much stronger than from water, more of the excitation light would reach the detector from the glass than from water solution. Indeed, scattered light was detected with a piece of unimpregnated PVG, which showed a decay within ca. 400 ns after excitation. Attempts to eliminate the scattering by using more filters (red-transparent),however, were not very succesful. The use of a monochromator in front of the detecting photomultiplier tube, on the other hand, reduces the emission intensity so much that reliable measurements could not be obtained.

To minimize the inteference of the fast component, therefore, all the emission lifetime measurements were made with a relatively long delay time, ca. 400 ns, i.e., only the

emission intensities 400 ns after excitation was measured and the emission lifetime was calculated using the intensity at t = 400 ns as the initial intensity. The lifetime thus obtained for the adsorbed complex is 780 $\pm$ 40 ns when measured in vacuum, and 490 $\pm$ 40 ns, when the sample was saturated with air, the decrease being the result of emission quenching by oxygen. The former value falls between the value for deaerated water, 580 ns, and acetonitrile, 860 ns.[11]

Despite the similarities in emission spectrum and lifetime of the adsorbed complex and that in fluid solutions, the emission quantum yield of $Ru(bpy)_3^{2+}$ in these two media differ significantly. The quantum yield of a luminescence is defined as the fraction of molecules that emit after direct excitation by light. Since a determination of absolute quantum yield is difficult, a relative measurement is often used where the emission intensity of the compound of interest is compared to a luminescent compound with known emission quantum yield.[169] This procedure requires a) the sample and the standard have the same absorbance at the excitation wavelength, b) the emission spectra of the sample and the standard are similar in shape, and c) since only a fraction of the emitted light can reach the detector in actual measurements, the recorded intensity is sensitive to the sample position in the spectrometer. Therefore, in the relative measurements the geometry and position of the sample should be arranged so that the detector "sees" the same emitting area in both. The standard used in these

measurements is aqueous solution of $Ru(bpy)_3^{2+}$, and the first two conditions, therefore, are easily met. To satisfy the geometry requirement, theoptical-dense method wasused in which emission intensities from the front face of the PVG samples are compared with those from a 1 mm cell containing deaerated aqueous solution of the complex. The optical density (absorbance) of the solution at the excitation wavelength, 450 nm, is adjusted to equal that of the PVG sample, and the 1 mm cell containing the solution is placed in the larger rectangular cell at the same positions as the PVG sample. The absorbance of the samples and the standard solutions at 450 nm were varied from 0.37 to 49. As shown in Figure 25, the emission intensity from the PVG sample parallels that from the solution except at the highest optical density, where there is a decline of ca. 30 % in the intensity from the PVG sample. The reduction occurs at close to monolayer coverage and, since the excitation intensity is low, is attributed to self-quenching(or concentration quenching), rather than excited state annihilation. The emission quantum yield for the adsorbed complex, fi, is calculated according to the following equation[169]

$$fi = fi_r(K_r/K_x)(I_x/I_r)(n_x^2/n_r^2) \quad (19)$$

where the subscripts x and r denote the adsorbed complex and the aqueous reference solution, respectively. I is the measured intensity and n, the refractive index, is 1.5 for PVG and 1.33 for water. The factor K_x/K_r is the wavelength dependence factor and is taken as 1 since the emission

Figure 25. Emission quantum yield of $Ru(bpy)_3^{2+}$ adsorbed onto PVG, measured relative to that of aqueous solution(see text).

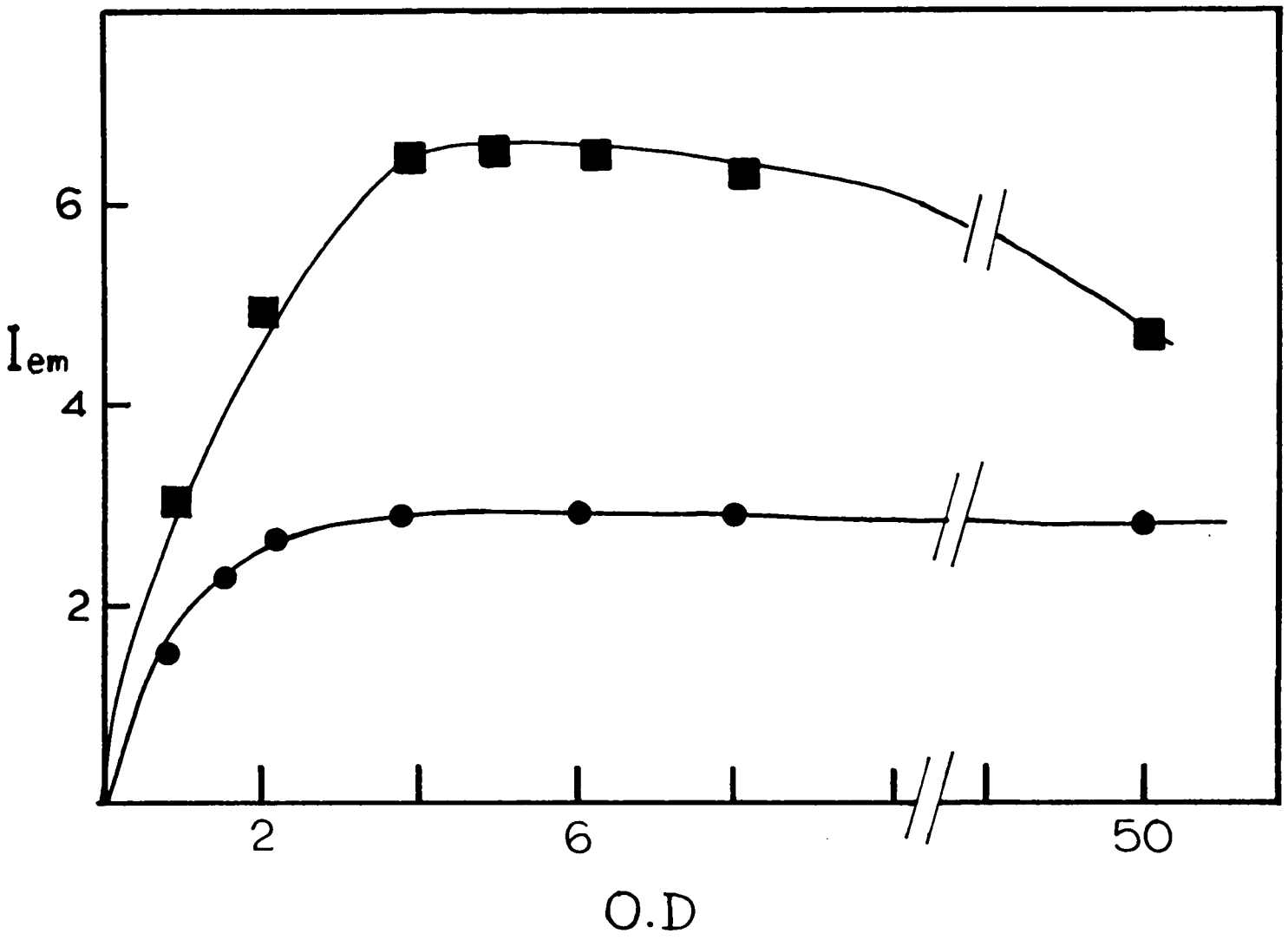
6
4
2
I_{em}
2
6
50
O.D

spectra are similar in shape in the two media. At less than monolayer coverage the calculated values of fi_x, as summarized in Table 5, are independent of the amount of complex adsorbed and ca. 3 times that in aqueous solution.

b) Polarization of Emission on PVG

In the crystalline form, $Ru(bpy)_3^{2+}$ shows polarized absorption and emission.[47,162] Emission polarization is also found with the complex in a frozen matrix.[45,46] Although the molecules are randomly oriented in a frozen matrix, excitation with linearly polarized light can selectively excite the molecules that have dipolar axes parallel to the incident polarization vector. The subsequent emission of these molecules will be preferentially polarized in the same direction as the original excitation. The relative polarization ratio P is defined by[45]

$$P = (I - I)/ (I + I) \qquad (20)$$

where the subscripts and denote emission intensities parallel and perpendicular to the incident polarization, respectively. Experimentally, eq. is modified to account for the polarization preference of the gratings in the spectrofluorometer:[45]

$$P = [I - I (T)]/[I + I (T)] \qquad (21)$$

where T is the instrumental factor.

Polarization of the emission from the adsorbed $Ru(bpy)_3^{2+}$

TABLE 5

Emission Quantum Yields for $RU(bpy)_3^{2+}$

Adsorbed Onto PV6

Moles Adsorbed $\frac{gm}{x\ 10^6}$	a. A_{450}	b. Φ_{em}
0.75	0.37	0.11 ± 0.01
2.0	1.00	0.12 ± 0.02
4.6	1.70	0.12 ± 0.01
10	3.50	0.12 ± 0.01
12	4.20	0.13 ± 0.02
140	49	0.09 ± 0.01

a. Absorbance of $Ru(bpy)_3^{2+}$ads at 450 nm.

b. Samples excited at 450 nm and emission monitored at 610 nm. Computed via equation 3 taking Φ_{em} for $Ru(bpy)_3^{2+}$ in aqueous solution as 0.042 ± 0.002.

on PVG was measured at room temperature, 22 ± 1°C, and the values of P obtained for various excitation wavelengths are listed in Table 6. The measurements were made with samples containing 1 x 10^{-7} - 1 x 10^{-5} moles $Ru(bpy)_3^{2+}$/g . No detectable concentration dependence of P was found within this concentration range.The maximum polarization , observed with 465 nm excitation, 0.16 + 0.01, is very close to that obtained in frozen glass at 77 K, 0.20 + 0.02.[45] In contrast, polarization of $Ru(bpy)_3^{2+}$ emission in the relatively high viscosity medium glycerol (η = 1430 cP at 20 C), is considerably lower, P = 0.015 at room temperature under similar experimental conditions. For comparison , Table 6 also lists the values of glycerol and low temperature EPA glass.

The temperature dependence of the emission polarization of the adsorbed complex was examined between the temperatures 5°C and 90°C, as well as that at 77 K, and the results are shown in Figure 26. Over this temperature range, no significant change in emission polarization of the adsorbed complex was found. By contrast, polarization of the complex dissolved in glycerol is essentially totally lost when the temperature is increased from 20°C to 40°C.

c) Temperature Dependence of Emission Quantum Yield

The emission quantum yield of $Ru(bpy)_3^{2+}$ adsorbed on PVG was measured as a function of temperature over the range 5°C to 90°C. The measured ϕ values are listed in Table 7, and a

TABLE 6

Emission Polarization Ratios for $Ru(bpy)_3^{2+}$ Adsorbed Onto PVG

Medium	Excitation Wavelength nm		
	400	465	510
77°ethanol[a]	0.08	0.20	0.10
PVG[b]	0.10±0.01	0.16±0.02	0.10±0.01

a. Reference .

b. Samples contain 2.0×10^{-6} or 1.0×10^{-5} moles of $Ru(bpy)_3^{2+}$/gm, at room temperature, 22±1°C, in vacuo.

Figure 26. Temperature independence of emission polarization of $Ru(bpy)_3^{2+}$ adsorbed onto PVG.

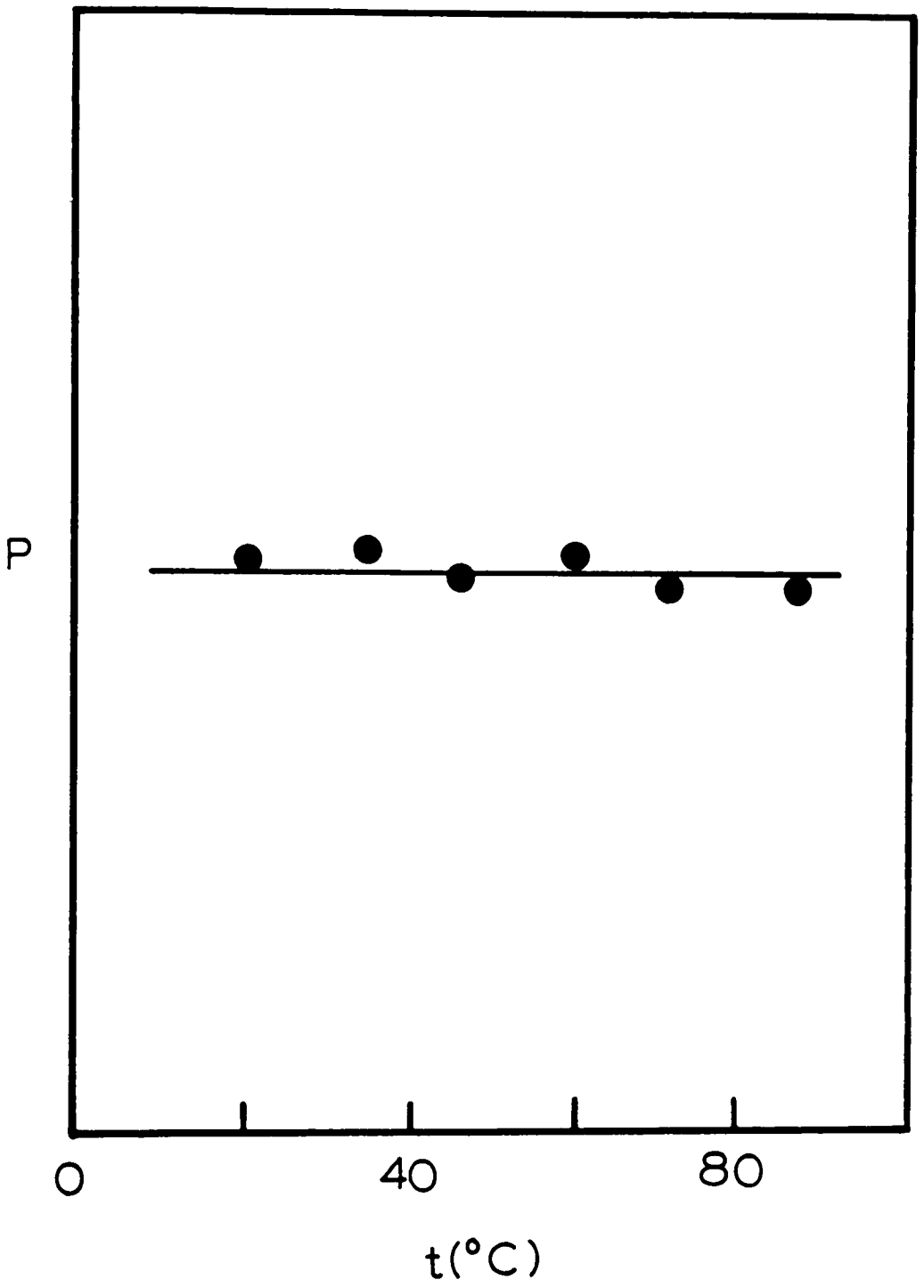
P
0
40
80
t(°C)

plot of ln(O) vs. 1/T is shown in Fig.ure 27. For comparison, similar measurements were carried out with deaered aqueous solution and the results, which are in excellent agreement with the literature values, are shown in Table 7 and Figure 27. In both media, the Ln(O) vs.1/T curves in Figure 27 are non-linear, indicating that the data are not fit by a simple Arrhenius type equation. According to the model proposed by Crosby and later modified by Van Houton and Watts, the temperature dependence of $Ru(bpy)_3^{2+}$ emission quantum yield O in fluid solutions can be described by the equation

$$fi = k_r tau(T) = k_r/(k_r + k_{nr} + k_o exp[- E/kT]) \qquad (22)$$

where k_r is the radiative rate constant, k_{nr} is the temperature-independent radiationless rate constant, and k_o is the pre-exponential constant of the temperature dependent term which represents all processes that occur through the dd state (see Discussion). Direct measurements of the excited state lifetime as a function of temperature were also carried out, but the experimental error in these measurements were so large that at T > 45 C, reliable data could not be obtained.

It is interesting to note from Figure 27 that the emission quantum yield of the adsorbed $Ru(bpy)_3^{2+}$ is approximately twice as sensitive to temperature as that of the aqueous solution.[42] When the temperature is increased from 5 C to 90 C, fi_{PVG} decreases by a factor of 12, whereas fi_{water} decreases by a factor of only 6. Consequently, the difference in emission quantum yields in these two media is

TABLE 7

Temperature Dependence of Emission Quantum Yield of $Ru(bpy)_3^{2+}$ Adsorbed onto PVG

t (^{o}C)	10^3x 1/T(K)	I_{em}(relative)
7	3.57	93
13	3.50	80
20	3.41	71
25	3.36	64
33	3.27	49
40	3.19	41
47	3.13	34
55	3.05	27
62	2.99	20
70	2.92	16
76	2.87	13
83	2.81	11
90	2.75	8

Figure 27. Temperature dependence of emission quantum yield of $Ru(bpy)_3^{2+}$ in water(lower curve) and adsorbed onto PVG (upper curve). Note that the adsorbed complex is more sensitive to temperature than the solution.

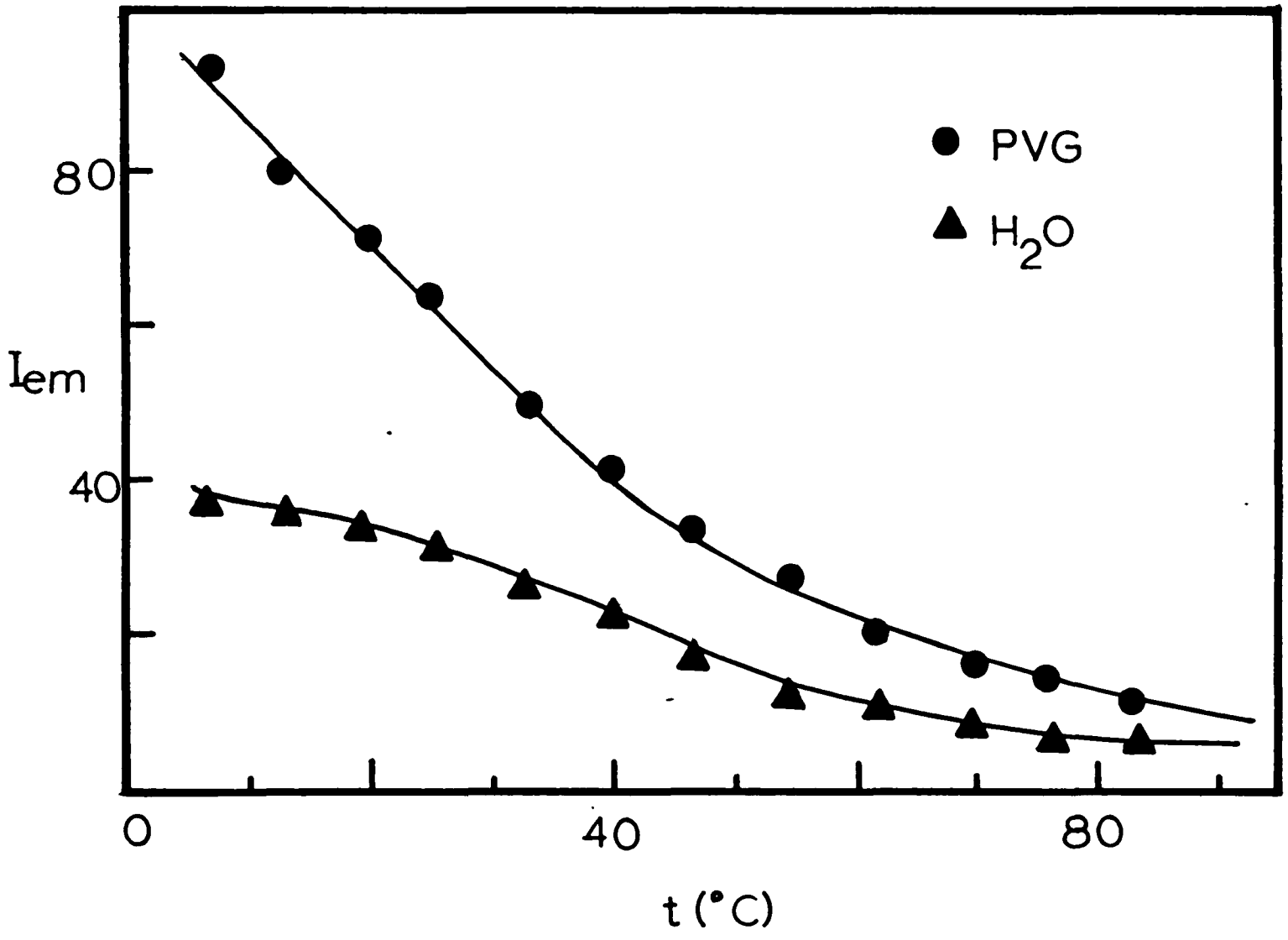
80
40
Iem
0
40
80
t (°C)
PVG
H2O

smaller at higher temperatures than at lower temperatures.

4. Biphotonic Emission Excited of $Ru(bpy)_3^{2+}$ Adsorbed on PVG

In contrast to emission spectrum of $Ru(bpy)_3^{2+}$ in aqueous solution, which is independent of excitation intensity, that of the adsorbed complex is dependent of excitation intensity. Under low intensity excitation, the emission of the adsorbed $Ru(bpy)_3^{2+}$ closely resembles that in fluid solution, as described in the preceding section. The maximum of the emission band occurs at 610 nm, and the excited state decay is exponential with a lifetime of 780 + 40 ns. High intensity excitation with a YAG laser (355 nm, 100 mJ, 10 ns pulses), however, causes a marked difference in emission spectrum and decay pattern. As shown in Figure 28, the emission spectrum of $Ru(bpy)_3^{2+}$ adsorbed on PVG in vacuo(10^{-4} torr) under these conditions exhibits a maximum at 510 nm and a shoulder at 610 nm. Control experiments with blank pieces of PVG under similar conditions indicate that this anomalous emission spectrum is not due to emission from the glass itself or impurities. Furthermore, visible absorption spectra recorded before and after the laser excitation establish no net chemical changes in the adsorbed complex. The emission spectrum, therefore, appears to be from the adsorbed complex rather than some possible new species formed during the laser pulse.

Concurrent with the new emission spectrum, the excited

Figure 28. Normalized emission spectra of $Ru(bpy)_3^{2+}$ adsorbed onto PVG with 355 nm laser pulses(●) and with a filtered 100 W Hg lamp(▲). Actual emission intensity of latter is 10% of that with laser excitation.

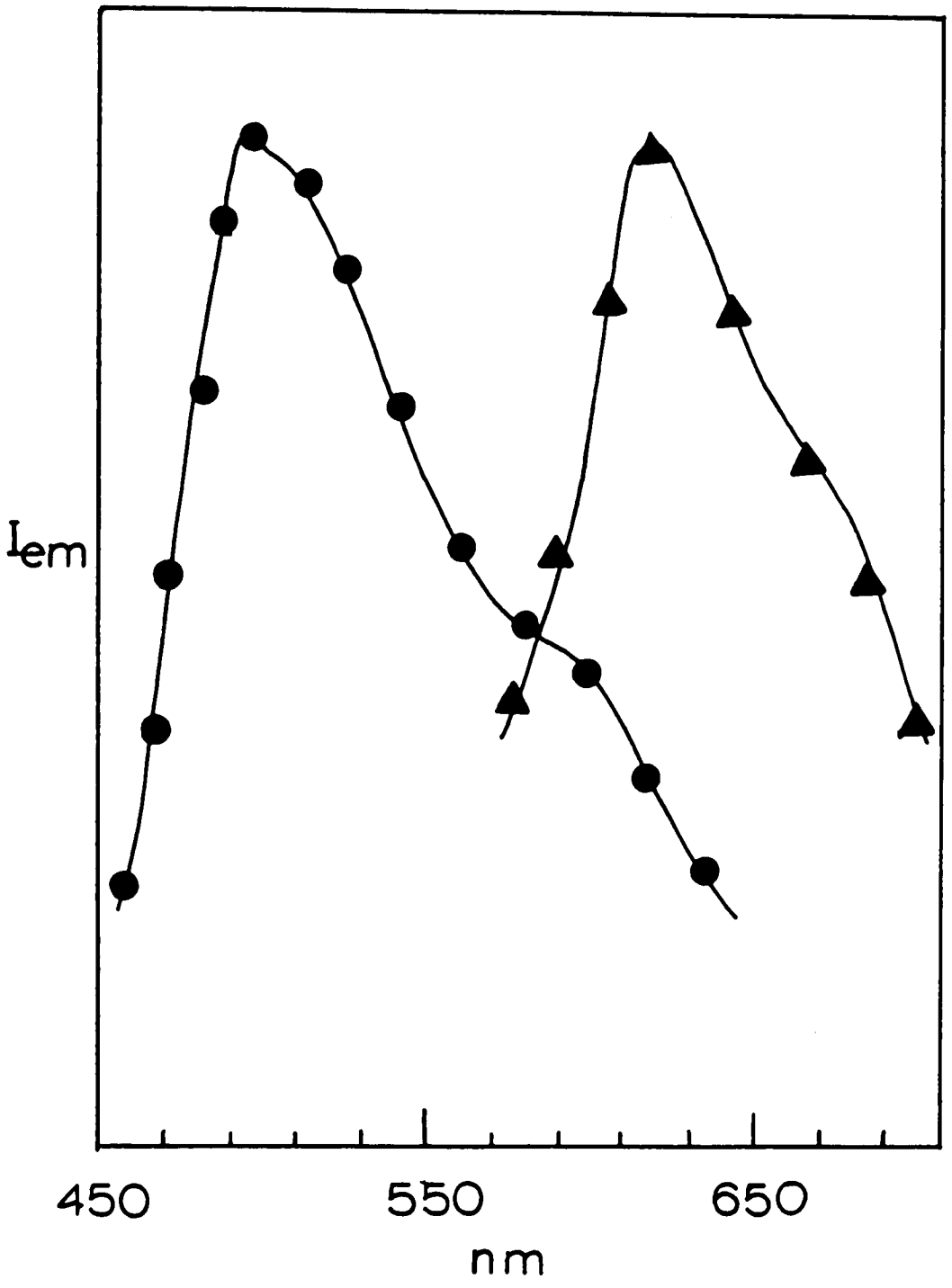
I_{em}
450
550
650
nm

state decay kinetics are also altered. The decay curve, monitored at 610 nm on a Tektronics 7834 oscilliscope, is shown in Figure 29. Unlike the first order decay observed with low intensity excitation, this decay is non-exponential and can be resolved into two first order components. The longer lived component is exponential and has a lifetime of ca. 800 ns, while the other decay within ca. 50 ns(Figure 30). Changing the monitoring wavelengh from 610 nm to 510 nm, however, leads to the disappearence of the slow decay and only the 50 ns decay is observed. These data establish that the 610 nm emission is associated with the slow decay whereas the 510 nm band is associated with the faster decay.

The dependence of the 510 nm emission on the excitation energy was determined. In Figure 31, log I_{em} is plotted against log I_{exc}. The slope of ca. 2 obtained from this plot suggests that the rapid 50 ns decay is a consequence of biphotonic excitation.

C. Photo-redox Reactions

1. Emission Quenching of $Ru(bpy)_3^{2+}$ on PVG

In fluid solutions, emission of $Ru(bpy)_3^{2+}$ is quenched by Fe^{3+}, Cu^{2+}, MV^{2+}, and Cr^{3+}. Previous experiments indicate that, in fluid solution, Fe^{3+}, Cu^{2+}, and MV^{2+} quench the excited state of $Ru(bpy)_3^{2+}$ by electron transfer whereas Cr^{3+} by energy transfer.

$$*Ru(bpy)_3^{2+} + Fe^{3+} \text{------>} Ru(bpy)_3^{3+} + Fe^{2+} \qquad (23)$$

Figure 29. Emissiobn decay excited with high intensity laser. Decay monitored at 610 nm (●) and the resolved Fast (●••) and slow components (■).

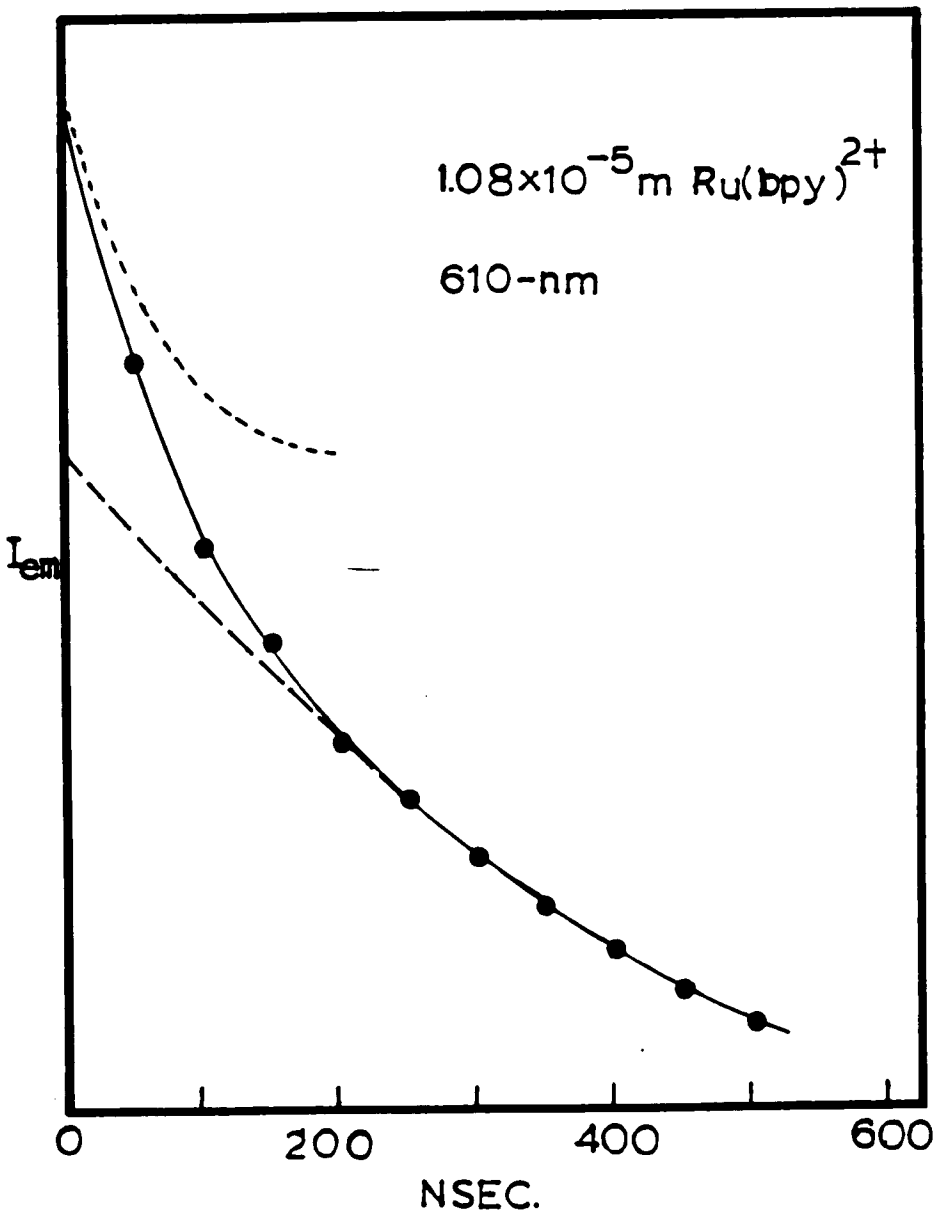
1.08×10⁻⁵m Ru(bpy)²⁺
610-nm
I_em
0
200
400
600
NSEC.

Figure 30 An oscilliscopic trace of the non-exponential emission from $Ru(bpy)_3^{2+}$ adsorbed onto PVG.

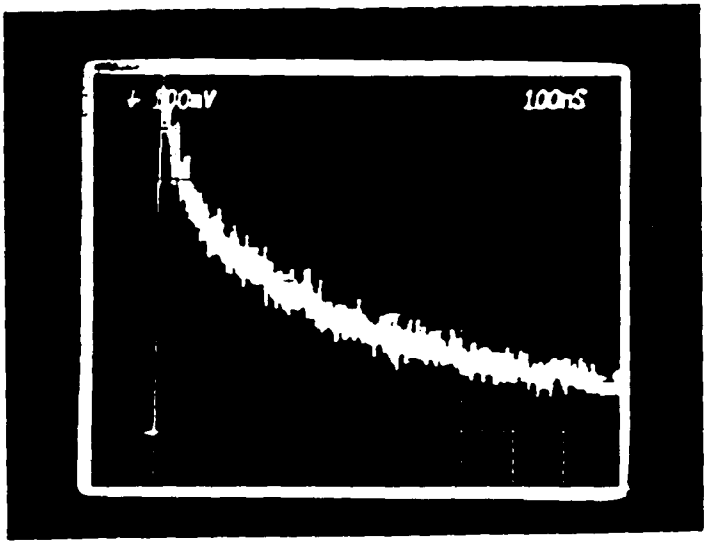
100mV
100nS

Figure 31. Dependence of initial emission intensity at 610 nm, I_0, on the relative laser excitation power, I_{ex}.

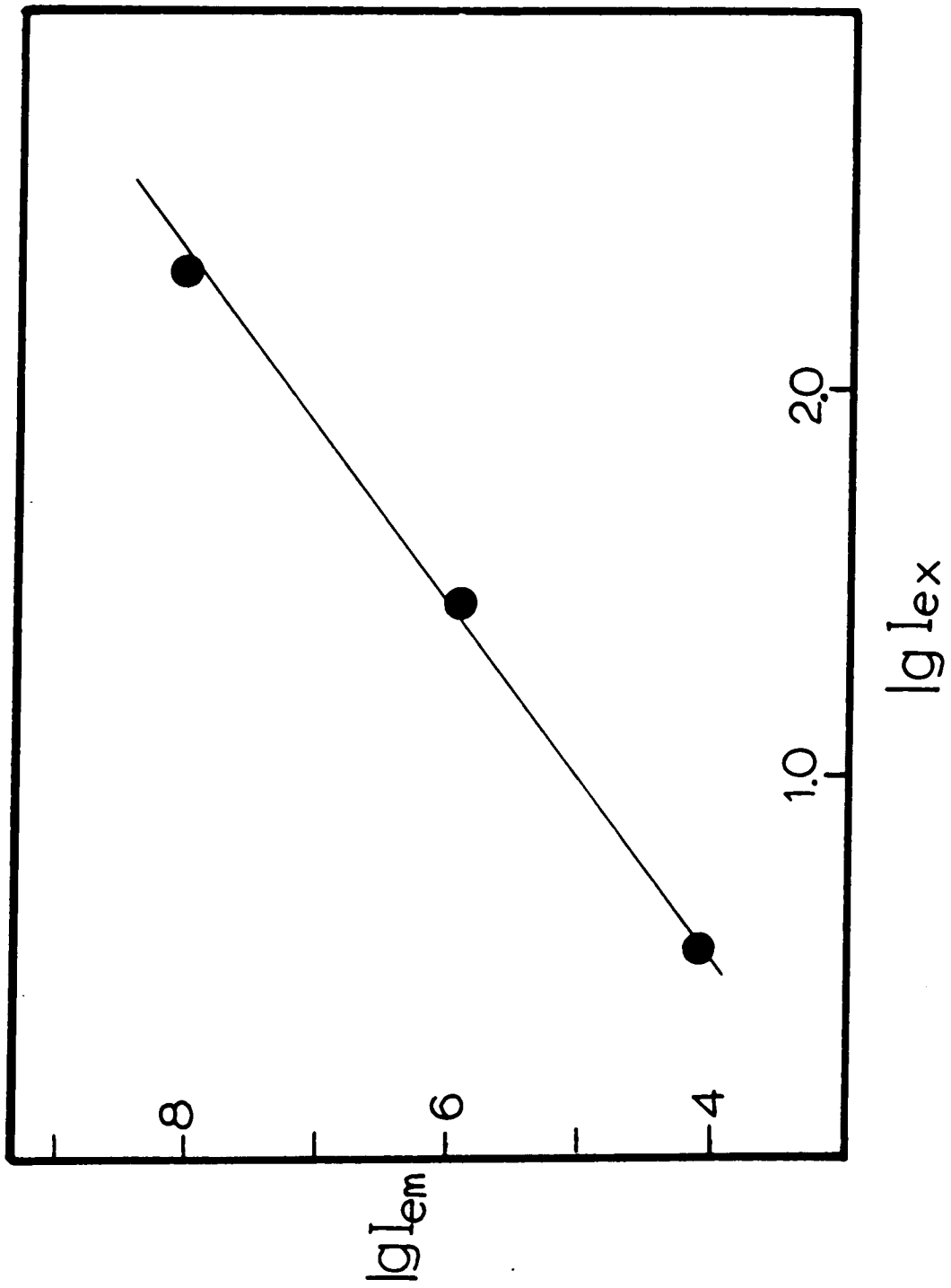
8
6
4
lg Iem
1.0
2.0
lg Iex

$$*Ru(bpy)_3^{2+} + Cu^{2+} \text{ ------> } Ru(bpy)_3^{3+} + Cu^{+} \quad (24)$$

$$*Ru(bpy)_3^{2+} + MV^{2+} \text{ ------> } Ru(bpy)_3^{3+} + MV^{+} \quad (25)$$

$$*Ru(bpy)_3^{2+} + Cr^{3+} \text{ ------> } Ru(bpy)_3^{2+} + *Cr^{3+} \quad (26)$$

a) Quenching by Cr^{3+}

The Cr^{3+} ion is adsorbed onto PVG from aqueous solution of $CrCl_3 6H_2O$. The rate of adsorption of the ion is unusually slow considering its charge and, as shown by grinding experiments, it penetrates only 0.1 mm into the glass. When coadsorbed with $Ru(bpy)_3^{2+}$, which penetrates ca. 0.4 mm into the bulk, the limited penetration depth of Cr^{3+} limits its access to the complex. A Stern-Volmer plot of the intensity and lifetime quenching is shown in Figure 32. In intensity quenching, where the ratio of the unquenched emission intensity to that of quenched, I_0/I, is plotted as a function of moles of Cr^{3+} adsorbed/g of PVG, an initial increase of I_0/I is followed by a region in which the ratio becomes independent of the amount of the quencher adsorbed. Apparently, this is caused by the limited adsorption area of the quencher ion. Increasing the quencher concentration beyond ca. 5×10^{-7} moles/g, as shown in the plot, has no effect on the emission intensity of $Ru(bpy)_3^{2+}$, since the Cr^{3+} ions adsorbed on the outermost surface can not diffuse into the interior where the Ru complex are adsorbed. The quenching rate constant, calculated from the initial region of the Stern-Volmer plot, is 2.2×10^6 $M^{-1}s^{-1}$. The ratio of t_0/t, the emission lifetime in the absence of the quencher to that in the presence of quencher, is nearly 1 on the Stern-

Figure 32. Stern-volmer plot of emission quenching of adsorbed $Ru(bpy)_3^{2+}$ by coadsorbed Cr^{3+}.

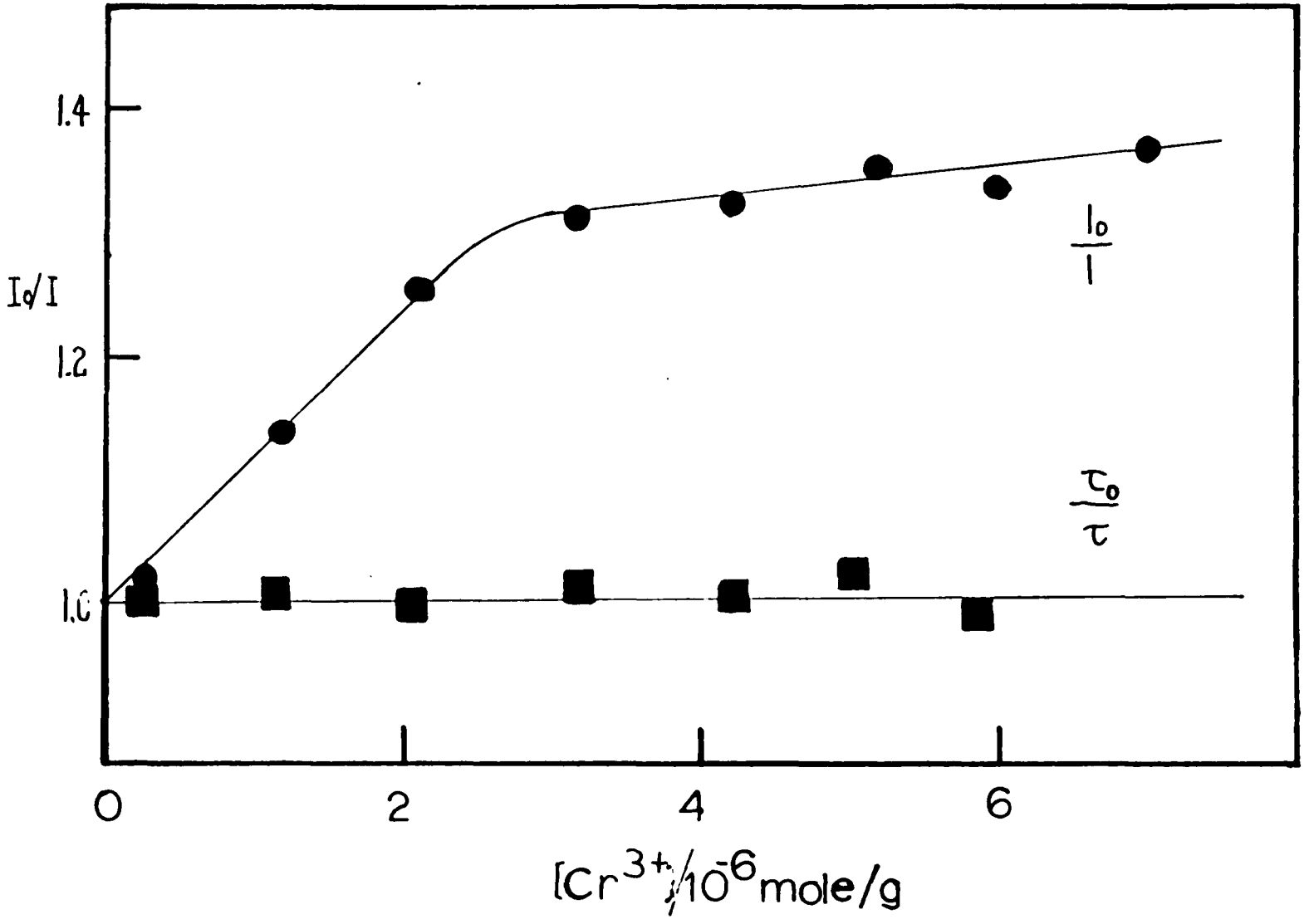
1.4
1.2
1.0
I_0/I
$\frac{I_0}{I}$
$\frac{\tau_0}{\tau}$
0
2
4
6
$[Cr^{3+}]/10^{-6}$ mole/g

Volmer plot (Figure 33). Consequently, quenching by Cr^{3+} on PVG is limited to a static mechanism.

b) Quenching by Cu^{2+}

Although Cu^{2+} is an efficient quencher of $*Ru(bpy)_3^{2+}$ in aqueous solution, $k_q = 1.0 \times 10^8$, no quecching occured below a certain level of impregnation when it was coadsorbed onto PVG with the complex. For example, when progressively larger amount of Cu^{2+} were adsorbed onto a piece of PVG containing 5×10^{-7} moles of $Ru(bpy)_3^{2+}$/g, the emission intensity, monitored at 610 nm, was independent of the Cu^{2+} concentration over the range 5×10^{-7} to 5×10^{-5} moles of Cu^{2+}/g. The Stern-Volmer plot for intensity quenching, shown in Figure 33, has a zero slope within this region. The result was unexpected because Cu^{2+} cation exchanges onto PVG and, since the surface covarege by $Ru(bpy)_3^{2+}$ in the 0.4 mm thick layer of the glass at the used impregnation level is $\leqslant$ 2 %, was expected to impregnate the same region of PVG. Yet, adsorption of 5×10^{-5} moles of Cu^{2+}/g , which corresponds to a surface coverage within the region impregnated with $Ru(bpy)_3^{2+}$ of $\geqslant$ 25 %, failed to result in detectable quenching. Similar results were also observed with MV^{2+}. Despite efficient quenching of $*Ru(bpy)_3^{2+}$ in fluid solution, k_q = ca. 10^9, the adsorbed MV^{2+} at concentrations up to 5×10^{-5} moles/g did not result in detectable emission quenching on PVG.

To determine whether the lack of quenching in the above

Figure 33. Stern-volmer plot of emission quenching of adsorbed $Ru(bpy)_3^{2+}$ by coadsorbed Cu^{2+}. The zero slope of the line indicates lack of quenching over the concentration range of 1 - 4 x 10^{-4} moles of Cu^{2+}/g.

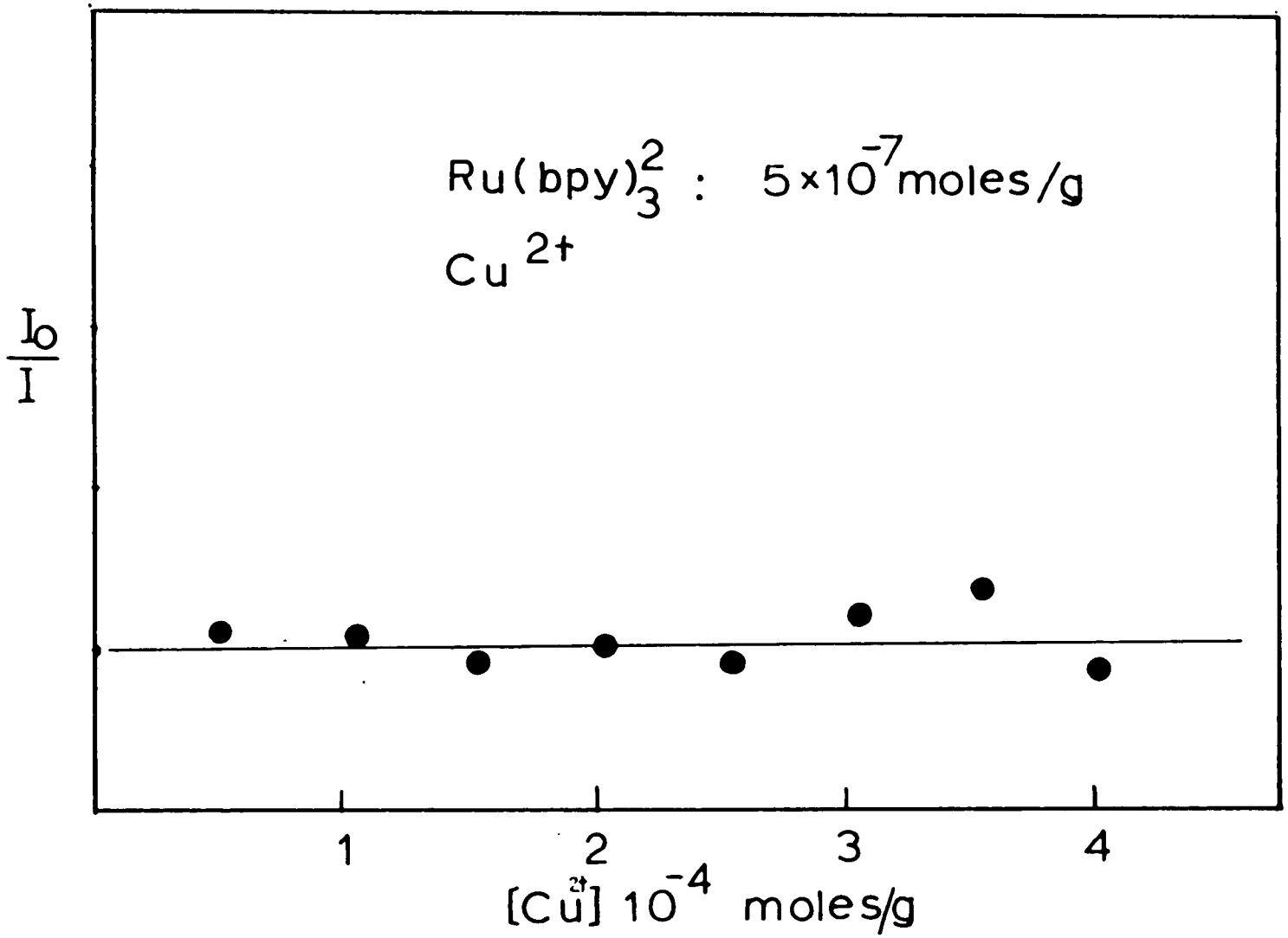
$Ru(bpy)_3^{2}$: 5×10^{-7} moles/g
Cu^{2+}
$\frac{I_0}{I}$
1
2
3
4
$[Cu^{2+}]\ 10^{-4}$ moles/g

experiments was due to changes in the redox properties of the reactants, PVG samples impregnated with $Ru(bpy)_3^{2+}$ were placed in water, and the emission intensities of the complex were measured as a function of the Cu^{2+} or MV^{2+} concentrations in the aqueous phase. As shown in Figures 34 and 35, the linear Stern-Volmer plots obtained in both cases indicate that the two compounds were capable of quenching the emission from the adsorbed complex. Also, MV^{2+} adsorbed on the glass can be reduced chemically by the reductant sodium dithionite, as demonstrated by the appearence of the blue color of the reduced ion, MV^{+}., when the sample was placed in a solution of the reductant. Thus, the absence of quenching does not appear to originate from chemical changes caused by adsorption of either the complex or the quenchers.

Since emission quenching presumes accessibility of the quencher ions to the complex, the absence of quenching found for these two molecules suggests their lack of access to the emitting complex on the PVG surface. This led to a re-examination of the distribution of these adsorbed ions. Indeed, a spectroscopic determination of the cross sectional distribution of Cu^{2+} and MV^{2+} on PVG shows that these ions preferentially adsorb in the interior of the bulk sample in the presence of $Ru(bpy)_3^{2+}$,which is exclusively adsorbed on the outer layer (see Section A, Ditribution of Ions). This partitioning of the adsorbates results in the physical separation of the donor and quencher on the PVG surface. Consequently, except at the interface of the two regions

Figure 34. Stern-volmer plot for quenching of $Ru(bpy)_3^{2+}$ emission in an interfacial systerm,in which the PVG sample impregnated with $Ru(bpy)_3^{2+}$ is placed in water and the quencher, MV^{2+}, is in the aqueous phase.

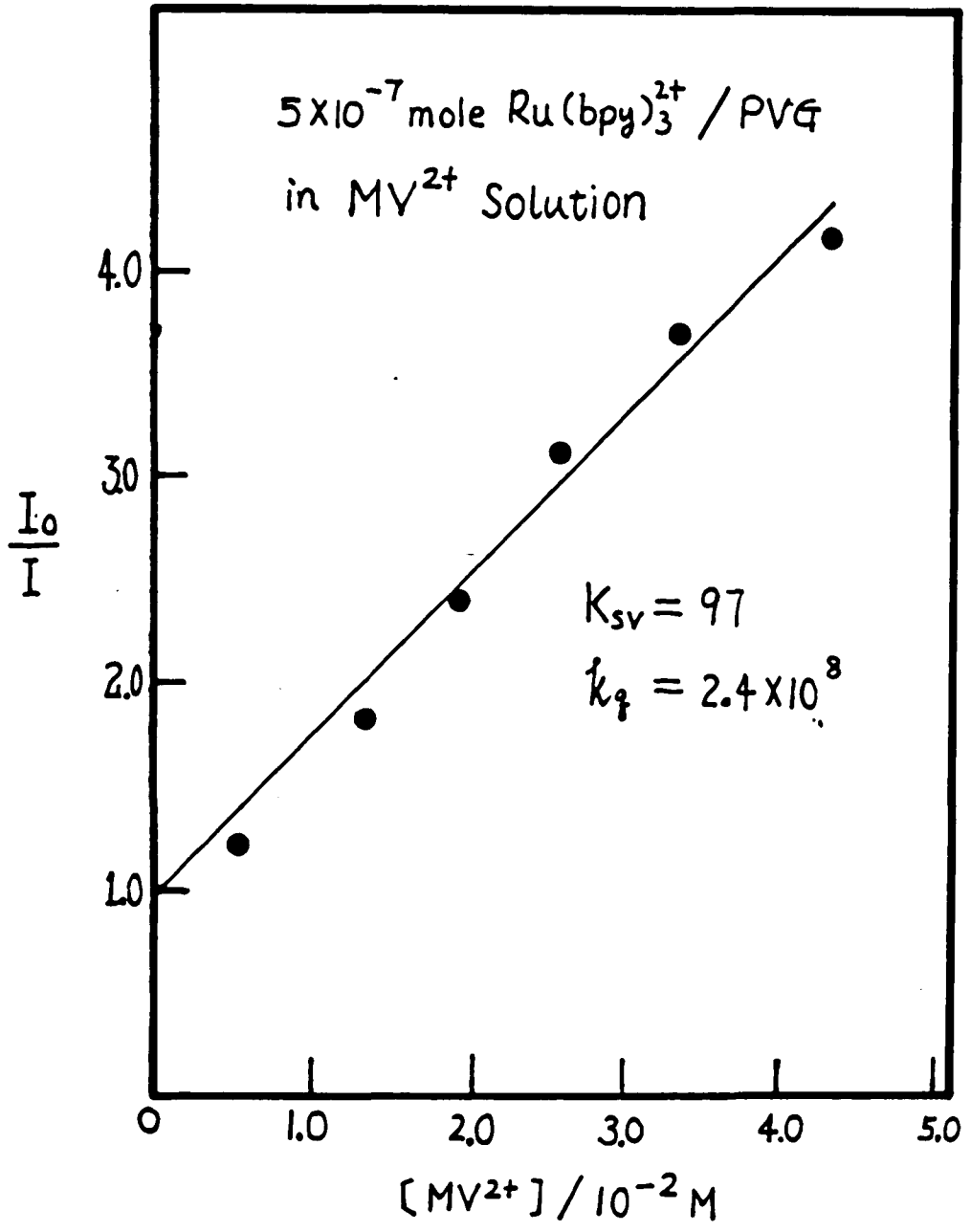
5×10^{-7} mole $Ru(bpy)_3^{2+}$ / PVG
in MV^{2+} Solution
$K_{sv} = 97$
$k_q = 2.4 \times 10^8$
$\frac{I_0}{I}$
4.0
3.0
2.0
1.0
0
1.0
2.0
3.0
4.0
5.0
$[MV^{2+}] / 10^{-2}$ M

Figure 35. Stern-Volmer plot of $Ru(bpy)_3^{2+}$ emission quenching in an interfacial system where the complex is adsorbed on PVG and the quencher, Cu^{2+} is in the aqueous phase.

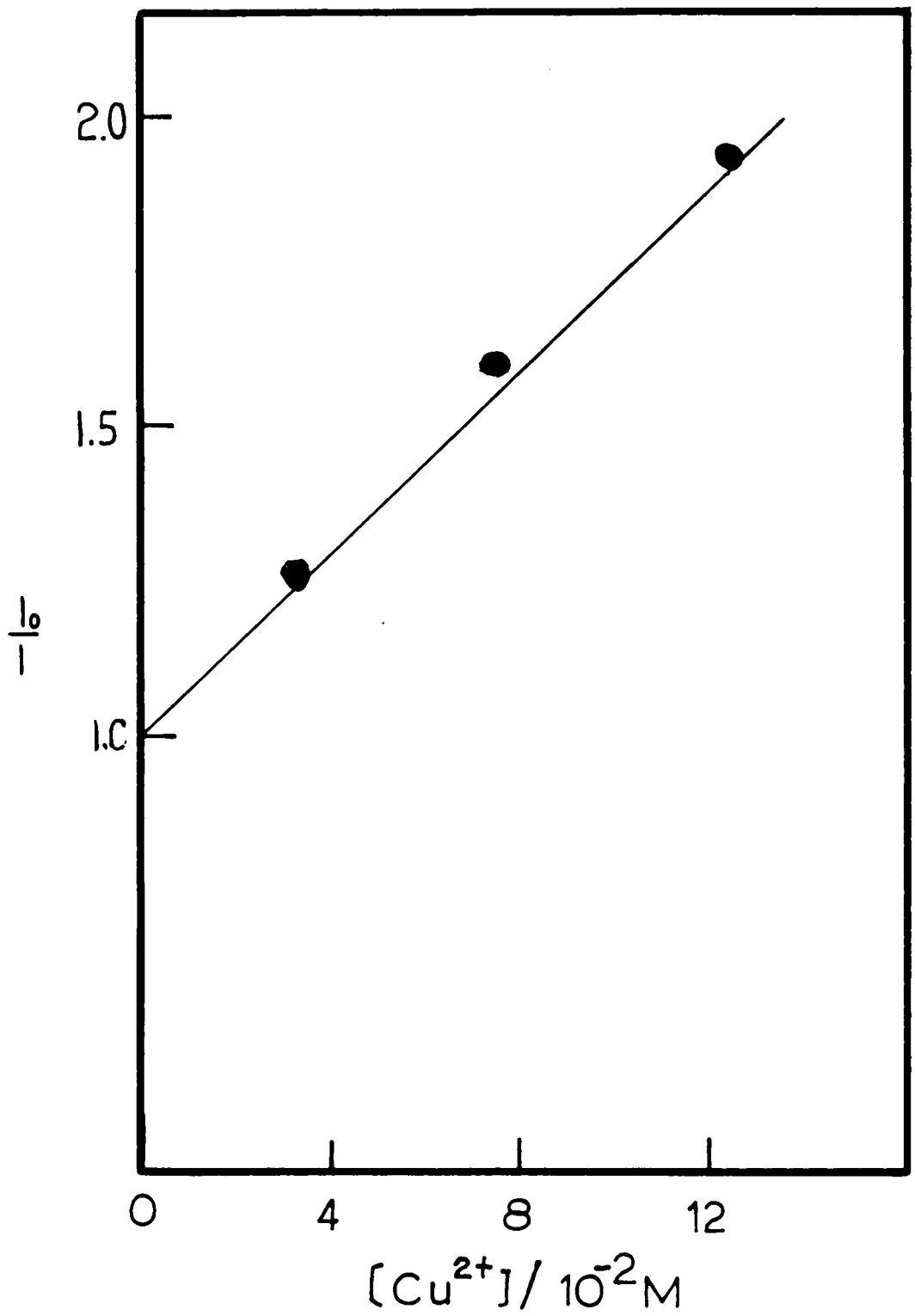
2.0
1.5
1.0
$\frac{I_0}{I}$
0
4
8
12
$[Cu^{2+}] / 10^{-2} M$

occupied by the adsorbates, quenching of $*Ru(bpy)_3^{2+}$ can not occur.

Since the $Ru(bpy)_3^{2+}$ concentration in the impregnated region is low (surface coverage $\leq$ 2 %), sufficiently high concentrations of quencher could lead to impregnation of the volumes of PVG impregnated with$Ru(bpy)_3^{2+}$. A "critical" concentration is achieved when > 7×10^{-5} moles of Cu^{2+}/g and $\geq 1.0 \times 10^{-4}$moles of MV^{2+}/g are adsorbed. At concentrations above each of these two values, emission quenching of the adsorbed $Ru(bpy)_3^{2+}$ by Cu^{2+} and MV^{2+} occurs. Shown in Figures 36 and 37 are the Stern-Volmer plots for the two quenchers at concentrations above their respective critical concentrations. The quenching rate constants, calculated from the slopes of the plots, are $(1.1 \pm 0.2) \times 10^7$ $M^{-1}s^{-1}$ for Cu^{2+}, and $(6.8 \pm 0.7) \times 10^6$ $M^{-1}s^{-1}$. The somewhat larger uncertainty for the Cu^{2+} data is due to the uncertainty in correction for copper absorption at 590 nm, where the emission was monitored (see Experimental Section).

c) Quenching by Fe^{3+}

Unlike Cu^{2+} and MV^{2+}, which partition into different regions of PVG, ferric ions adsorbed in the same regions as the Ru complex. No significant partitioning is detected. Consequently, the quenching behavior of Fe^{3+} more closely resembles that in aqueous solution., as shown by the linear Stern-Volmer plots for both intensity and lifetime quenching (Figure 38). However, unlike in solution, where the intensity

Figure 36. Stern-Volmer plot of $Ru(bpy)_3^{2+}$ emission quenching by coadsorbed MV^{2+} on the PVG surface.

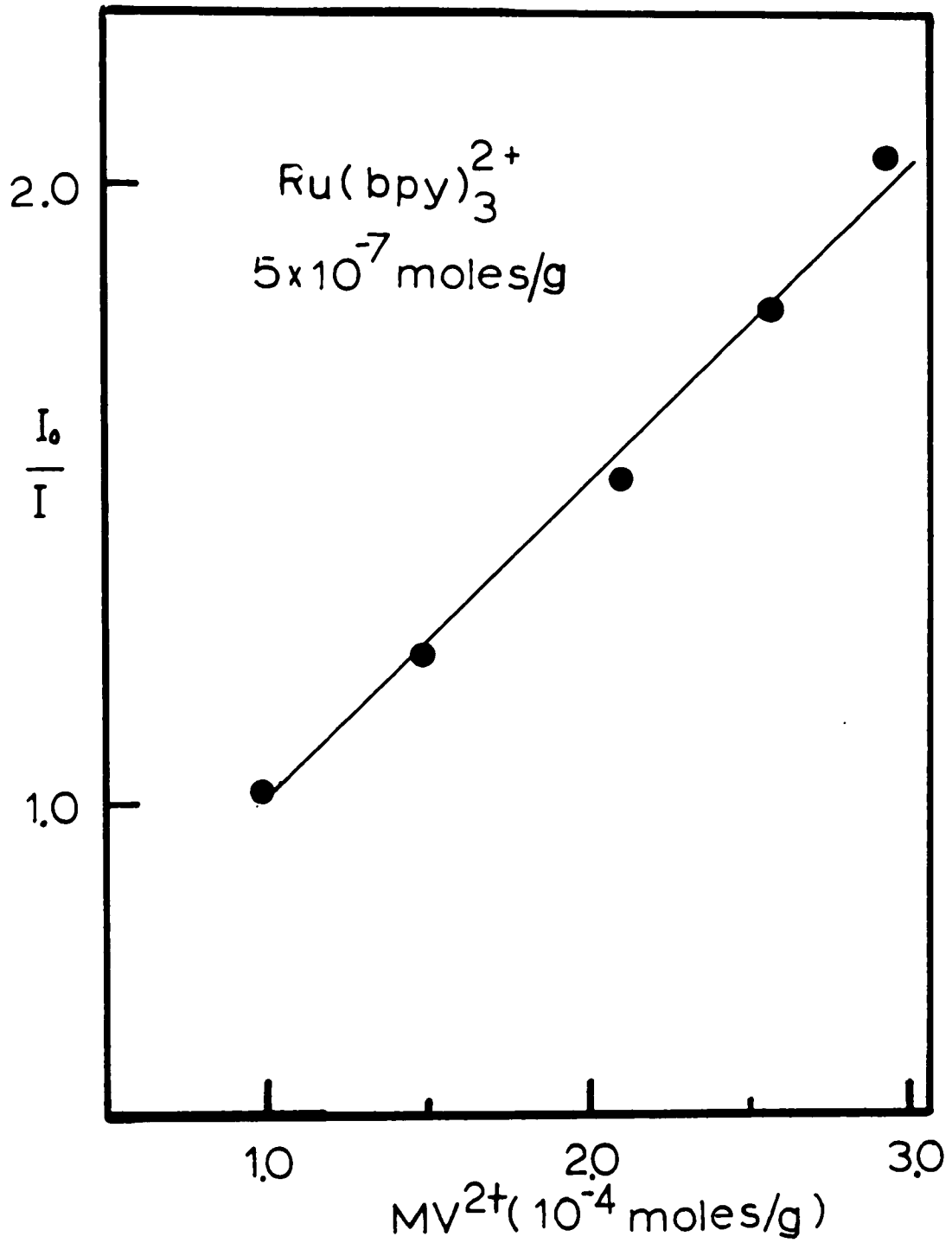
2.0
1.0
$Ru(bpy)_3^{2+}$
5×10^{-7} moles/g
$\frac{I_o}{I}$
1.0
2.0
3.0
MV^{2+} (10^{-4} moles/g)

Figure 37. Stern-Volmer plot of emission quenching of adsorbed $Ru(bpy)_3^{2+}$ by coadsorbed Cu^{2+} on PVG.

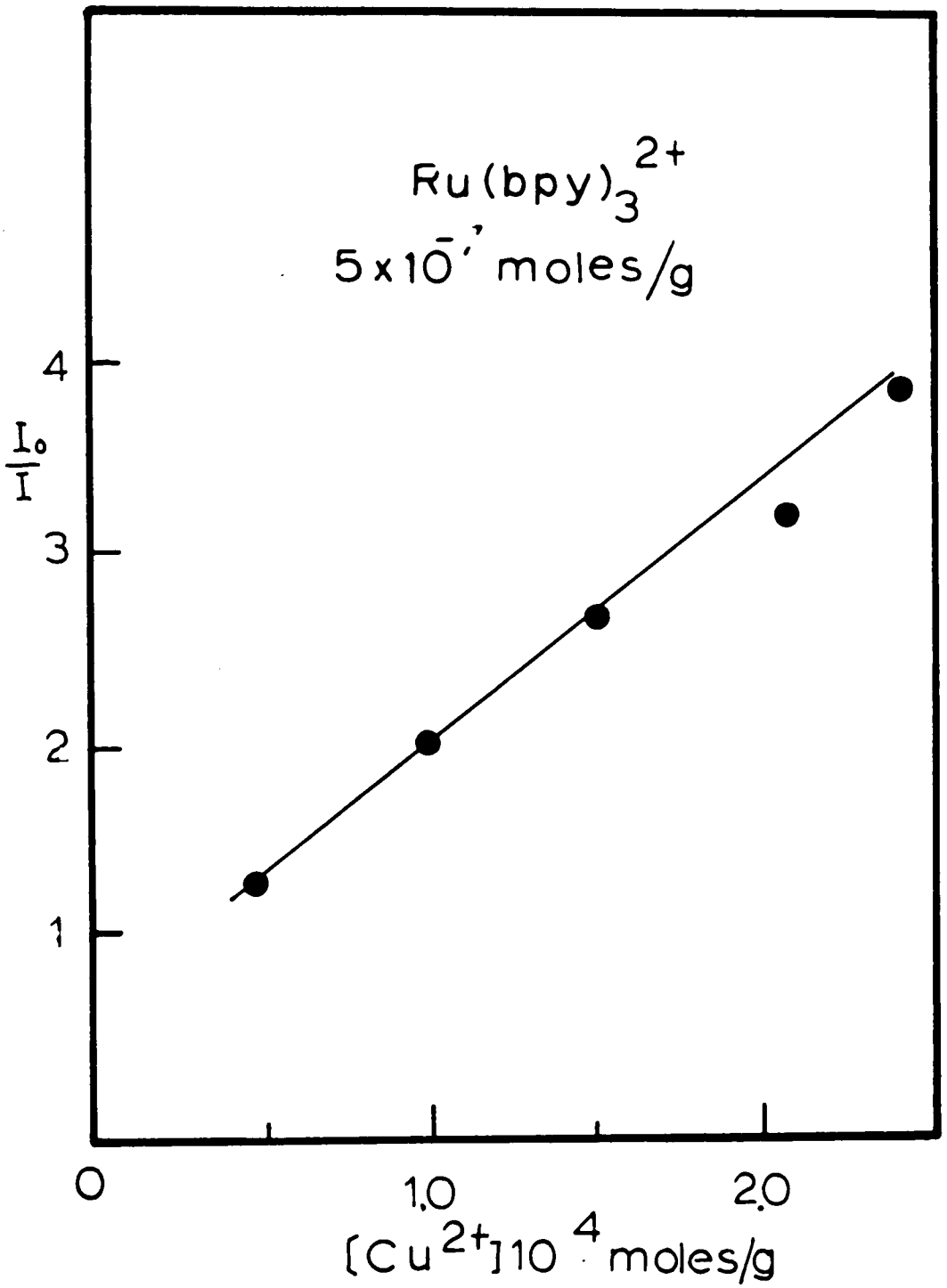
Ru(bpy)3 2+
5x10-7 moles/g
4
3
2
1
Io/I
0
1.0
2.0
[Cu2+]10 4 moles/g

Figure 38. Stern-Volmer plot for emission quenching of adsorbed $Ru(bpy)_3^{2+}$ by coadsorbed Fe^{3+}. Note the difference between intensity and lifetime quenching.

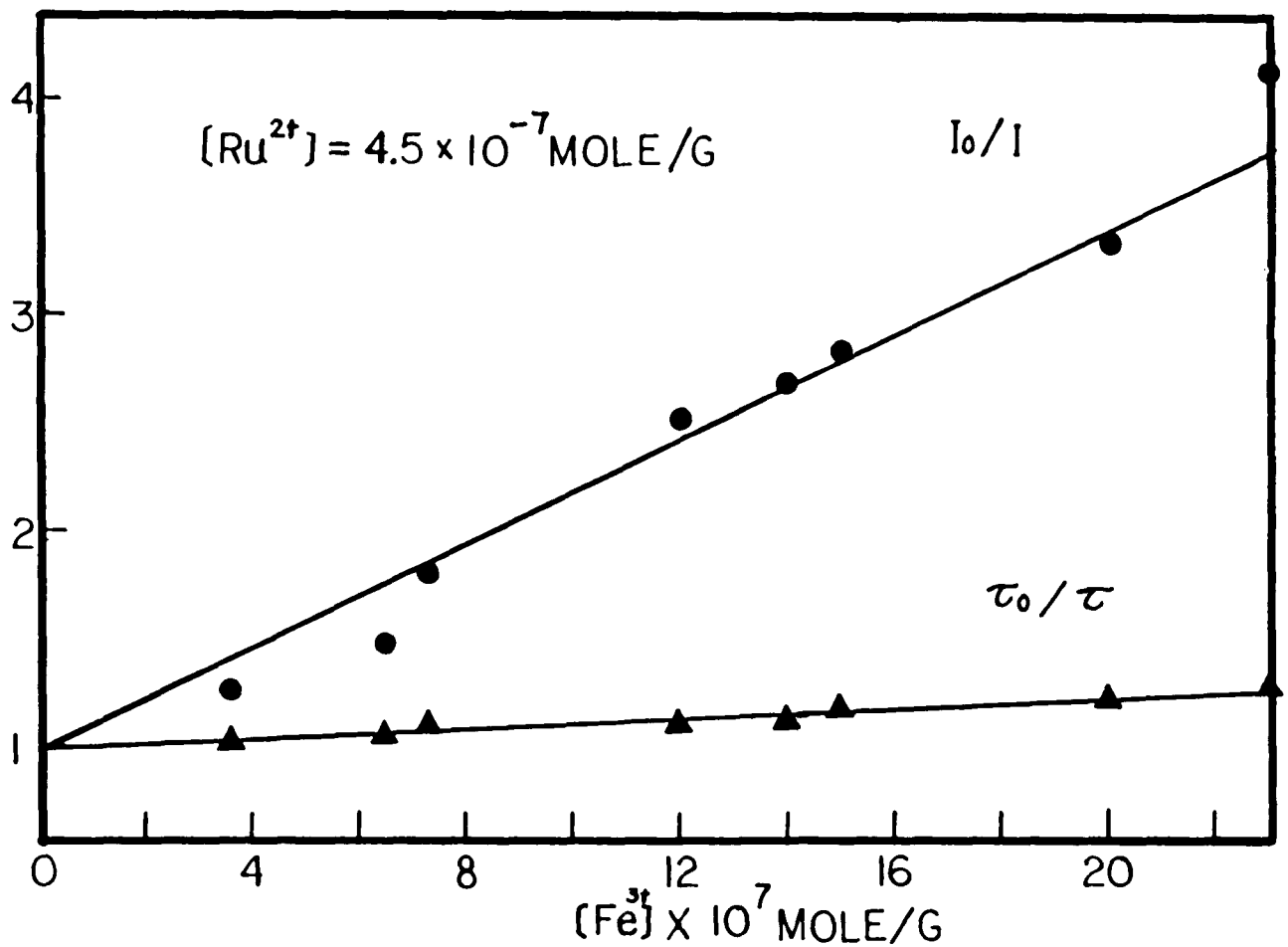
[Ru2+] = 4.5 x 10-7 MOLE/G
I0/I
τ0/τ
4
3
2
1
0
4
8
12
16
20
[Fe3+] X 10^7 MOLE/G

quenching and lifetime quenching are parallel, the extent of lifetime quenching is significantly smaller than that of intensity quenching on the PVG surface. The bimolecular rate constant calculated from the lifetime data, which represents the dynamic component of the quenching process, is $\lesssim 1 \times 10^7$ $M^{-1}s^{-1}$. Compared to the constant obtained from the intensity quenching (I_0/I), which reflects the overall degree of quenching, 1.5×10^8 $M^{-1}s^{-1}$, it is obvious that emission quenching by Fe^{3+} on PVG is predominately a static process. Two additional differences between the quenching in water and on the PVG surface should also be noted. First,the rate of quenching on PVG is substantially reduced compared to that in aqueous solution, which proceeds with a rate constant of 2.7×10^9 $M^{-1}s^{-1}$. Second, quenching on PVG does not result in detectable accumulation of the photoproducts, i.e., $Ru(bpy)_3^{3+}$ and Fe^{2+}, which are readily observed in aqueous solution.[70]

2. Photochemical Reactions of $Ru(bpy)_3^{2+}$

a) Temperature Dependence of Photo-induced Disproportionation of $Ru(bpy)_3^{2+}$

Previous work in this laboratory has shown that 450 nm photolysis of $Ru(bpy)_3^{2+}$ adsorbed on PVG leads to disproportionation[157]

$$Ru(bpy)_3^{2+} + h\nu \text{ -----> } {}^*Ru(bpy)_3^{2+} \qquad (27)$$

$${}^*Ru(bpy)_3^{2+} + h\nu \text{ -----> } Ru(bpy)_3^{3+} + e^- \qquad (28)$$

$$e^- + Ru(bpy)_3^{2+} \text{-----> } Ru(bpy)_3^{+} \qquad (29)$$

$$2\ Ru(bpy)_3^{2+} + 2\ hv \text{-----> } Ru(bpy)_3^{3+} + Ru(bpy)_3^{+} \qquad (30)$$

This reaction occurs by biphotonic photoionization of the adsorbed complex and migration of the photodetached electron on the PVG surface.[160] To probe the surface conduction of the photodetached electron the temperature dependence of the quantum yield of the photoinduced disproportionation of the Ru complex on the glass (eq 30) was examined. PVG samples impregnated with 1 x 10^{-6} M/g of $Ru(bpy)_3^{2+}$ were irradiated with 457.9 nm laser light from an argon ion laser (intensity ca. 10 mW), and the formation of the photoproduct, $Ru(bpy)_3^{+}$, was monitored spectrally at 510 nm (ϵ = 12000 $M^{-1}cm^{-1}$). the temperature was varied from 0 C to 65 C, and the relative quantum yields of $Ru(bpy)_3^{+}$ formation measured at different temperatures are listed in Table 8. A plot of ln vs. 1/T (Figure 39) is linear and the activation energy calculated from the slope is 4.5 kcal/mole.

b) Formation of Long-lived MV^+ on PVG

A 457.9 nm irradiation of a PVG sample containing 1.5 x 10^{-7} moles of $Ru(bpy)_3^{2+}$/g and 1.0 x 10^{-4}moles of MV^{2+}/g in vacuo results, as shown in Figure 40, in the appearence of a weak absorption at 510 nm and more intense absorptions at 395 nm and 605 nm.The latter bands agree exactly with the spectrum of adsorbed MV^+ generated by reduction of adsorbed MV^{2+} with a basic solution of $Na_2S_2O_4$. The formation of MV^+

TABLE 8

Temperature Dependence of Quantum Yield of $Ru(bpy)^{+}$ Formation

Temperature (°C)	10^3 x 1/T	Quantum Yield [a]	log ϕ
0	3.66	0.45	- 0.34
22	3.36	1.00	0
45	3.14	1.63	0.21
65	2.96	2.34	0.37

[a] Relative to the quantum yield at 22 C.

Figure 39. Aplot of the quantum yield of $Ru(bpy)_3^+$ as a function of 1/T. The slope of the curve gives the activation energy of the photoinduced disproportionnation of adsorbed $Ru(bpy)_3^{2+}$.

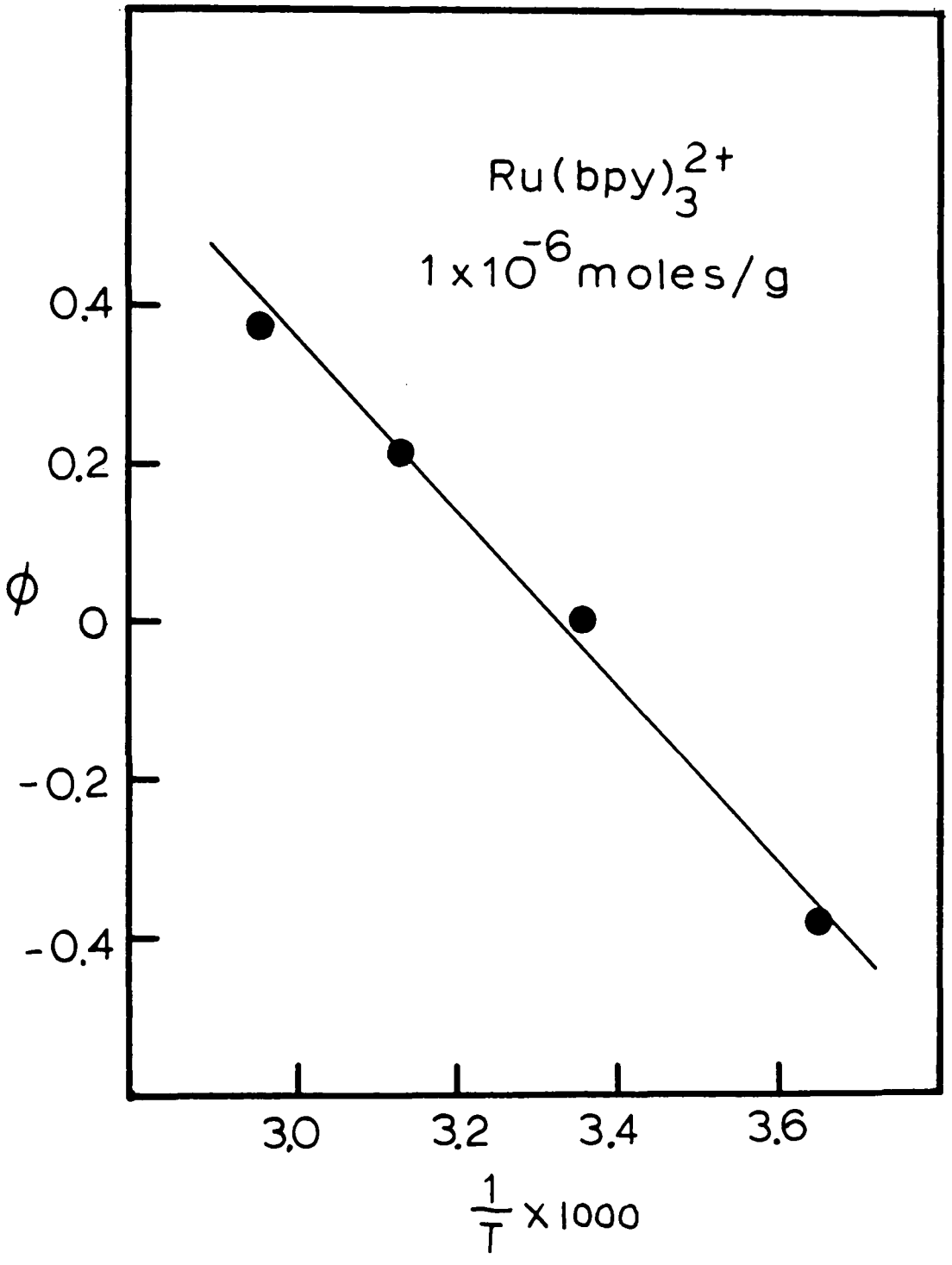
Ru(bpy)$_3^{2+}$
1x10^{-6}moles/g
0.4
0.2
ϕ
0
-0.2
-0.4
3.0
3.2
3.4
3.6
$\frac{1}{T}$ X 1000

Figure 40. Formation of MV^{+} upon laser photolysis of a PVG sample containing $Ru(bpy)_3^{2+}$(1.5×10^{-7} moles/g) and MV^{2+}(1×10^{-4}moles/g). The increase of absorption at 610nm,and 395 nm are due to MV^{+} formation. The weak absorption at 510 nm is due to $Ru(bpy)_3^{2+}$. The light source is the 457.9 nm line from an Ar ion laser.

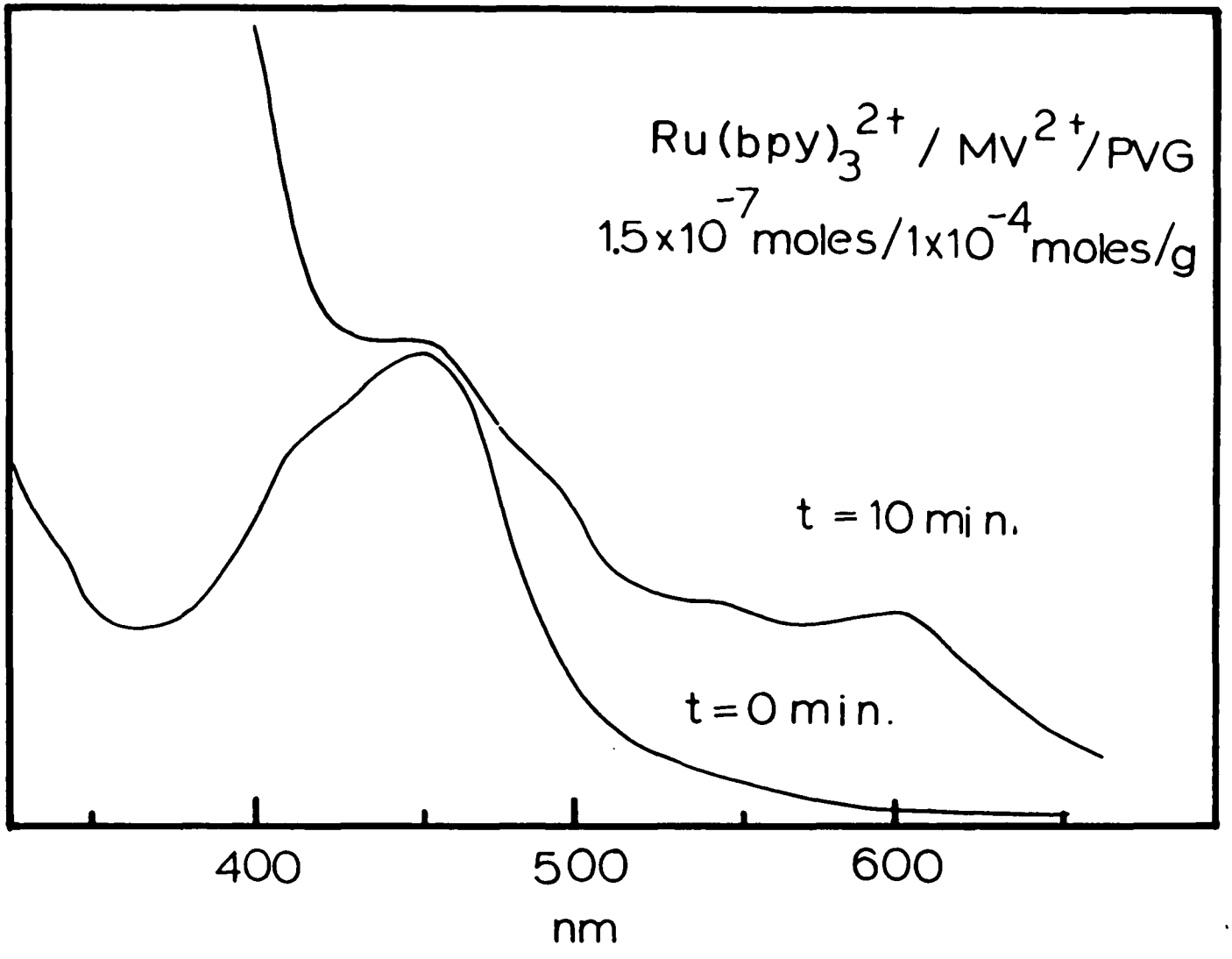
Ru(bpy)3 2+ / MV2+/PVG
1.5x10-7 moles/1x10-4 moles/g
t = 10 min.
t=0 min.
400
500
600
nm

is limited to a narrow range of samples containing (1.5 - 2.0) x 10^{-7} moles of $Ru(bpy)_3^{2+}$/g and (0.8 - 1.2) x 10^{-4} moles of MV^{2+}/g. Also, MV^+ is not generated throughout the sample, but is visually aparent only in the regions where there is an overlap between the two partitioned compounds. In vacuo, the photogenerated MV^+ is stable for hours, but exposure to air causes the 395 nm and 605 nm bands to disappear. Consistent with the generation of MV^+ within the support and the time required for O_2 to diffuse into the bulk, the rate of oxidation is relatively slow in comparison with the instantaneous oxidation of MV^+ generated chemically on the surface of PVG. The quantum yield of MV^+ formation during 45o nm photolysis of a sample containing 1.5 x 10^{-7} moles of $Ru(bpy)_3^{2+}$/g and 1.0 x 10^{-4} moles of MV^{2+}/g is ca. 10^{-4}. The calculated value, which is based on the total light absorbed, is a lower limit, however, since the absorption of light does not parallel the distribution of the photoproducts within PVG.

The formation of MV^+ and its stability can not be attributed to an impurity effect. A 450 nm photolysis of a sample, in vacuo, containing 10^{-4} moles of MV^{2+}/g does not yield MV^+. Furthermore, the reaction can be cycled by oxidizing MV^+ with O_2 as many as 10 times without a significant decline in efficiency. The cross sectional absorptivity of $Ru(bpy)_3^{3+}$, 4.0 x 10^5 cm^2/mole at 675 nm, precludes optical detection under these conditions. However, attributing product stability to a rapid scavenging of the

oxidized complex by PVG, as is in the case in cellulose,[123] is inconsistent with EPR spectra which establish that $Ru(bpy)_3^{3+}$ is stable in PVG.[160]

DISCUSSION

A. Characterization of the PVG Suface

1. General Considerations

Chemical processes at interfaces are governed primarily by three parameters: a) the chemical and physical properties of the functional groups at the surface, b) the distribution of the binding, or active sites at the surface, and c) the geometry of the surface. The chemical and physical properties determine the types of binding between the surface and the adsorbate, e.g.,hydrogen bonding, cation or anion exchange, or physisorption. The distribution of binding sites determines adsorbate location on the surface, e.g., whether the adsorbate distributes randomly or aggregates inlocalized regions. The first parameter, and, to certain extent the second, can be examined by physical techniques developed for homogeneous solutions. The extrapolation from solution to surface is possible, particularly with hydroxylated surfaces, since the chemistry of the OH^- group is basically the same whether it is part of a solvent or a surface moity. With low loadings, the adsorbate can be randomly dispersed on the surface and approximates the random distribution in fluid solution. However, this is not true for the surface geometry, which largely determines the dynamic processes(diffusion) of the molecule on the surface. In solution, a solute molecule

is surrounded by a spherecally symmetric solvent shell, e.g., solvent cage, where its translational motion is governed by Brownian collisions, concentration gradients, and convections. In contrast,the surface environment of an adsorbate and its surface mobility are strongly dependent on surface geometry. Adsorbate" solvation" on a surface is nonisotropic, and the immediate environment of the adsorbate does not necessarily posses the dynamic flexibility of a solven cage. Consequently, adsorbate diffusion is governed by the wiggles of the surface. Therefore,chemical processes on surfaces of similar chemical composition, but differrent geometry, can lead to different results in terms of kinetic behavior. In the studies of photochemical reactions on a surface, particularly an amorphous materials such as the porous Vycor glass, it is necessary to examine both chemical and geometric properties of the surface to understandand their effects on the reaction system.

2. The Chemical and Physical Properties of PVG Surface

Chemically, the surface of porous Vycor glass(PVG) falls within the large family of silica surfaces which are of practical importance in a number of applications. Prepared by acid leaching of a conventional borosilicate glass, the finished PVG is comprised of 96% SiO_2, 3% B_2O_3, and 1% of principally Na and Al metal oxides.[170] Although this composition closely resembles that of silica, PVG does possess a higher B/Si ratio (1:3) on the surface than in the

bulk (1:18).[171] The surface boron is present as Lewis acid sites leading to the presence of a large number of Lewis acid type sites of active surface area in PVG than in conventional silica gel. In addition to Lewis acid sites, PVG also has Bronsted acid sites, present predominately in the form of SiOH and hydrogen bonded H_2O.[172-174] The decrease in pH of the surrounding aqueous phase and the development of a negative zeta potential when powdered PVG is dispersed in H_2O establish that the surface hydroxyl groups are relatively acidic. A number of reports have commented on the acidity of porous silica in the presence of metal ions.[175] Ahrland and co-workers, for example, have shown that for each equivalent of metal ions adsorbed, one equivalent of protons dissociates from the silica into the aqueous phase. Similarly, studies of the adsorption of metal ions and cationic metal complexes onto PVG from aqueous solutions show that adsorption occurs without a concurrent adsorption of the anion (see below). Rather, a concurrent decrease of the pH of the surrounding solutions phsae indicates a cation exchange process in which the metal ions displace the weakly acidic protons of the Bronsted acid sites.[176]

At room temperature, the surface of PVG is extensively hydrated. Diffuse reflectance Fourier transform IR spectra taken at room temperature shows a broad band centerd at 3500 cm^{-1} that is assigned to chemsorbed water (Figure 41). This band disappears on heating in vacuum and at 550 C the spectrum (Figure 42) consists of a sharp band at 3750 cm^{-1}

assigned to free SiOH and a shoulder at 3650 cm^{-1} assigned to hydrogen bonded SiOH units. Thermal gravimetric analysis of PVG (Figure 43) shows that the loss of bulk water at 100 - 120 C is followed by the slow loss of chemisorbed water up to 650 C. Thesedata establish the presence of considerable amount of chemisorbed, or hydrogen bonded, water even after removal of bulk water by pumping in vacuum at room temperature.

3. Geometry of the PVG Surface

The porous Vycor glass is an amorphous material possessing a random array of interconnected cavities, or pores, throughout its entire volume. The average diameter of the pores is 70 + 20 A, and the surface area of the glass, measured by the nitrogen BET method, is 140 m^2/g.[177] Although the latter gives a simplified picture of an irregular surface,it does not give any information, particularly on the level of molecular dimension, of the surface geometry. Very few surfaces in Nature are truely flat, two-dimensional planes. Rather, at the molecular or supermolecular levels, most materials possesses fractured surfaces. The traditional treatment of surface irregularity had been to regard it as a deviation from an ideal reference, i.e., a plane.[178] However, a new approach, suggested by Mendelbrot several years ago, takes an entirely different stand.[179] Instead of treating the irregularity as deviations,

Fire 41. Diffuse reflectance Fourier Transform IR spectrum of an uncalcined PVG sample.

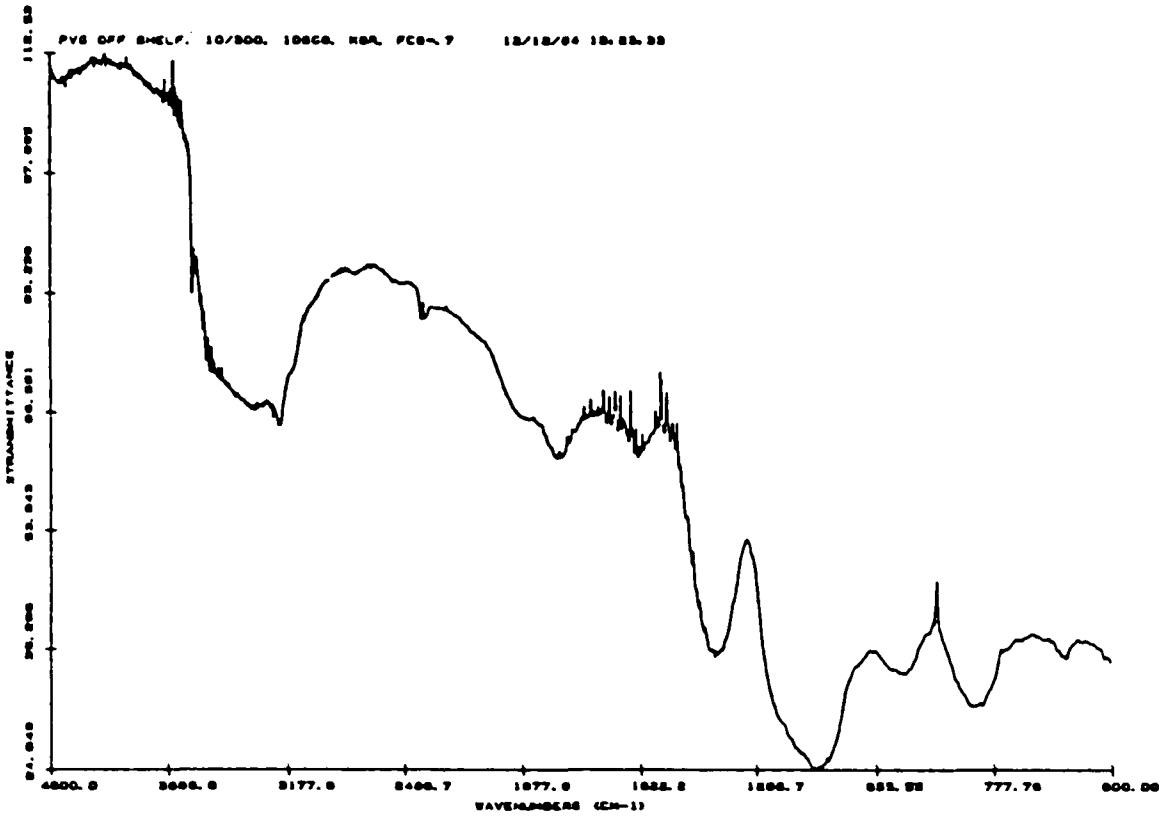

Figure DRIFT spectrum of uncalcined PVG.

Figure 42. Diffuse reflectance Fourier transform IR spectrum of a calcined PVG sample.

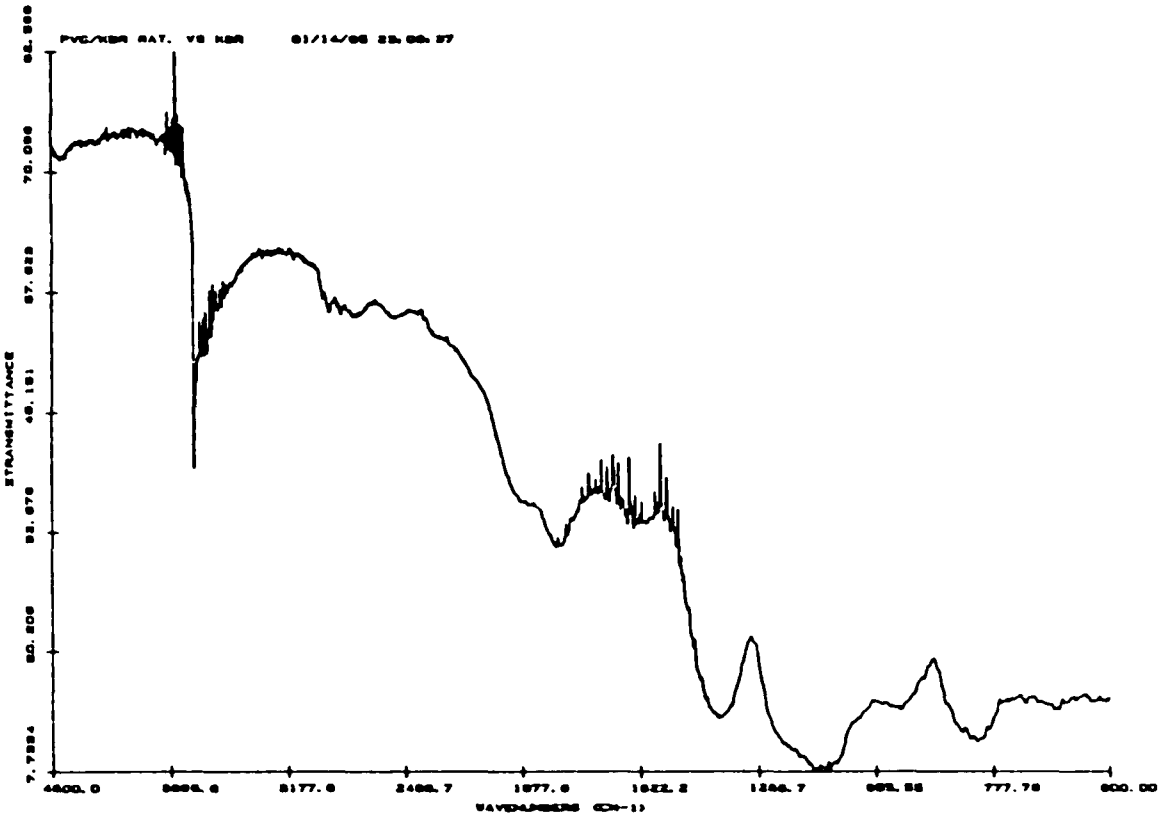

Figure . DRIFT spectrum of calcined PVC.

Figure 43. Thermal gravimetrivc analysis of PVG.

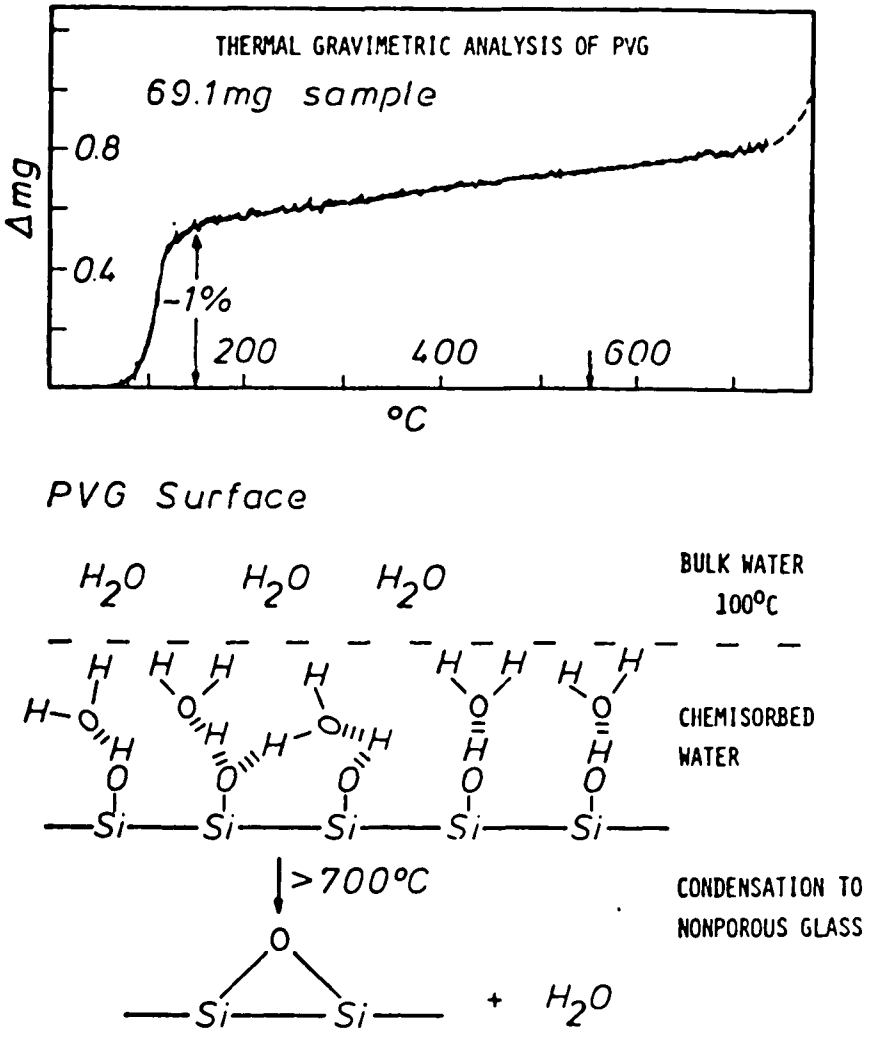

Figure . Thermal gravimetric analysis of PVG.

this new method measures the degree of irregularity by a universal parameter called "fractal dimension" or the Hausdorf dimension, d. For straight lines and flat surfaces, d equals the Euclidian dimensions, i.e., 1 and 2, respectively. For irregular lines and surfaces, d varies between 1 and 2, and 2 and 3, respectively. Thus, the larger the difference from the Euclidian dimension, the larger the irregularity in the geometric entity. d can be obtained by resolution analysis, where the rate of appearence of new features of irregularity is determined as a function of the probing yard stick, or the degree of magnification. This is given by the power law

$$n \propto r^{-D} \qquad (31)$$

where n is the number of yardsticks of size r needed to cover the total length of the irregular line. For a smooth line, d = 1, and eq.31 becomes the familiar $n \propto r^{-1}$. For a wiggly curve, d > 1, and the number n increases faster than the decrease inthe size of the yardstick.

Avnir and Pfeifer and co-workers have developed an approach based on the adsorption data for the determination of fractal properties of surfaces at the molecular level.[180-184] They have shown that most materials, amorphous or crystalline, are fractal, i.e., with d > 2. The values of d for a representative number of surfaces are listed in Table 9. Of special interest is the fractal dimention of silica. The d value of 2 .94 $\pm$ 0.06, determined from adsorption data,

TABLE 9

MOLECULAR FRACTAL SURFACES

MATERIAL	FRACTAL DIMENSION
POROUS SILICIC ACID	2.94±.04
ACTIVATED ALUMINA F-20 (ALCOA)	2.79±.03
POROUS FeOOH MAGNETIC TAPES	2.57±.04
CARBON BLACK	2.25±.09
AEROSIL NONPOROUS FUMED SILICA (DEGUSSA)	2.02±.06
GRAPHITE VULCAN 3G	2.07±.01
POROUS VYCOR GLASS CORNING 7930, 70A°	1.74±.12

D. AVNIR, D. FARIN, P. PFEIFER, NATURE, (1984), 308, 261

points to an extremely irregular surface.[180] The value has been recently confirmed by independent experiments with several types of mesopore silicas (silicas with average pore sizes 20 - 200 Å and surface areas 50 - 500 m^2/g).[185]

In contrast to silica, the chemically similar PVG surface posseses an unusually low Hausdorff dimension. Jortner and coworkers have reported a d value of 1.74 $\pm$ o.12 for PVG.[186] Since the lower limit of the surface dimensionality is 2, this value may be taken essentially as 2. In a recent report, the d value of PVG has been remeasured and a value close to 2.0 has been obtained.[185] Thus, although the two media have basically identical surface chemical composition, their geometric properties, as characterized by the fractal dimention, are very different. In fact, the d values of the two surfaces represent the two extremes of surface dimensionality.

B. Binding and Immobilization of $Ru(bpy)_3^{2+}$ on PVG

1. The Nature of the Binding

Adsorption of $Ru(bpy)_3^{2+}$ onto PVG from aqueous solution occurs without concurrent adsorption of the Cl^- counterion (Figure 7). This result establishes that the complex binds onto the surface by cation exchange with acidic hydroxyl groups. The increasing rate of adsorption and the total amount of cations adsorbed with increasing pH of the solution further illustrates the role of the surface charge in cation

adsorption.

Cation exchange, however, may not be the sole mode of adsorption of $Ru(bpy)_3^{2+}$. Because of the presence of Bronsted acid sites, PVG develops a negative surface charge when placed in aqueous solutions.The surface charge declines with decreasing pH of the aqueous phase. The isoelectric point (i.e.p.), or point of zero surface charge, varies with the mode of preparation and (for example) heat pretreatment. Normally, however, the i.e.p. falls in the range of pH 3-4 for silica surfaces.[187] Since $Ru(bpy)_3^{2+}$ adsorption on PVG can occur at pH below 4, where the PVG surface is thought to consist of neutral surface groups, the adsorption at low pH is probably due to nonelectrostatic mechanisms.

Two forces other than electrostatic attraction have been suggested for metal ion adsorption on silica surfaces.[188] The first involves the formation of covalent bonds between the metal and the surface groups.The second involves hydrophobic binding, in which the surface tension of water forces the adjacent hydrophobic groups of the adsorbates together whereas the cationic part of the adsorbate is bonded to the SiOH surface. For $Ru(bpy)_3^{2+}$ adsorbed onto PVG, a covalent bond between the metal and the surface site requires dissociation of a Ru-N bond. This is neither energetically likely nor supported by spectroscopic data. The absorption spectrum of the adsorbed complex shows no significant shifts or splitting of the ligand centered *pi-pi transition at 285

nm and the MLCT transition at 450 nm. In addition, the resonance Raman spectrum of the adsorbed complex, with the exception of changes in relative intensity, is identical to that in aqueous solution. Nor are the data consistent with formation of a covalent bond to the bpy periphery since this generally produces significant spectral changes. For example, Van Damme and co-workers find that the absorption spectra of $Ru(bpy)_3^{2+}$ intercalated between clay layers differ significantly from the solution spectra. The 285 nm band of the adsorbed complex splits into two band at 272 and 290 nm, and the extinction coefficients of both the ligand pi-pi transition and that of the MLCT transition change considerably. These authors suggest that a covalent bond formed between the bipyridine ligand and surface water causes for the observed spectral changes.[118] Rather, the similarities of the UV-visible and resonance Raman spectra of $Ru(bpy)_3^{2+}$ on the PVG surface with the solution spectra establish the retention of the primary coordination sphere of the complex and the absence of any bond interruption.

The question of the hydrophobic binding, between the adsorbed complex and the PVG surface, is more difficult to answer with certainty. Direct experimental data are not available for this system. On the other hand, the conditions for this type of interaction appear to be easily met, given the considerable amount of chemisorbed water on the PVG surface and the hydrophobicity of the bipyridine ligands of the complex. Non-ionic organic compounds, such as pyrene, can

be adsorbed onto PVG from organic solvents.[189] Studies of pyrene fluorescence on PVG indicate a restricted mobility of the adsorbed molecule. Although not directly related to the binding of $Ru(bpy)_3^{2+}$, these results are consistent with the presence of hydrophobic binding on PVG. It seems possible that, in addition to the dominant coulombic attraction, the hydrophobic binding also contribute to the interaction between $Ru(bpy)_3^{2+}$ and the surface, albeit to a less extent.

2. Immobilization of $Ru(bpy)_3^{2+}$ on PVG

Despite the obvious cation exchange character of the silica surface, many metal ions are strongly and irreversiblly held by various forces on the surface. In colloidal silica suspensions, $Ru(bpy)_3^{2+}$ has been shown to reside primarily in the so called "Stern layer"[110] in which the cations are tightly bonded to the negative surface and essentially immobilized against the surface, forming a "compact double layer". Since the Stern layer is as close to the surface as the the incoming adsorbate can be, short of covalent bond formation, a strong interaction between the adsorbed complex and the surface is clearly implied.[190]

Since surfaces consist of fixed arrays of surface functional groups, strong interaction of adsorbate with surface groups results in restricted motions of the adsorbate on the surface. Since $Ru(bpy)_3^{2+}$ exhibits polarized absorption and emission, a sensitive method to probe the rotational motion of the adsorbate is the measurement of

emission polarization. In the crystalline form and in a rigid, 77 K, glassy solvent,polarized excitation gives rise to an emission polarized in the same direction as the incident light.[37,45,46] However, if the molecule can rotate between the time of excitation and emission, the polarization is lost. The polarization ratios for $Ru(bpy)_3^{2+}$ adsorbed on PVG at room temperature, and in 77 K EPA glass are essentially identical (Table 7). The agreement between these data is a conclusive indication that the rotational motion of the adsobred complex is severly restricted or non-existent, at least on the time scale of the complex's excited state lifetime, ca. 1 us. Since translational motion of the molecule along the surface most likely involves rotation, the lack of rotational freedom of the adsorbed complex implies that the translational motion of the complex on PVG surface is also curtailed or non-existent during the excited state lifetime.

The rigidity of the environment surrounding the adsorbed $Ru(bpy)_3^{2+}$ shows no detectable change in the temperature range of 0 ^{o}C - 85 ^{o}C. Emission polarization measured at various temperatures within this range is virtully constant (Figure 26). Furthermore, polarization of the adsorbed complex at 77 K is, within the rather large experimental uncertainty, in keeping with the value reported for 77 K EPA glass.

These results are consistent with earlier observations

that macroscopic diffusion of adsorbed $Ru(bpy)_3^{2+}$ is absent. For example, PVG samples impregnated with $Ru(bpy)_3^{2+}$ show no detectable changes in cross sectional distribution after several months in contact with pure water at room temperature, nor when maintained at 100 C for 8 hrs in boiling water. Apparently, the activation energy of diffusion on the PVG surface is very high and beyond that that can be overcome by the elevated temperatures used in these experiments. Similar results have been reported with $Ru(bpy)_3^{2+}$ doped into poly(methyl methacrylate), where the emission polarization is found to be independent of temperature between 2 K and 305 K.[46]

Immobilization of various (mostly organic) compounds on PVG has been noted. Avnir and coworkers report that Rhodamine 6G, which usually aggregates in aqueous or alcoholic solutions at concentrations > 10^{-4} M,does not aggregate on PVG at much higher concentrations, > 10^{-3} M.This result is attributed to the lack of diffusion of the dye molecules on the glass surface.[191] Nakashima and Phillips find that the rotational motion of 9,9'-bianthryl about the anthracene-anthracene bond is non-existent when the molecule is adsorbed onto PVG.[192]

Restricted mobility of $Ru(bpy)_3^{2+}$ adsorbed to other supports has also been reported, although in most cases the degree of curtailment is less than that on PVG. Emission polarization of $Ru(bpy)_3^{2+}$ bonded to clay minerals is 0.11 + 0.02.[134] Independent measurements of the diffusion coefficient of the complex in clays show that translational

motion is negligiblly small within the complex's excited state lifetime.[132] The distance traveled by the molecule during its excited state lifetime is given by

$$L = 1/2(\tau D)^{1/2} \qquad (32)$$

where tau is the excited state lifetime and D the diffusion coefficient. For $Ru(bpy)_3^{2+}$ adsorbed on the clay surface, D = 1×10^{-12} cm^2s^{-1}, and tau = 700 nsec.[132] This leads to a L value of ca. 0.07 A. This is to be compared with the size of the complex, r = 7.5 Å. Although the diffusion coefficient of $Ru(bpy)_3^{2+}$ on PVG is unknown, the higher degree of polarization suggests that translational motion of the complex on PVG is unlikely to exceed that on clays, which is essentially zero.

C. Distribution and Partitioning of Reagents on PVG

1. Distribution of Metal Ions

Despite the large pore size and the open structure of porous Vycor glass, distribution of various adsorbates in this matrix is not always uniform, which suggests that not all parts of the glass are equally accessible to every compound. This phenomenon was first noticed with $Ru(bpy)_3^{2+}$ adsorption. Under the usual experimental conditions, i.e., solution concentration of 1×10^{-5} M to 1×10^{-3} M, impregnation time of 24 - 72 hours, and room temperature, 22 $\pm$1 ^{o}C, thecomplex adsorbs onto the outer surfaces and

penetrating no more than 0.4 mm into the 4.5 mm thick glass sample. Similar distributions were also found for a number of other transition metal complexes.[167,193]

The distribution of the metal ions used as quenchers, i.e., Cr^{3+}, Fe^{3+}, and Cu^{2+}, however, can differ from that described above. Under similar impregnation conditions, the penetration depth of the ions increases in the order

$$Cr^{3+} < Fe^{3+} < Cu^{2+}$$

In fact, Cr^{3+} only distributes on the outermost surface of the PVG sample and, consequently, the total amount of the ion adsorbed is limited to $< 5 \times 10^{-6}$ mole/g. Ferric ion, on the other hand, penetrates ca. 0.5 mm into the glass, and impregnates the same volume as $Ru(bpy)_3^{2+}$. Cu^{2+} adsorbs in both the outer surfaces and the interior of the PVG sample and, unlike the other adsorbates, is leached from the impregnated glass when in contact with pure water.

The differences in the distribution of metal ions on the PVG surface may arise from a number of factors. The most important ones, however, are their sizes, their kinetic labilities, and the types and strength of their binding with the surface groups.

a) The sizes of the Ions

The role of adsorbate size in determining adsoption onto a porous support has long been recognized and is the basis of partition chromotography.[195] A molecular sieve, for example,

differentiates a spieces by adsorption of small spieces into the body of the sieve. The PVG samples used in this study possess 70 $\pm$ 20 Å diameter pores in a three dimensional array. Although The sizes of the adsorbates are small comprared to the pore size, it is possible that narrower segments exist between the pores. These could be plugged by the first few ions adsorbed, thereby blocking the path of other ions to the interior. Congestion in the pores is quite likely for the relatively bulky $Ru(bpy)_3^{2+}$ that has a diameter of 15 A,[194] since penetration $\geq$ 0.5 mm requires that PVG remains in the impregnating solution for several months. Furthermore, complexes of similar size, e.g. $Cr(bpy)_3^{3+}$, $Ru(bpy)_2(CN)_2$, all show similar cross sectional distributions, despite their differences. However, the size factor fails to explain the different distributions of the metal ions Cr^{3+}, Fe^{3+}, and Cu^{2+} which, if considering only the primary coordination sphere, are of similar sizes and all are considerably smaller than $Ru(bpy)_3^{2+}$. Other factors, therefore, must determine their distributions within PVG.

b) Kinetic Lability vs. Inertness

One of these additional factors, particularly with a coordination complex, may be the lability of the adsorbate. On a surface such as PVG, where the silanol and chemisorbed water can be viewed as ligands,[187] exchange from site to site may be crucial for a metal ion to move about.In fact, formal coordination to the metal may not be necessary since a large

number of water molecules are bound to the metal in various degrees. For example, Cr^{3+} may have as many as50 water molecules when fully hydrated.[195] The hydration number for the ferric and cupric ions are 69 and 24, respectively.[195] Considering the size of the fully hydrated ions, the metal ions must rid themselves of some of this burden in order to move amongst the PVG pores. Ironically, it is also true that Cr^{3+}, a d^3 metal, is among the most inert transition metal ions. This is readily apparent from its extremely slow water exchange reaction

$$Cr(H_2O)_6^{3+} + L \text{ -----} \rightarrow Cr(H_2O)_5^{3+}L + H_2O \qquad (33)$$

where L is another water molecule that displaces the coordinated water. The rate constant of this reaction is 2.5 x $10^{-6}s^{-1}$, which corresponds to a half life of 100 hours for hexaquochromium(III).[196] In contrast, Cu^{2+}, one of the most labile transition metal ions, has a rate constant of > 10^{9} s^{-1} for water exchange.[196] The differnce of nearly 15 orders of magnitute will certainly affect the ability to switch from site to site. It is conceivable that, once the PVG surface is in contact with the aqueous solution, the copper ion will move rapidly into the interior of the glass, because of both its smaller hydration shell and much higher kinetic lability. Cr^{3+},onthe other hand,stays where it first adsorbed on the outer surface of the glass, since its hydration and slow rate of exchange prevent further motion. These differences are the basis for the separation of the two metals on supports such as alumina and cellulose in early chromatograhy

experiments.[195] Interestingly, however, Fe^{3+} behaved more like Cr^{3+} in those experiments than like Cu^{2+}, although ferric ion is fairly labile, with a water exchange rate constant ca. 10^{4} s^{-1}.[196] Apparently, while kinetic lability plays a role in affecting the rate of adsorption and the distribution of the metal ions, other factors, which involve the chemical interactions between the adsorbed ions and the surface, must also be taken into consideration.

c) Binding of Metal Ions on PVG

The primary mode of interaction between cationic metal complexes and ions and the negatively charged silica surface is undoubtedly that of the electrostatic attraction. However, as pointed out in the preceeding section, other types of binding may also exist. One such possiblity is the formation of covalent bonds between the adsorbate and the surface silanol groups according to the equation:

$$SiOH + (H_2O)_xM^{Y+} \longrightarrow SiOM(H_2O)^{(Y-1)}_{x-1} + H_2O + H^+ \quad (34)$$

Either or both of the two bindings, the electrostatic and the covalent, can contribute to the interactions between the metals and the surface.[187] For the three metal ions examined in this work, the tendency to form covalent bonds on silica falls in the order $Fe^{3+} > Cr^{3+} > Cu^{2+}$.[187] Since covalent binding requires bond specificity, ions that are more readily to form covalent bonds are more likely to be fixed on the surface and less free to move. Studies of rare earth metal

ions adsorbed onto PVG reveal that the ions bind to the surface in a manner similar to binding with bulk glass.[197]

For electrostatic binding, the most important factor that determines the binding strengh is the ionic potential of the metal ion, since the surface negative charge is always monovalent. The values of ionic potential, Z/r, where Z is the positive charge on the metal and r is the ionic radius, for the three metals are: Cr^{3+} 4.69, Fe^{3+} 4.49, and Cu^{2+} 2.00.[195] Therefore, the copper ion, with the smallest ionic potential, is the least strongly bound by electrcstatic forces whereas Cr^{3+} is the most strongly bound. Fe^{3+} more closelyresembles Cr^{3+} rather than Cu^{2+} and, in this respect, is consistent with the separation of the ions on alumina and cellulose. Parallel trends also occur in the dialysis coefficients, λ, and the relative diffusion coefficients D. When measured on alumina columns, Cu^{2+} has the lowet $1/\lambda$ and 1/D values, whereas the corresponding values for Cr^{3+} and Fe^{3+} are both considerably higher.

In the above discrimination, it has been, in a sense, assumed the integrity of the adsorbate. Another process that affects adsorption and distribution of metal ion is the tendency to hydrolyze on the surface:

$$M(H_2O)_6^{n+} + H_2O \text{ ------} \rightarrow MOH(H_2O)_6^{(n-1)+} + H_3^+O \qquad (35)$$

Extensive hydrolysis of hydrated metal ions leads to strong adsorption to the surface, since, as illustrated in Figure 44, the more polarized water molecules in the metal

Figure 44. Surface hydolysis of metal ions on PVG.

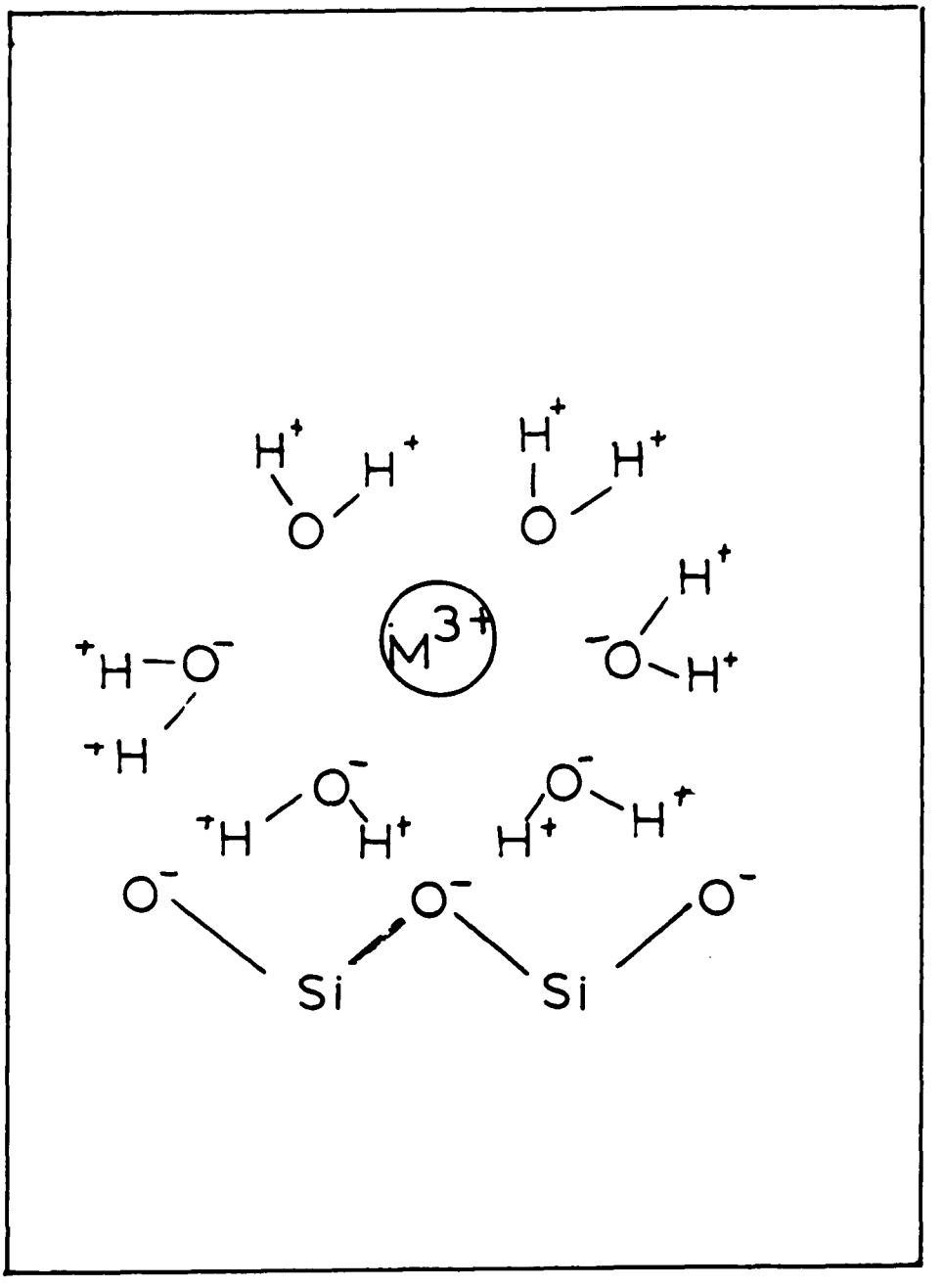
H+
H+
O
H+
H+
O
M3+
+H—O−
+H
H+
−O
H+
+H
O−
H+
H+
O−
H+
O−
O−
O−
Si
Si

coordination sphere tend to be more strongly bound to the surface Si-O-Si groups. In terms of the ability to hydrolize, Fe^{3+} and Cr^{3+} again differ substantially from Cu^{2+}. The K_a values in eq. 35 for Fe^{3+}, Cr^{3+}, and Cu^{2+} are 3.05, 4.00 and 8.15, respectively.[196] In fact, since the PVG surface has a pH 4-5, hydrolysis of the ferric ion on the surface is favorable. PVG samples impregnated with various amounts of ferric ion appear yellow and the absorption spectra show increasing absorption in the UV region. (Figure 19). Since similar absorption spectra was also obtained with partially hydrolized ferric solutionswhere pH > 4, the spectral change that occurs on PVG indicates significant hydrolysis of hexaquoiron(III).

Evidence for the hydrolysis of Cr^{3+} comes from the absorption spectral shifts observed when the ion is adsorbed from aqueous solution onto PVG. The acidic solution of $CrCl_3 6H_2O$ used for PVG impregnation (pH < 3.5, adjusted with HCl) shows two absorption maxima at 440 nm and 630 nm. Adsorption onto PVG shifts the two peaks to 420 nm and 600 nm, respectively. Since in a pH 10 solution of the chromium ion the two peaks are at 420 nm and 585 nm (Figure 45), the species on the glass appears to be intermediate between the species in acidic and that in basic solutions. Considering the pK_a for $Cr(H_2O)_6^{3+}$, 4.0, hydrolysis in pH 10 solution is highly favored and perhaps even complete. However, the spectral changes suggest that the adsorbed species is best described as a partially hydrolized chromium ion.

Figure 45. Absorption spectrum of Cr^{3+} in a) acidic solution(pH 2), b) basic solution(pH = 10) and c) adsorbed on PVG.

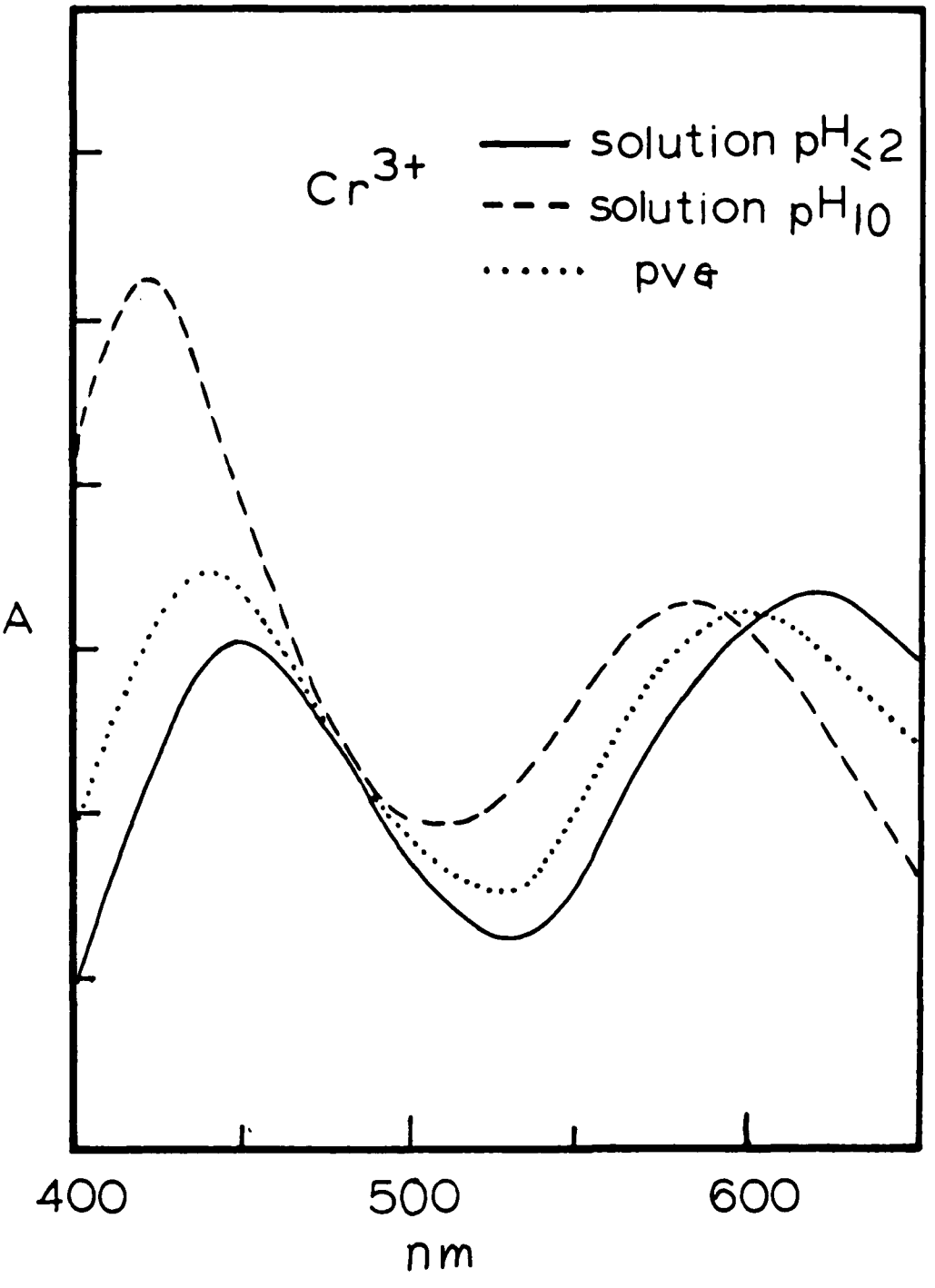
Cr^{3+}
solution $pH \leq 2$
solution pH_{10}
pvc
A
400
500
600
nm

In contrast to Cr^{3+} and Fe^{3+}, the identical absorption spectra of Cu^{2+} in aqueous solution and adsorbed on PVG establish that Cu^{2+} does not undergo hydrolysis on the PVG surface.(Figure 46). Judging by the extent of hydrolysis, Fe^{3+} and Cr^{3+} should adsorb more strongly on PVG than Cu^{2+}. This, and the factors discussed in the preceeding section, consistently point to the strongly adsorbed Fe^{3+} and Cr^{3+} and more weakly adsorbed Cu^{2+}. The observed cross-sectional distribution patterns, i.e., the penetration depth increase in the order of $Cr^{3+} < Fe^{3+} < Cr^{2+}$, is a reflection of the different adsorbability of the metal ions on the glass.

2. Partitioning of $Ru(bpy)_3^{2+}$ and Cu^{2+}

In the presence of $Ru(bpy)_3^{2+}$, which adsorbs only on the outer surfaces of the glass sample, the cross sectional distribution of Cu^{2+} is no longer uniform. Rather, as shown in Figures 14 and 15, it is dependent on the amount of Cu^{2+} adsorbed. At impregnation levels below 5×10^{-5} mole/g, the copper ion distributes almost entirely in the interior of the glass where no $Ru(bpy)_3^{2+}$ is adsorbed, despite the fact that the surface coverage due to $Ru(bpy)_3^{2+}$ in the those region where it distributes is $\leq$ 2 %. Taking 18 % as the percent of the volume of the glass that is occupied by $Ru(bpy)_3^{2+}$, adsorption of 5×10^{-7} moles/g corresponds to the effective concentration in the impregnated region of ca. 2.6×10^{-6} mole/g. This 20-fold difference in adsobate concentrations in different regions of the support is rather surprising in view

Figure 46. Absorption spectrum of Cu^{2+} in aqueous solution adn adsorbed on PVG.

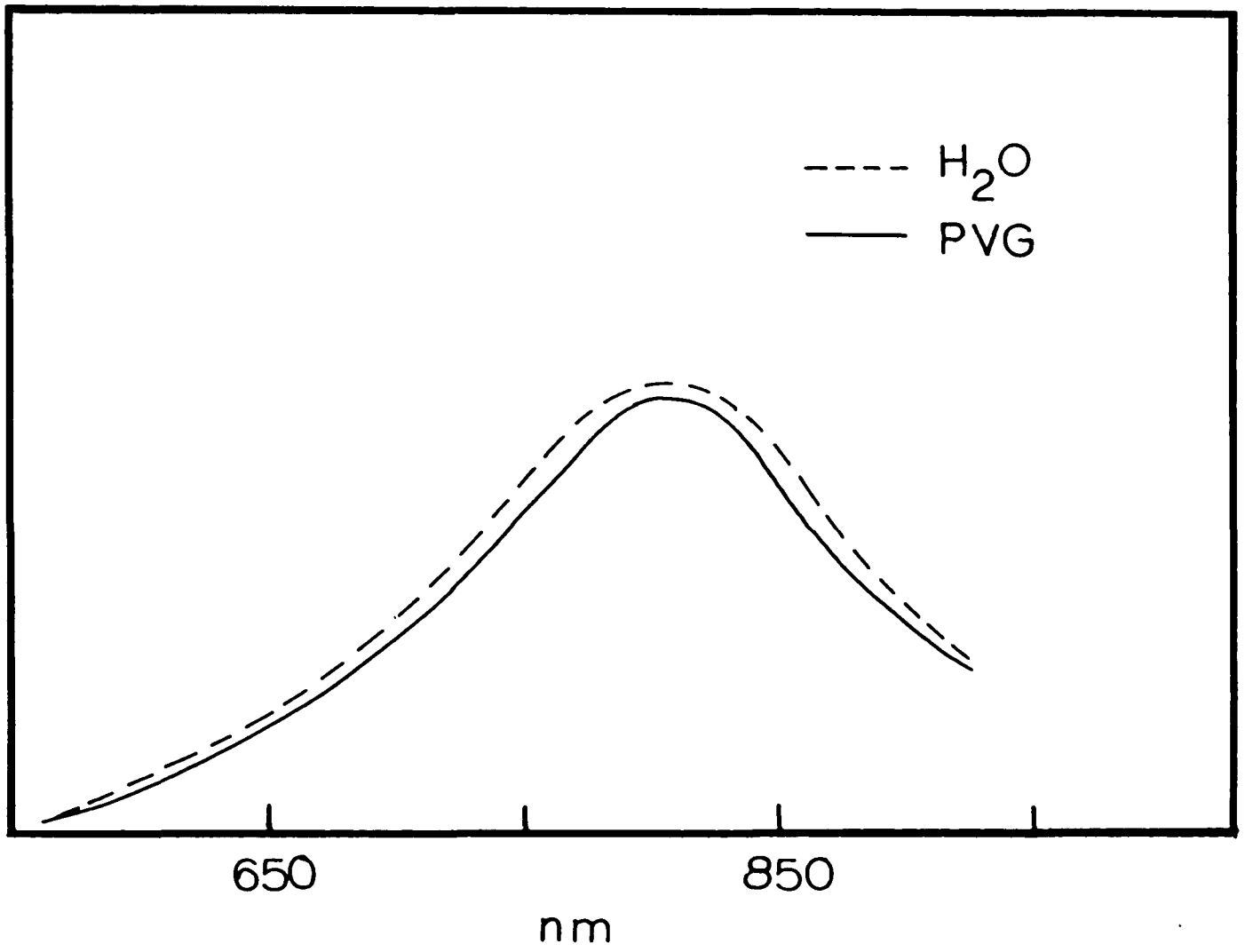
H2O
PVG
650
850
nm

of the random distribution of the surface adsorption sites. It is, however,understandable if the nature of the adsorption process and the differences between the two molecules are taken into consideration. First, the different adsorbate concentrations in different volume of the glass sample does not result in net charge unbalance. This is due to the fact that the adsorption is, to a large extent, an cation exchange process in which the incoming metal ions displace the hydrogen ions from the surface silanol groups, and as such the total surface charge will remain nearly constant at constant solution pH. Secondly, the two molecules have very different sizes. $Ru(bpy)_3^{2+}$ has a radius of ca. 7.5 Å, whereas the hydrated Cu(II) ion has a radius of ca.2.5 Å. The cross sectional area of the two molecules, therefore, differ by a factor of 9. If it is assumed that distribution of adsorbates on the PVG surface requires uniform coverage of the surface area, then areas covered by the two compounds will have a different number of adsorbates per unit area, due to the molecular size difference. Since $Ru(bpy)_3^{2+}$ can only adsorb on the outer surface of the glass, whereas Cu^{2+} can penetrate into the interior, the presence of the complex in the glass will affect the distribution of the copper ions so that the first ions will penetrate into the interior of the glass until a surface coverage in that volume of the glass reaches that on the outer surface that is covered by $Ru(bpy)_3^{2+}$. Thus, distribution of Cu^{2+} on the outer surface will not begin until after this critical concentration is reached. Quantitatively, the distribution of the copper ion

on the outer surface already impregnated with $Ru(bpy)_3^{2+}$ can be described by the following equation

$$n_{Cu}/\text{per Ru} = V_{Ru}/V_t \left(N_{Cu}/N_{Ru} - V_{Cu}/V_{Ru}\, A_{Ru}/A_{Cu}\right) \qquad (36)$$

where n_{Cu} is the number of copper ions in the $Ru(bpy)_3^{2+}$ impregnated region for every molecule of the complex, and N is the total amount of the adsorbate (Cu^{2+} or $Ru(bpy)_3^{2+}$). V_t, V_{Cu}, and V_{Ru} are the total volume of the glass sample, the volumes that is occupied by the copper ion and the complex, respectively. A_{Ru} and A_{Cu} are the cross sectional areas of the two adsorbates.

Equation 36 yields the effective concentration of the copper ion in the 0.4 mm thick framwork of the 4.5 mm PVG sample. Substituting the cross sectional areas of $Ru(bpy)_3^{2+}$ and Cu^{2+}, 170 $\mathring{A}^2$ and 20 $\mathring{A}^2$, respectively, and the respective volumes, i.e., V_{Ru}/V_t = 18 %, and V_{Cu}/V_{Ru} = 4.6 , equation 36 reduces to

$$n_{Cu}/\text{per Ru} = 0.18\ (N_{Cu}/N_{Ru} - 41) \qquad (37)$$

A schematic representation of equation 37 is shown in Figure 47. For every $Ru(bpy)_3^{2+}$ adsorbed on the glass, more than 41 Cu^{2+} must be adsorbed in the interior of the glass before it begins to distribute into the area occupied by $Ru(bpy)_3^{2+}$. This means that for a $Ru(bpy)_3^{2+}$ concentration of 5×10^{-7} mole/g, at least 2×10^{-5} mole/g of the copper ions must be adsorbed in the interior in order to have a non-zero distribution of copper on the outer surface. After this

Figure 47. Schematic representation of Cu^{2+} distribution on PVG in the presence of $Ru(bpy)_3^{2+}$. $Ru(bpy)_3^{2+}$ adsorbs exclusively on the outer surfaces of PVG. The first Cu^{2+} ions tend to adsorb in the interior of the PVG sample. Only after the surface coverage of the interior by Cu^{2+} approaches that on the outer surface by $Ru(bpy)_3^{2+}$, Cu^{2+} begin to distribute on the outer surface.

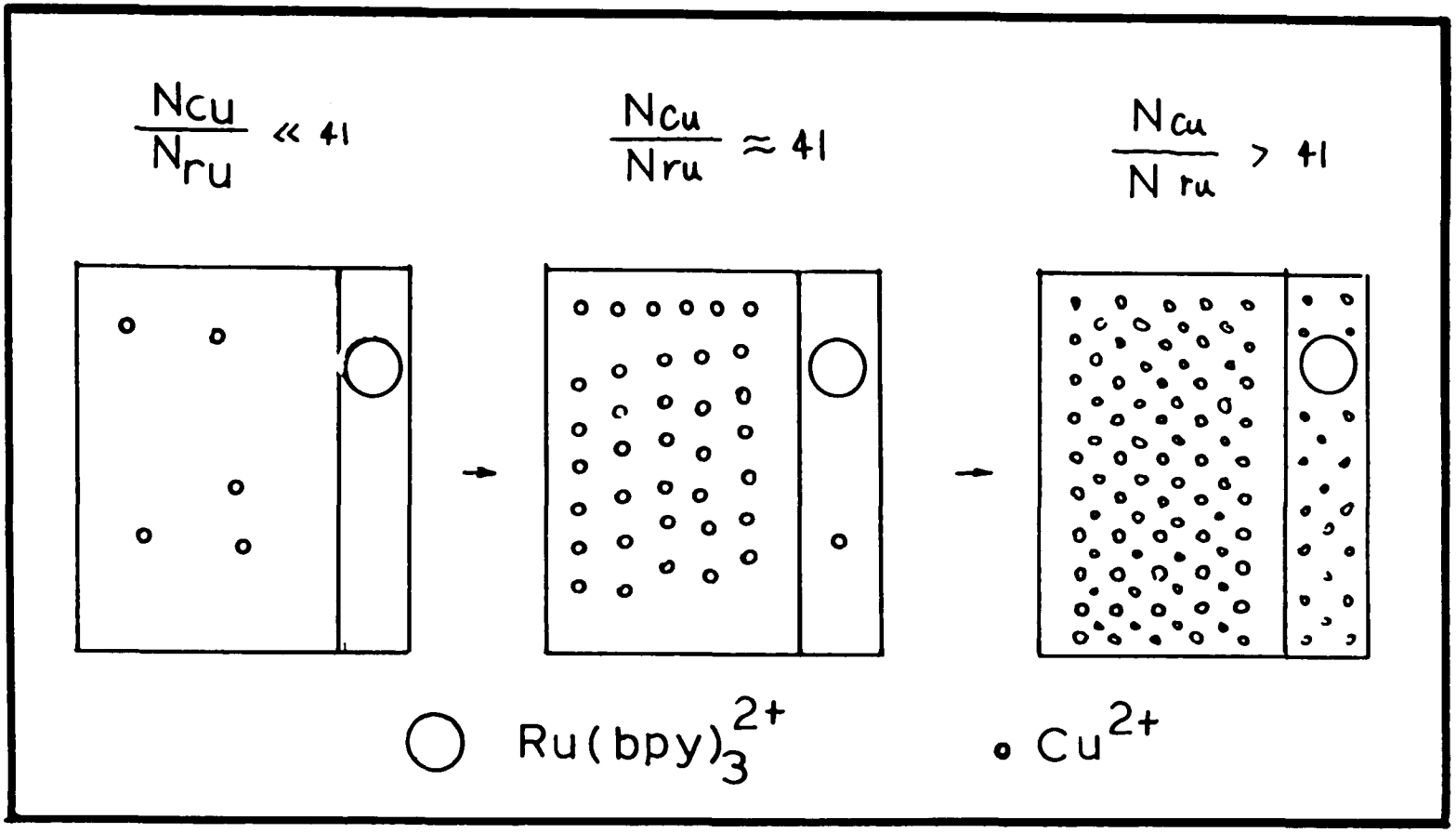
$\frac{N_{Cu}}{N_{Ru}} \ll 41$
$\frac{N_{Cu}}{N_{Ru}} \approx 41$
$\frac{N_{Cu}}{N_{Ru}} > 41$
$Ru(bpy)_3^{2+}$
Cu^{2+}

"critical concentration" is reached, the concentration of Cu^{2+} in the outer surface increases linearly with the total amount of the adsorbed ion. This was indeed observed experimentally. Figure 48 compares the values of n_{Cu} predicted by eq. 37 and that obtained by grinding experiments, as a function of the ratio of the total amount of the copper ion to that of adsorbed $Ru(bpy)_3^{2+}$.

This description of the adsorption of Cu^{2+} on the PVG samples is also consistent with the observed quenching of $*Ru(bpy)_3^{2+}$ by adsorbed copper ion, as shown in Figures 33 and 36. No quenching is observed with increasing copper impregnation until ca. 5×10^{-5} mole/g of the ion is adsorbed. This occurs because only those copper ions that are distributed in those regions where $Ru(bpy)_3^{2+}$ adsorbs can react with the excited complex. Since there is no Cu^{2+} in those regions at concentrations below 5×10^{-5} mole/g, no quenching will occur. At higher Cu^{2+} concentrations, however, the Stern-Vlomer plot becomes "normal" because the effective copper concentration begins to increase linearly with the total amount of the adsorbed ion. The "critical concentration" obtained from the experiments, 5×10^{-5}mole/g, is somewhat higher than the value predicted by eq. 37, ca. 2×10^{-5} mole/g. However, considering the approximations made regarding the size of the adsorbed ions and their corresponding volumes, the agreement between the two values must be considered within experimental error.

Figure 48. Number of Cu^{2+} ions on the outer surface of PVG per $Ru(bpy)_3^{2+}$ ion as a function of the total Cu^{2+} amount. Solid curve is the calculated value using eq.37, and points are the experimental values.

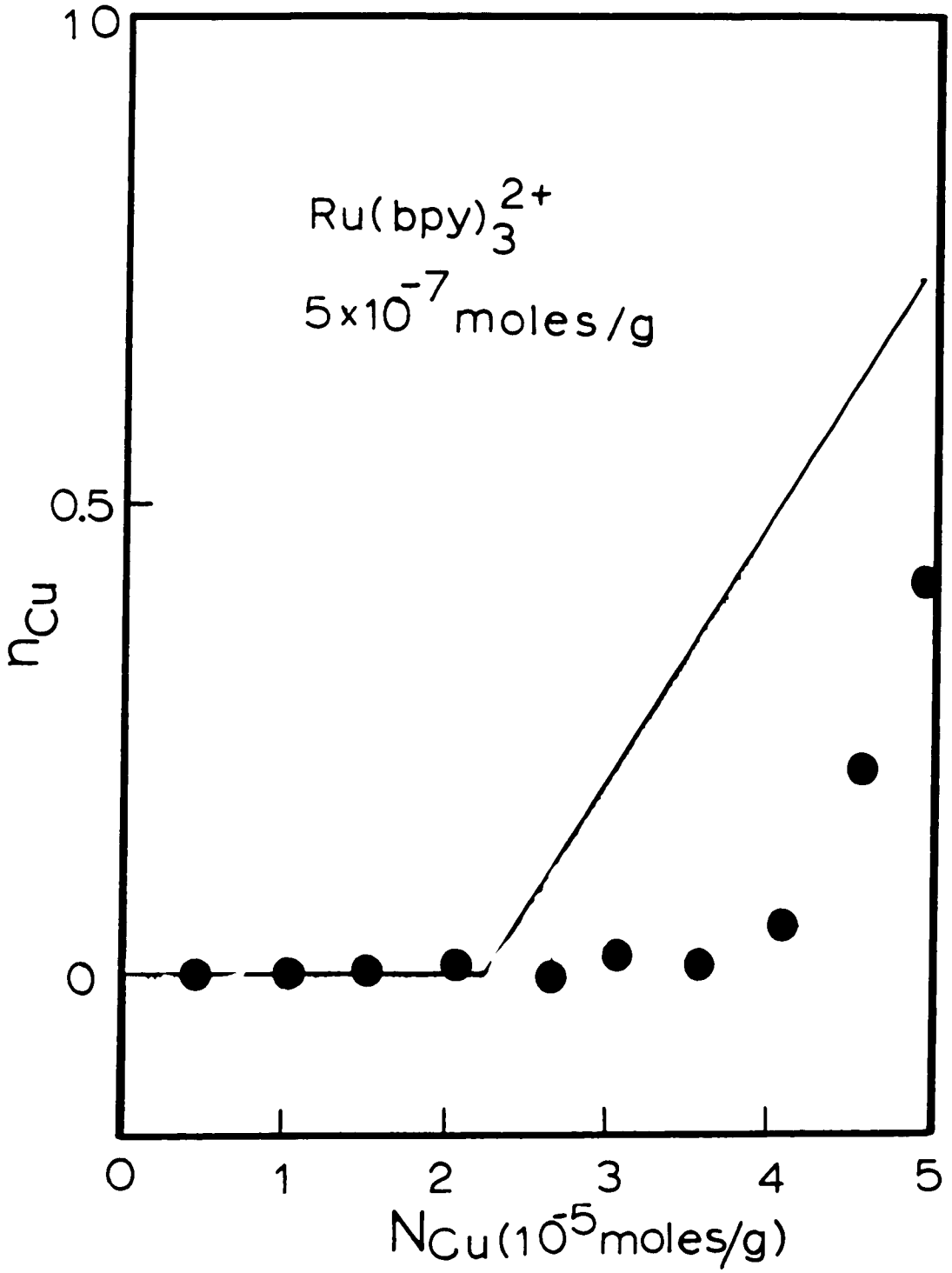
10
0.5
0
n_{Cu}
$Ru(bpy)_3^{2+}$
5×10^{-7} moles/g
0
1
2
3
4
5
$N_{Cu}(10^{-5}$ moles/g)

D. Excited State Properties of Adsorbed $Ru(bpy)_3^{2+}$

1. Resonance Raman Studies

Resonance Raman spectroscopy provides a powerful tool for investigating the structural and geometrical features of both ground state and excited state properties of transition metal complexes. The resonance Raman spectroscopy of $Ru(bpy)_3^{2+}$, in particular, has been extensively examined. As shown in Figure 22, excitation of aqueous solution of $Ru(bpy)_3^{2+}$ with 457.9 nm laser light reveals seven resonance bands in the 1000 cm^{-1} - 1600 cm^{-1} frequency region. These bands, which are typically observed in the charge transfer and pi-pi* transition enhanced resonance Raman spectra of other bipyridine complexes, have been assigned to the symmetric in-plane C-C and C-N stretches of the bipyridine rings of $Ru(bpy)_3^{2+}$. Adsorption of $Ru(bpy)_3^{2+}$ onto PVG does not shift the positions of the seven vibrational bands, $v \leq 1$ cm^{-1}, from the aqueous solution spectrum (Figure 22). The spectral agreement establishes that adsorption does not structually distorted the complex in its electronic ground state. This is consistent with the similarity of the UV-visible spectra of the complex in the two media which shows that adsorption does not disrupt the primary coordination sphere of the complex. However, the significant change in the relative intensity of the 1492 cm^{-1} band, the most intense band in the spectrum, is worth noting. The intensity of a Raman band resonant with an electronic transition is related to the change in the

equalibrium position of the corresponding vibrational mode upon excitation to the electronically excited state[199]

$$I = \Delta_s^2 \nu_s^4 [(\nu_{em} - \nu_0 + i\Gamma)(\nu_{em} + \nu_s - \nu_0 + i\Gamma)]^{-2} \qquad (38)$$

The origin shift, Δ , represents the shift in equilibrium position of the vibrational mode with an electronic transition. ν_{em}, ν_s, and ν_0, represent the frequencies of the 0-0 electronic transition, the Raman scattering, and the laser excitation,respectively. Γ is a damping factor which is generally taken as the absorption band width. Since the electronic absorption spectrum and the resonant bipyridine frequencies of the adsorbed complex are within experimental error of those in aqueous solution, the frequecy portion of eq 38 are equivalent in both media. Substituting the relative intensities of the 1492 cm^{-1} band, measured relative to the intensity of the 1609 cm^{-1} band, 4.4 in water and 2.5 when adsorbed on PVG, into eq. 38, leads to a change in the origin shift of the corresponding vibrational mode

$$\Delta_{PVG}^{1492} = 0.75\, \Delta_{water}^{1492} \qquad (39)$$

which indicates that the origin shift of the 1492 cm^{-1} vibration is reduced by 25 % when the complex is adsorbed onto PVG from aqueous solution. Since the origin shifts characterize the excited state geometry of a molecule, their changes in different media reflect the effects of the environment on the excited state properties of the molecule and, in this particular example at least, the excited state is more susceptible to environmental changes thanis the

ground state, since no structural distortion of the ground state molecule is observed for the surface adsorbed complex.

The cause of the change in the excited state geometry can be sought from the differences between the two media. Since the primary interaction between the adsorbed complex and the surface is electrostatic, change in polarity on going from aqueous solution to PVG might cause the observed reduction in the excited state origin shifts. In the MLCT excited state, where the charge has been transferred to a ligand, the complex is more polar than the ground state of the complex. The surface polarity of silica, which possesses hydroxylated surface like PVG, has been estimated to be greater than methanol but smaller than water.[191] Consequently, the more polar excited state may be less able to distort on PVG than in water. This explanation, however, is inconsistent with the observation that the relative intensities of the seven bands are identical in solutions of different polarities, e.g. water, ethanol, and methanol. The similarity of the Raman intensities in water and in the alcohols indicates that polarity is not the cause of the intensity change observed in PVG.

A more plausible explanation is the rigidity of the environment experienced by the adsorbed complex. The complex is rigidly held on the PVG surface and, as shown by the emission polarization data, is not free to rotate. Hence, it is considerably more constrained by PVG than by water, where

no emission polarization occur at room temperature. Although such constraints are not detectable when the complex is in the ground state, it could be "felt" by the molecule in the electronically excited state where the molecule is geometrically different and, generally, is larger. The 1492 cm^{-1} band, being the most intense band in the spectrum, plays a significant role in distorting the ground state to the excited state. Indeed, the displacements of bond lengths in the excited state have been examined for a series of Os bipyridine complexes and it has been shown that the vibration represented by the 1492 cm^{-1} band in these complexes shows the greatest displacement upon electronic excitation. The average bond length displacement for this vibration is 0.0173 A, as compared to 0.0134 A for the next most significant displacement.[197] As such, this particular mode can be the most sensitive to any constraints imposed by a rigid environment. Similar reduction of the 1492 cm^{-1} band intensity has also been observed when $Ru(bpy)_3^{2+}$ is bonded to DNA molecules, where the complex is held within the grooves of the double helix.[198] Intercalation of the complex into certain clay layers appears to produce the same effect, although the authors did not offer any detailed explanations.[119]

2. Emission Quantum Yields

The emission spectrum of $Ru(bpy)_3^{2+}$ adsorbed onto PVG closely resembles that in aqueous solution (Figure 20).

However, the excited state lifetime of the adsorbed complex, 780 ns, is 35 % longer than that in the aqueous solution, 580 ns, and the emission quantum yield of the adsorbed complex at room temperature, 0.12, is larger than that in solution, 0.042 (Table 6). Both the excited state lifetime and the emission quantum yield are determined by the radiative (k_r) and non-radiative (k_{nr})decay rate constants according to the equations[56]

$$\phi = k_r \times \tau(T) \times \eta_{isc} \qquad (40)$$

$$\phi(T) = 1/(k_r + k_{nr} + k_0 \exp[-\Delta E/kT]) \qquad (41)$$

where τ is the measured emission lifetime and the exponential term represents a temperature dependent deactivation route. At room temperature, the intersystem crossing efficiency for the complex in aqueous solution is unity. Substituting the values 0.12 and 780 ns for quantum yield and lifetime for the adsorbed complex, and 0.042 and 580 ns for aqueous solution, k_r values in the two media are $1.54 \times 10^5 s^{-1}$ and $0.72 \times 10^5\ s^{-1}$, respectively.
Using these values of the radiative rate constant, the overall non-radiative rates constant k_{nr}'

$$k_{nr}' = k_{nr} + k_0 \exp(-\Delta E/kT) \qquad (42)$$

can be calculated from eq. (41). The values thus obtained are $1.13 \times 10^6\ s^{-1}$ for PVG and $1.65 \times 10^6\ s^{-1}$ for aqueous solution.

As shown in eq.(41), the non-radiative deactivation of

the $Ru(bpy)_3^{2+}$ MLCT state proceeds by a temperature independent vibrational coupling to the surrounding solvent molecules, and by thermal population to the non-emissive, dd states. The latter, lie ca. 3600 cm^{-1} above the emisive MLCT state, either decay directly to the ground state, or undergo a photosubstitution reaction.[42] A recent estimate shows that the dd states account for ca. 25 % of the non-radiative decay at room temperature in aqueous solution.[56] Since the dd states are in thermal equilibrium with the MLCT state, an increase of the energy diffrence between the two states, E, will decreased the deactivation via this pathway. However, a change in E will not account for the observed decrease in non-radiative decay rate of the adsorbed complex. The similarities in the emission spectra establish that the energy level of the emissive MLCT state of the complex in both PVG and water are essentially identical. In addition, these is no evidence that the energy level of the dd states changes when $Ru(bpy)_3^{2+}$ is adsorbed onto to PVG from aqueous solution. Non-radiative decay of the excited state through dd states seems to proceed at the same rate in both media.

The decrease in the non-radiative decay rate of the adsorbed complex must then arise from the vibrational deactivation through solvent, which is represented, in eq.41, by the rate constant k_{nr}. In aqueous solution, this is thought to occur by hydrogen bonding of the surrounding water molecules to the bipyridine ligands. In D_2O, k_{nr} is ca. 40 % of the value found in H_2O.[42] The rigid environment of

SiO_2 powders,[111] polymerized silica,[110] and cellulose matrices,[120] for example, affect the deactivation of adsorbed $Ru(bpy)_3^{2+}$. Although the PVG surface is hydrated at room temperature, the tight binding of the complex to the surface groups may impose a similar rigidity and curtail non-radiative relaxation. The temperature dependence of the emission quantum yields in PVG and water is also consistent with this mechanism. As shown in Figure 27, the difference in emission quantum yields at high temperatures is smaller than that at lower temperature. Since deactivation pricipally occurs through the dd state at high temperatures, and both wates and PVG have the same decay rates for this pathway, the difference in emission quantum yields at high temperatures become less than that at lower temperatures. At room temperature, deactivation through the dd state accounts for only 25 % of the non-radiative deactivation. Consequently,the gap in emission quantum yields in the two media widens due to their differnt efficiencies in vibrational coupling, which is now the major deactivation mode.

The other factor that contributes to the increased emission quantum yield of the adsorbed $Ru(bpy)_3^{2+}$ is an increase in the radiative rate, k_r. k_r is related to the Einstein coefficient for sponteneous emission[200]

$$k_r = 4E_{em}^3/3h^4 \left| \psi \, d \, {}^*\psi \right|^2 \qquad (43)$$

where E_{em} is the emission energy, ψ and ${}^*\psi$ are the wave functions of the excited state and the ground state,

respectively, and d is the transition dipole moment operator. A difference in emission energy could result in different radiative rate constant, but as metioned above, the emission energy of $Ru(bpy)_3^{2+}$ in PVG and in water are identical and the different rate constants in the two media is not due to the energy factor. A possible mechanism involving the transition moment integral can be suggested, however. Resonance Raman intensity measurements in the two media suggest that the excited state geometry of the adsorbed complex is less able to distort relative to the ground state structure than it is in aqueous solution. Although this structural change occurs with the spectroscopically allowed 452 nm transition which populates not the emissive triplet MLCT state but that prior to intersystem crossing, it is possible that this change can be carried over to the emissive state. As such the emissive state is more closely related, structually, to the ground state than in fluid solution. Hence, the nuclear displacements accompanying the radiative transition may be less demanding and the radiative rate of the adsorbed complex larger than in the solutions. Increases in the emission quantum yield have been reported for $Ru(bpy)_3^{2+}$ incorporated into polymerized silica and attributed to an increased radiative rate.[110]

3. Biphotonic Processes on PVG

a) Biphotonic Emission of Adsorbed $Ru(bpy)_3^{2+}$

The emission, which occurs at 510 nm following high intensity laser excitation of $Ru(bpy)_3^{2+}$ adsorbed on PVG,exhibits a second order dependence on the excitation intensity (Figure 31). Thus the occurence of the 510 nm emission follows biphotonic excitation. Such an emission has not been reported for the complex in solutions or adsorbed on other solid supports. Although a detailed mechanism for this anomalous emission has yet to be developed, the data gathered in this study suggest possible origins of this emission. Attributing the 510 nm emission to formation of a luminescent photoproduct or a blue shift in the normal 610 nm emission caused by binding to PVG is not consistent with the available experimental results. UV-visible absorption spectra of the impregnated PVG sample recorded before and after exposure to the laser pulses are identical within experimental error. Also, the emission intensity is independent, at least through twenty excitation pulses, of the number of times the sample was exposed to the laser pulse. Absorption, low intensity excited emission, and resonance Raman spectra of the adsorbed complex offer no indication of an adsorbate-adsorbent interaction that might account for a blue shift of the 610 nmband. Furthermore, the difference in emission maxima, 3200 cm^{-1}, is considerably larger than the 1100 cm^{-1} shift found when the complex is adsorbed onto colloidal silica surface, although both materials have similar anionic surfaces.

The available data suggest two possible explanations. First, the 510 nmband is actually a difference spectrum in

which the 610 nm emission is being partially absorbed. Flash photolysis experiments show that the adsorbed complex undergoes biphotonic photoionization similar to that found in aqueous solution, and that the photodetached electron persists ca. 0.5 - 2 microseconds on PVG. Since the absorption spectrum of the electron, λ_{max} = 650 nm, overlaps the $Ru(bpy)_3^{2+}$ charge transfer emission, the latter will be partially absorbed, giving the impression of a blue shift.

Alternatively, the 510 nm band is a emission from a higher energy excited state. Although this is contrary to the currently accepted picture that only the lowest energy MLCT of $Ru(bpy)_3^{2+}$ is emissive, the increase in energy found in these experiments, ca. 3200 cm^{-1},is similar to the calculated energy gap, 3600 cm^{-1}, between the emissive MLCT state and the dd states.[42] In aqueous solutions, the latter are non-luminescent, but do initiate photosubstitution.[43,44,45] With the adsorbed complex, however, the emission intensity of the 510 nm band is proportional to I_{exc}^2, indicating that the emissive state is populated from higher excited state. Relaxation of this initially populated state may pass through a previouly unknown luminescent level or a component of the dd manifold which, because of the constraints imposed by PVG surface, is unable to photosubstitute, but will luminesce.

b) The Activation Energy of $Ru(bpy)_3^{2+}$ Disproportionation

Previous experiments have established biphotonic photoionization of $Ru(bpy)_3^{2+}$ on PVG and the subsequent

reduction of a second $Ru(bpy)_3^{2+}$ molecule by the photodetached electron. The proposed mechanism for this reaction (equations 27-29) involve surface conduction where the photodetached electron resides in shallow surface trap before its reaction with the second complex molecule,

$$Ru(bpy)_3^{2+} + hv \text{ -----> } {}^*Ru(bpy)_3^{2+} \quad (27)$$

$${}^*Ru(bpy)_3^{2+} + hv \text{ -----> } Ru(bpy)_3^{3+} + e^- \quad (28)$$

$$e^- + Ru(bpy)_3^{2+} \text{ -----> } Ru(bpy)_3^{+} \quad (29)$$

where e^- represents the detached electron on the PVG surface. A detailed analysis of flash photolysis data suggests that the reduction of the complex (reaction 29) is thermally activated.[160] Consequently, the temperature dependence of the quantum yield of $Ru(bpy)_3^{+}$ was determined. Continueous photolysis of PVG samples impregnated with 1.5×10^{-6} mole of $Ru(bpy)_3^{2+}$ per gram of PVG at various temperatures indeed results in different quantum yields of the photoproduct, $Ru(bpy)_3^{+}$ (Table 8). The energy of activation , calculated from the slope of plot in Figure 39, is 4.5 kcal/mole. The temperature dependence of emission polarization establishes that the translational barrier of the adsorbed complex is very high. Therefore, this relatively small activation energy must correspond to the activation of the surface trapped electron.

E. Photoredox Chemistry of $Ru(bpy)_3^{2+}$ on PVG

1. Intensity Quenching of $*Ru(bpy)_3^{2+}$ Emission

A comparison of the rate constants for $*Ru(bpy)_3^{2+}$ emission quenching in aqueous solution and on the PVG surface listed in table 10 shows substantial reduction in the reaction rates. For Cr^{3+}, Fe^{3+}, Cu^{2+}, and MV^{2+}, the rates of quenchingon PVG are considerably slower than those in aqueous solutions. The reduction in the rate constants may arise from a number of causes, but one of particular importance is the curtailed mobility of the reagents on the PVG surface. In the interfacial systems, where the $Ru(bpy)_3^{2+}$ impregnated PVG samples were placed in aqueous solutions of Cu^{2+} or MV^{2+}, emission quenching occurs at rates that are two or three times lower than that in fluid solution (Figures 34 and 35). In view of the similarities of the absorption and emission spectra of the complex in aqueous solution and on PVG, it is unlikely that the reduced rate is due to any change in the redox properties of the adsorbed complex. Rather, since the quenching by Cu^{2+} and MV^{2+} are essentially diffusion limited in fluid solutions, the reduction in rates most likely reflectsa reduced rate of diffusion. Although the quenchers are free to move in the aqueous phase, the excited complex is immobilized on the glass surface. Furthermore, the access of the quenchers to the excited complex may also be hampered by the finite sizes of pores on the PVG surface and diffusion of molecules in PVG is not as rapid as in solvent.

When both the complex and the quencher molecules are adsorbed on PVG, the reaction rate is affected by the

TABLE 10

A Comparison of $Ru(bpy)_3^{2+}$ Emission Quenching Rates in Water and on Porous Vycor Glass

Quencher	H_2O	H_2O/PVG [a]	PVG
Fe^{3+}	2.7×10^9	--	1.2×10^8
Cr^{3+}	1.2×10^7	--	1.0×10^7
Cu^{2+}	7.6×10^7	2.3×10^7	1.3×10^7
MV^{2+}	5.6×10^8	2.2×10^8	5.6×10^6

a. $Ru(bpy)_3^{2+}$ adsorbed on PVG, quencher in aqueous phase.

diffusion rate of the particular quencher, which varies considerably, depending upon the adsorption characteristics. As discussed in the preceding section, Cu^{2+} is the least strongly bound metal ion on the PVG surface and appears to be able tomoverelatively freely.On the other hand, Fe^{3+} adsorption is strong and its mobility on the surface appears to be more severly retarded. The quenching rates of these two metal ions on PVG reflect this difference. Compared to their respective quenching rates in aqueous solutions, the rate of Fe^{3+} adsorbed on PVG is reduced by a factor of 14, whereas that of the adsorbed Cu^{2+} is reduced by 6 fold (Table 10). Curtailment of quenching rate by Cu^{2+} has been reported for the clay-$Ru(bpy)_3^{2+}$-Cu^{2+} system.[134] The rate constant, 1.9 x 10^7 M^{-1} s^{-1} is similar to the value found for the reagents adsorbed PVG. Differences in the diffusion rate also appear to be responsible for $Ru(bpy)_3^{2+}$ quenching by coadsorbed Fe and Cu on a cation exchange resin. In those experiments, the quenching rate constant for Cu^{2+} is essentially the same as that in aqueous solution, but that for adsorbed Fe^{3+} is reduced to ca. 30 % of the solution value.[115]

Another factor that influences bimolecular reaction rate on a support is the surface dimensionality. For long distance electronic energy transfer between a donor and an acceptor Klafter and Blummen have shown that the reaction rate depends on the medium's Hausdorf dimension d according to the equation[201]

$$P(t) = \exp[-r(t/\tau)^{d/6} - (t/\tau)] \qquad (44)$$

where P(t) is the survival probability of the excited state (the energy donor) at time t, τ is the excited state lifetime, d is the Hausdorff demension of the medium, and r is related to the concentrations of the donor and quencher. Experiments based on this model have been carried out on the surfaces of silica and PVG by examining energy transfer between Rhodamine B and malachite green.[185,186] The energy transfer rate obtained for silica, which has a Hausdorff dimension of 3.0, is identical to that observed in methanol solution, which is also three-dimensional. The rate of reaction on the PVG surface, however, is substantially slower, despite the close resemblence of the two supports in their surface chemical properties. Although the specific quantitative treatment of electron transfer processes may differ from the energy transfer reactions in terms of the dimension effects, a qualitative comparison of electron transfer rates in silica and PVG clearly demonstrates the difference. In porous silica colloids, $Ru(bpy)_3^{2+}$ emission is quenched by MV^{2+} with a bimolecular rate constant of ca. 2×10^9 $M^{-1}s^{-1}$.[110] This value is within experimental error of that found in aqueous solution, 1.0×10^9 $M^{-1}s^{-1}$. On the other hand, the corresponding rate constant for the PVG adsorbed reagents is $\leqslant 6 \times 10^6$ $M^{-1}s^{-1}$. Although the currently available d values for PVG, 1.74 + 0.12 and 2.0, do not agree exactly with each other, they both are substantially lower than the d value for silica, 3.0, which has been consistently

obtained by a number of indepndent measurements. A quenching rate constant of $k_q = 1.8 \times 10^6\ M^{-1}s^{-1}$ has been reported when the $Ru(bpy)_3^{2+}$ and MV^{2+} are adsorbed into clay membranes. Molecular adsorption data indicate that the clay has a Hausdorff dimention of 2.0.[202] Although the exact cause of the unusually low quenching rate in the clays is not clear, the similarity of the Hausdorff dimensions between the clays and PVG, and their parallel quenching rates does suggest the possible presence of links between the bimolecular reaction rates and the dimensionality of the media.

The effect of the Hausdorff dimension of the surface on a bimolecular reaction can be described as a limitation of accessibility that the surface imposes on the reacting molecules. Simplified illustrations of this accessibility in 1,2, and 3-dimensional environments are shown in Figure 49. In case A, where the reagents are in three dimensional space, e.g., a solution, the molecule that is to undergo a bimoleclar reaction with a second molecule can, in priciple, be approached by the latter from all directions in the space. In case B,on a two-dimensional plane, however, the central molecule can now be reached only by those that are on the same plane. In other words, the number of molecules that have access to the central molecul is reduced because of the reduced dimensionality of the space in which the reaction is to take place. When the dimensionality of the environment is further reduced to 1, as in Figure 49 case C, the reacting

Figure 49. A simplified representation of the effects of environment dimensionality on bimolecular reactions. In 3-dimentioal space, the molecule at center can be approached by many other molecules. The number of molecules that have access to the ceter molecule declines as the dimensionality of the environment decreases.

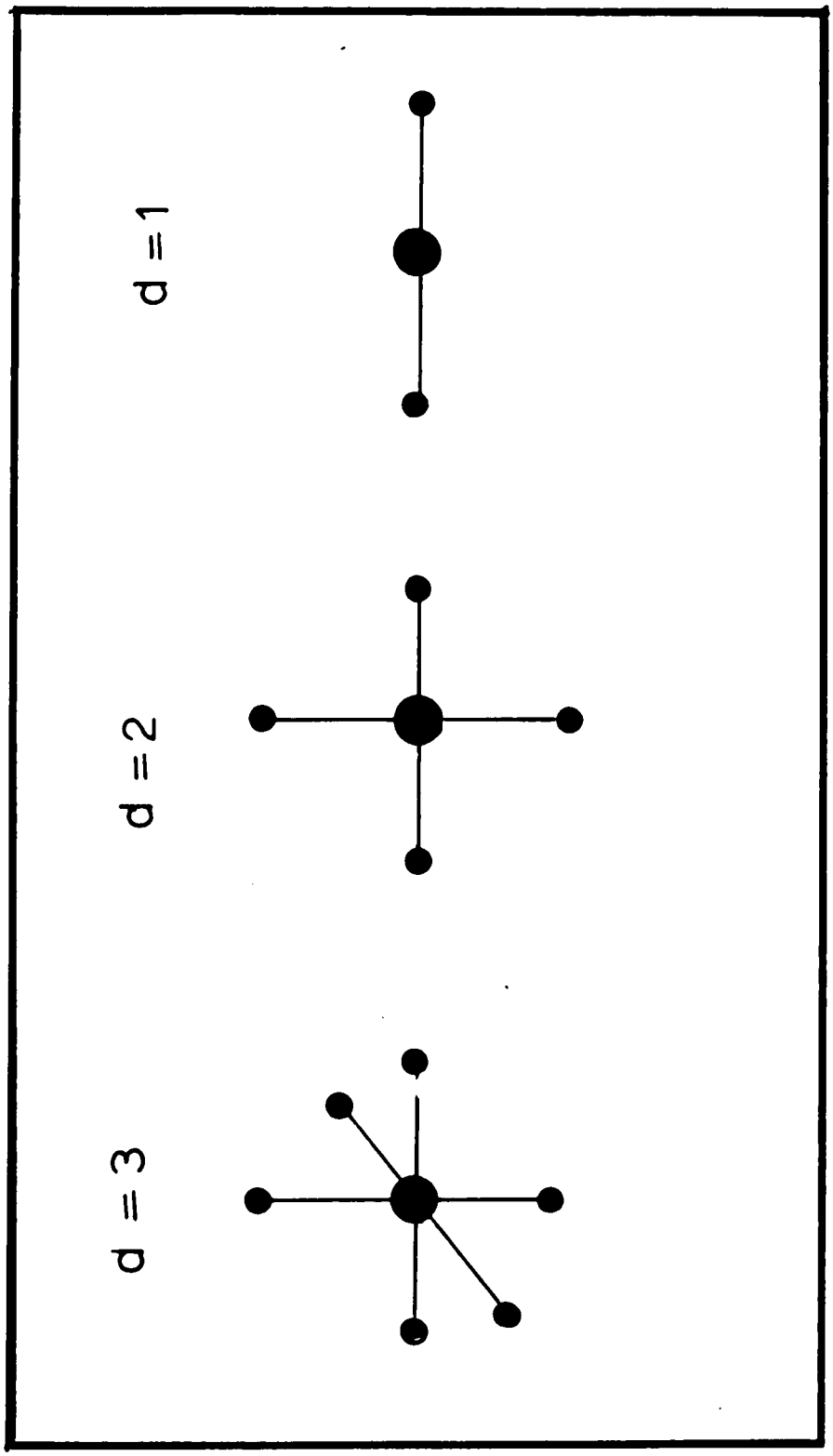
d = 1
d = 2
d = 3

molecules are situated in a "tunnel-like" environment, and the accessibility of any of them by the others is extremely limited. Thus, the Hausdorf dimensions serve to define, in a sense, the degree of accessibility for an object in a given space.

This picture, alghough oversimlified, illustrates the geometric effect on a chemical process. The effect is usually neglected in solution rections since all solutions are three-dimensional. However, when a reaction is to take place on surfaces, the question of surface dimensionality arises because, in general, the surface is not a perfect plane and may have a dimensionality $2 < D < 3$, determined only by the actual surface geometry of the particular material.

2. Lifetime Quenching of $*Ru(bpy)_3^{2+}$

In fluid solutions where the molecules can move freely, the excited state emission of $Ru(bpy)_3^{2+}$ is quenched, either by cationic or neutral quenchers, by a pure dynamic process, where quenching takes place within the collisional distance of the two molecules. The Stern-Volmer plot for such a process can be obtained from either the intensity quenching(I_0/I vs. [Q]) or lifetime quenching (τ_0/τ vs.[Q]), with identical slopes. When the emission quenching takes place on the PVG surface, however, large discrepancy between the two plots is found for each of the quenching reactions studied (Figures 32, 36-38). In all cases, the extent of lifetime quenching is substantially less than that of the intensity

quenching. For example, in the presence of 2.0 x 10^{-6}mole of Fe^{3+}/g of PVG, an intensity ratio (I_0/I) of 6 is observed for a PVG sample containing 5 x 10^{-7} mole of $Ru(bpy)_3^{2+}$/g PVG. However, the ratio of lifetimes, tau_0/tau, of this sample remains essentially 1, i.e., no change in the excited state lifetime occurs (Figure 38).

In general, intensity and lifetime quenching differ when one of the following situations occurs: a) the donor(electron or energy) and the acceptor form a complex before excitation. In this case the excited donor will be quenched the moment it is excited, since there is no need for the reactants to migrate together. For those donor molecules which are not associated with the acceptor, their emission will not be quenched at all and the excited state decays as if no quencher is present. The experimentally observed excited state lifetime is then the lifetime of the unquenched donors, $\tau_0/\tau = 1$. This situation is schematically depicted in Figure 50. Such purely static quenching processes have been observed when the donor and the acceptor bear opposite charges, e.g., $Ru(bpy)_3^{2+}$ quenching by $Fe(CN)_6^{2-}$ in aqueous solution.[203]

b) When diffusion of the reactants is slow compared to the excited state's natural lifetime, or, in an extreme case, when the reactants are in a fixed array and do not move. The decay profile in this case can become quite complicated. A theoretical treatment for a random distributionof acceptors

Figure 50. A schematic representation of lifetime quenching in A) a pure dynamic process, B) a pure static process where the donor and quecher forms a ground state complex, and C)ina process where the quenchers and donors are immobilized. The quenched decay in a dynamic process is single exponential but with a shorter lifetime than the unquenched decay. In a static process no change in lifetime occurs. For the fixed quencher-donor system, decay is non-exponential with a fast component and a slow component which approaches the unquenched decay at long t mes.

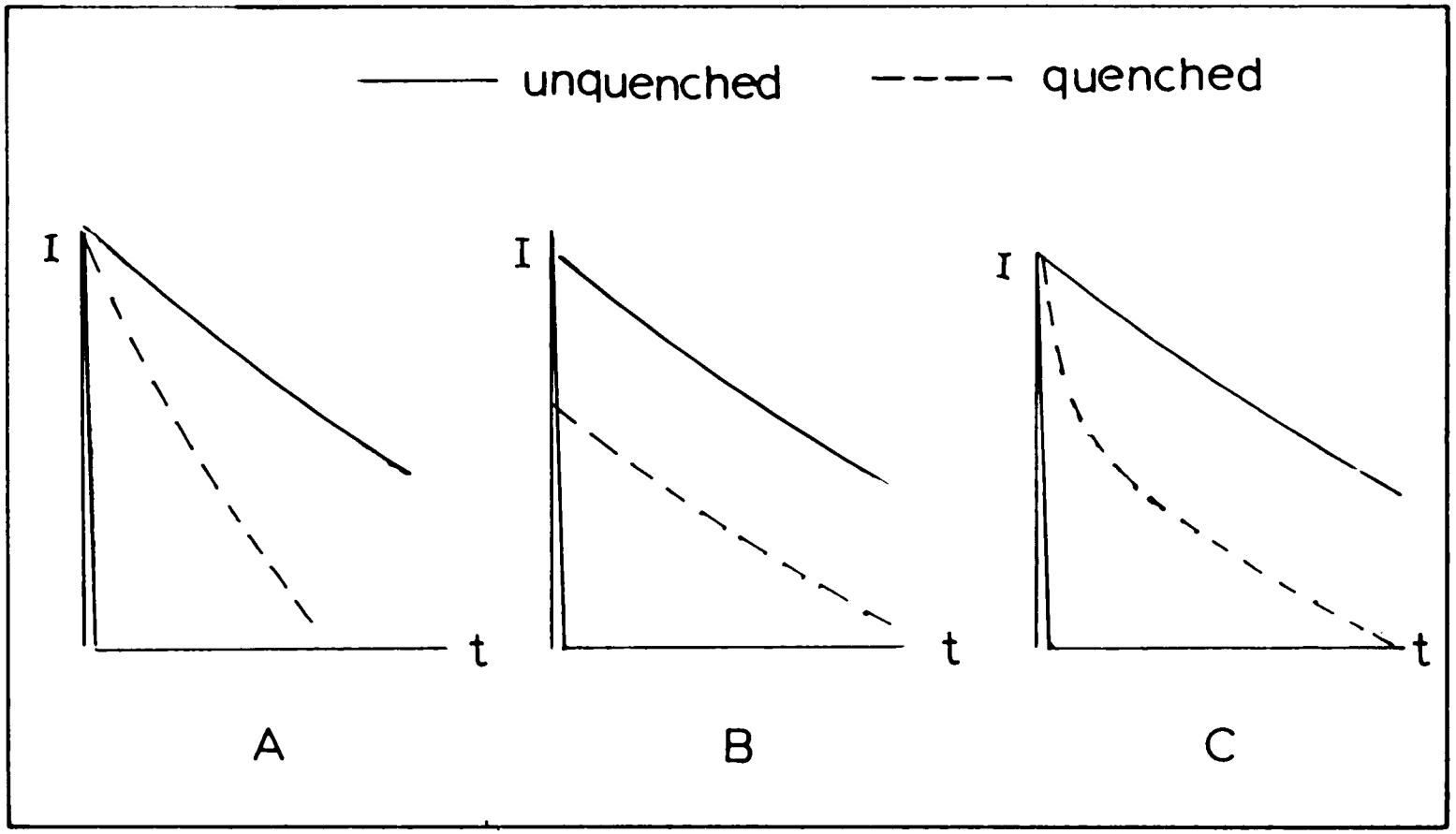
unquenched
quenched
I
t
A
B
C

has led to the equation describing the time dependence of the number of the excited state donor.[204]

$$P(t) = \exp[-t/\tau_0 - \Gamma^{-3} c/c_0 \, g(e\, t/\ _0] \qquad (45)$$

where P is the survival prtobability of the excited state at time t,tau is the lifetime in the absence of quencher, c the concentration of the acceptor,andc_0 the critical concentration ofthe acceptor (concentration at which the quenching rate equals the natural decay rate). The equation, derived by Inokuti and Hirayama for electronic energy transfer processes, also applies to electron transfer reactions. At short times, $t << \tau$, the decay is very fast but, as time passes, the second term in the exponential becomes smaller and the decay approaches a single exponential form. The over all decay pattern, therefore, is one that is grossly non-exponential. Physically, this represents the situation where those donors surrounded by acceptors in close proximity are quenched rapidly. Hence, the fast decay at short times. As the number of such donors declines, the decay approaches a natural decay. This occurs because limited diffusion prevents donors that are far away from the acceptors from being quenched. These isolated donors can only deactivatevia unimolecular processes. A somewhat different model has been suggested by Van Damme and coworkers for electrontransferin clays.[135] However,thismodelalso predicts a rapid initial decay followed by a near-single exponential tail with increasing time (Figure 50 c).

For the emission quenching of $Ru(bpy)_3^{2+}$ by the cationic quenchers on PVG, the first mechanism, ground state complexation of the donor-acceptor pair, seems unlikely in view of the positively charged reactants. Such complexation, in general, results in significant spectral shifts in absorption and excitation spectra,[203] but none observed in these experiments. The more likely explanation for the absence of lifetime quenching on PVG involves the slow diffusion rates of the reactants on the surface. Because of the instrumental limitations, emission lifetimes in these experiments could only be measured with a delay time > 200 - 400 ns, namely, 200 - 400 ns after the excitation pulse. Since the faster component of the non-exponential decay may well be over within this time, what has been observed, according to the Innokuti-Hirayama model, most likely is the "tail" of the real decay. According to eq.45 this appears as a nearly single exponential and with a "lifetime" similar to the unquenched emission. A more quantitative examination is necessary in order to provide a conclusive answer to this question.

3. Mechanism of Formation of Reduced Methyl Viologen on PVG

Due to the rapid, back electron transfer, net formation of the reduced methyl viologen, MV^+, in fluid solutions, has only been observed with the presence of sacrificial electron donors such as EDTA or triethanolamine(TEOA), which reduce

$Ru(bpy)_3^{3+}$ complex in competitively with the back reaction and allow the built-up of the radical cation. In heterogeneous systems, the back reaction rate can be reduced by as much as a thousand fold by the presence of interfacial barriers. Gratzel et al, for example, report the evolution of H_2 during photolysis of a heterogeneous reaction system composed of Pt impregnated n-type TiO_2 colloids, $Ru(bpy)_3^{2+}$, and MV^{2+}. Although no sacrificial reagents were added in this case, TiO_2 was thought to have provided the separation of the photoproducts.[147,148] However, recent evidence indicates that the polyalcohols used to stablize the semiconductor particules were really the ultimate electron source.[152] Thomas and coworkers describe the formation of MV^+ by electron transfer from $Ru(bpy)_3^{2+}$ in a cellulose matrix. The absence of back reaction here was attributed to the reduction of $Ru(bpy)_3^{3+}$ by the cellulose support.[123] Direct evidence of net MV^+ formation, in the absence of external electron donor, obtained in this experiment, appears to be the first system to achieve $Ru(bpy)_3^{2+}$-MV^{2+} charge separation.

The formation of MV^+ or its stability on the glass can not be attributed to an impurity effect. Photolyses of PVG samples containing only MV^{2+}, 1×10^{-4} moles of MV^{2+} /g of PVG under similar conditions do not yield the reduced viologen. Furthermore, the reaction can be cycled by oxdizing MV^+ with oxygen for as many as 10 times without a significant decline in efficiency. The cross sectional absorptivity of $Ru(bpy)_3^{3+}$, 4.0×10^5 cm^2/mole, precludes its optical

detection under these conditions. However, attributing product stability to a rapid scavenging of the oxidized complex by PVG, as is the case of cellulose, is inconsistent with EPR spectra which establish that $Ru(bpy)_3^{3+}$ is stable on the glass.

Although the mobility of MV^{2+} and $MV^{+\cdot}$ on the PVG surface could not be directly determined in these experiments, studies in the clay membranes and Nafion films show that the diffusion coefficients of these species are only slightly higher than that of $Ru(bpy)_3^{2+}$ on the same support.[119,132,154-156] Since $Ru(bpy)_3^{2+}$ is essentially immobilized on the surface, the reaction with MV^{2+} can be viewed as occuring between a fixed array of adsorbed ions, and in this sense, is subject to the constraints which stablize the products of the disproportionation of $Ru(bpy)_3^{2+}$ on PVG.[160]

Photoexcitation of $Ru(bpy)_3^{2+}$ initiates the reaction sequence, but the absence of intensity quenching in the dry samples, i.e., the conditions under which the net formation of MV^{+} occurs, preclude direct oxidative quenching. In addition to the 395 nm and 610 nm, spectra reveal a weak absorption at 510 nm that closely resembles the spectrum of $[Ru(bpy)_2(bpy)^{-}]^{+}$(Figure 40). Its appearance provides a rational for the formation and stability of $MV^{+\cdot}$. Previous experiments show that disproportionation occurs when the adsorbate ions are within the electron transfer distance, 50+10 Å,[160] and the products are stable, inspite of the 2.5

eV driving force of the back reaction, when this distance exceeds that for the thermal back reaction, < 13 Å.[160] Since the mean separation between the adsorbed $Ru(bpy)_3^{2+}$ in these samples is in the order of 160 Å, the formation of $MV^{+\cdot}$ is attributed to two reaction pathways. One is photoionization of $Ru(bpy)_3^{2+}$ where the photodetached electrons, which is mobile on the PVG surface,[160,205] reduces MV^{2+} within the electron migration distance. Since $[Ru(bpy)_2(bpy)^-]^+$ is detected and its oxidation potential, 1.3 V, exceeds the reduction potential of MV^{2+}, 0.44 V, formation of $MV^{+\cdot}$ may also arise from the secondary thermal reaction

$$[Ru(bpy)_2(bpy)^-]^+ + MV^{2+} \longrightarrow Ru(bpy)_3^{3+} + MV^{+\cdot} \quad (46)$$

where the reactants are within the thermal electron transfer distance. Since Kaneto and coworkers report that electron transfer distance between $*Ru(bpy)_3^{2+}$ and MV^{2+} in cellulose, which has a driving force of 0.4 eV, occurs when the separation is $\lesssim$ 14 Å, [140,141] the driving force of reaction 47, 0.9 eV, suggests that the reaction will occur between adsorbates 15-20 Å apart.[160,206] Reaction 47 is not burdened by a corresponding back reaction. In fact, its occurence promotes product stability by reducing the driving force for the back reaction from 2.5 eV for the disproportionation products to 1.6 eV for the $Ru(bpy)_3^{3+}$-$MV^{+\cdot}$ reaction. McLendon and coworkers report that the thermal reactions between $*Ru(bpy)_3^{2+}$ and various viologens, having driving forces of 0.1 to 0.6 eV, require a mean separation ranging from a

contact distance to10Å in glycerol at0 °C.[207] In both reactions on PVG, product stability occurs provided the mean separation between the redox products exceed that for the thermal back reaction, which the available data indicate is ≤ 20 A. Our experiments indicate that this spatial array occurs within the bounary region between thse partioned reagents. Although further experiments are necessary to elucidate the parameters which control MV^{+} stability, this study illustrates that formation of MV^{+} in PVG can be achieved in the absence of an external electron donor.

REFERENCES

1. Gafney, H.D. and Adamson, A.W., J. Amer. Chem. Soc.(1972) 94, 8238-8241.

2. Adamson,A. and Fleischaur,P.D.(Eds.), Concepts in Inorganic Photochemistry, Wiley: New York, 1975.

3. Balzani,V., Moggi,L., Manfrin, and Bolletta, F., Coor.Chem.Rev., (1975) 15, 321-433.

4. Meyer,T.J., Acc.Chem.Res., (1978) 11, 94-112.

5. Sutin, N. and Cruetz,C., Pure Appl.Chem., (1980) 52, 2717-2738.

6. Balzani,V., Bolletta,F., Scandola,F., Ballarad,R., Pure Appl.Chem (1979) 51, 299-311.

7. Whitten,D.G., Acc.Chem.Res. (1980) 13, 83-90.

8. Meyer,T.J., Prog.Inorg.Chem. (1983) 30, 389-441.

9. Tatzuke,S.and Kitamura,N., Pure Appl.Chem. (1984) 56, 1269-1280.

10. Darwent,J.R., Douglas,P., Harriman,A., Porter,G., and Richoux,M.L., Coor.Chem.Rev. (1982) 44, 83-126.

11. Kalyanasundaram,K., Coor.Chem.Rev. (1982)46, 159-244.

12. Heinlein,A., Pure.Appl. Chem. (1984) 56, 1212-1224.

13. Kalyanasundaram,K. and Gratzel, M., Photochem.Photobiol. (1984) 40, 807-821.

14. Creutz, C. and Sutin, N., Proc. Natl. Acad. Sci.USA, (1975)72, 2858-2861.

15. Porter, G., Proc.R. Soc. London Ser. (A1978) 362, 281-303.

16. Kirch, M., Lehn, J-M., and Sauvage, J.P., Helv. Chim. Acta (1979) 62, 1345-1384.

17. Brown, G.M., Gray, H.B., Brunschwig,B.S., Creutz, C., and Sutin, N., J.Aem.Chem.Soc. (1979) 101, 1298-1299; (1981)

103, 2141-2142.

18. Maveric,A.W. and Gray,H.B., Pure.Appl.Chem. (1980) 52, 2339-2348.

19. Connolly,J. Ed., Photochemical Conversion and Storage of Solar Energy, Academic Press: New York, 1981.

20. Gratzel,M., Energy Resources Through Photochemical Catalysis, Academic Press: New York, 1983.

21. Sutin, N., J.Photochem. (1979) 10, 19-35.

22. Lehn,J-M, Sauvage,J.P., Nouv.J.Chim. (1977) 1, 449-469.

23. Kalyanasundaram,K., Kiwi,J., Gratzel,M., Helv.Chim.Acta (1978) 61, 2720- 2730.

24. DeLaive,P.J., Sullivan,B.P., Meyer,T.J., and Witten,D.G., J.Amer.Chem.Soc. (1979) 101, 4007-4008.

25. Kiwi,J., Kalyanasundaram,K., and Gratzel,M., Visible Light Induced Cleavage of Water, in " Structure and Bonding", Vol. 49, Spring Verlag: Berlin, 1982.

26. Barber,J., Photosythesis in Relation to Model Systems, Elsevier: New York, 1979.

27. Gerischer,H., and Katz,J.J., Light Induced Separation in Biology and Chemistry, Verlag Chime: New York, 1979.

28. Lytle,F.E. and Herculers,D.M., J.Amer.Chem.Soc. (1969) 91, 253-260.

29. Demas,J.N. and Crosby,G.A. J.Mol.Spectr. (1968) 26,72-77.

30. Crosby,G.A., Acc.Chem.Res. (1975) 8, 231-238;

31. Harrigan,R.W. and Crosby,G.A., J.Chem.Phys. (1973) 59, 3468-3476.

32. Crosby,G.A. and Hipps,K.W., J.Amer.Chem.Soc. (1975) 97, 7042-7048.

33. Crosby,G.A., Hipps,K.W., and Elfring,W.H., J.Amer.Chem.Soc. (1974) 96, 629-630.

34. Hager,G.D. and Crosby,G.A., J.Amer.Chem.Soc. (1975) 97, 7031-7048.

35. Balzani,V., Bolletta,F., Gandolfi,M.T., and Maestri,M., Topics Current Chem. (1978) 75, 1-64.

36. Allsop,S.R., Cox,A.,and Kemp,T.J., J.Chem.Soc.Faraday Tran.1, (1975) 74, 1275-1289.

37. Felix,F., Ferguson,J., Gudel,H., and Ludi,A., Chem.Phys.Lett. (1979) 62, 153-157.

38. Felix,F., Ferguson,J., Gudel,H., and Ludi,A., J.Amer.Chem.Soc. (1980) 102, 4096-4102.

39. Demas,J.N. and Tayler,D.G., Inor.Chem. (1979) 18, 3177-3179.

40. Kober,E.M. and Meyer,T.J., Inor.Chem. (1982) 21, 3978-3989.

41. Creutz,C., Chan,M., Netzel,T.L., Okumura,M., and Sutin,N., J.Amer.Chem.Soc. (1980) 102, 1309-1319

42. Van Houton,J., and Watts,R.J., J.Amer.Chem.Soc. (1976) 98, 4853-4858.

43. Van Houton,J. and Watts,R.J., Inor.Chem. (1978) 17, 3381-3388.

44. Durham,B., Caspar,J.V., Nagle,J.K., and Meyer,T.J., J.Amer,Chem.Soc. (1982) 104, 4803-4810.

45. Kobayashi,T, Inorg.Chem. (1973) 12, 2758-2762.

46. Hipps,K.W., Inorg.Chem. (1980) 19, 1390-1392.

47. Ferguson,J., Mau,A.W.H., Sasse,W.H.F., Chem.Phys.Lett. (1979) 68, 21-24.

48. Bradley,P.G., Kress,N., Horberger,B.A., Dallinger,R.F., and Woodruff,W.H., J.Amer.Chem.Soc. (1981)103, 7441-7446.

49. Dallinger,R.F. and Woodruff,W.H., J.Aerm.Chem.Soc. (1979) 101, 4391-4397.

50. Foster,M. and Hester,R.E., Chem.Phys.Lett. (1981) 81, 42-47.

51. Ferguson,J., Krausz,E.R., and Maeder,M., J.Phys.Chem. (1985) 89, 1852-1854.

52. Krausz,E.R., Chem.Phys.Lett. (1985) 116, 501-504.

53. Cherry,W.R. and Henderson,L.J., Inorg.Chem. (1984) 23, 983-986.

54. Barigelletti,F., Juris,A., Balzani,V., Belser,P., and Zelewsky,A.V., Inorg.Chem. (1983) 22, 3335-3339.

55. Caspar,J.V. and Meyer,T.J., J.Amer.Chem.Soc. (1983) 105, 5583-5590.

56. Allen,G.H., White,R.P., Rellima,D.p., and Meyer,T.J., J.Amer.Chem.Soc. (1984) 106, 2613-2620.

57. Bock,C.R., and Meyer,T.J., J.Amer.Chem.Soc. (1974) 96, 7410-7412.

58. Bock,C.R., Meyer,T.J., and Witten,D.G., J.Amer.Chem.Soc. (1975) 97, 2909-2911.

59. Navon,G. and Sutin,N., Inor.Chem. (1974) 13, 2159

60. Sutin,N. and Cruetz,C., J.AMer.Chem.Soc. (1976) 98, 6384-6385.

61. Laurence,G.S. and Balzani,V., Inor.Chem. (1974) 13, 2976-2982.

62. Lin,C.T. and Sutin,N., J.Phys.Chem. (1976) 80, 97-105.

63. Sutin,N. and Cruetz,C., Adv.Chem.Ser. (1978) 168, 1-27.

64. Sutin,N., J.Photochem. (1979) 10, 19-40.

65. Demas,J.N. and Adamson,A.W., J.Amer.Chem.Soc. (1971) 93, 1800-1801.

66. Lin,C.T., Bottcher,W., Chou,M., Creutz,C., and Sutin,N., J.Amer.Chem.Soc. (1976) 98, 6536-6540.

67. Boletta,F., Maestri,M., Moggi,L., and Balzani,V., J.Chem.Soc.Chem.Commun. (1975) 901-902.

68. Juris,A., Manfrin,M., Maestri,M., and Serpone,N., Inor.Chem. (1978) 17, 2258-2261.

69. Lin,C.T. and Sutin,N., J.Amer.Chem.Soc. (1975) 97, 3543-3544.

70. Young,R.C., Keen,F.R. and Meyer,T.J., J.Amer.Chem.Soc. (1977) 99, 2468-2472.

71. Fereira,M.I.C. and Harriman,A., J.Chem.Soc.Faraday Trans.2 (1979) 75, 874-879.

72. Hazelton,M.A., Lin,C.T., Schwartz,H.A., and Sutin,N., J.Amer.Chem.Soc. (1978) 100, 2383-2388.

73. Demas,J.N. and Addington,J.W., J.Amer.Chem.Soc. (1976) 98, 5800-5806.

74. Brunschwig,B.S. and Sutin,N., Chem.Phys.Lett. (1981) 77, 63-66.

75. Natarajan,P. and Endicott,J.F., J.Phys.Chem. (1973)

77,1823-1830.

76. Demas,J.N. and Adomson,A.W., J.Amer.Chem.Soc. (1973) 95, 6864-6865.

77. Juris,A., Gandolfi,M.T., Manfrin,M.F., and Balzani,V., J.Amer.Chem.Soc. (1976) 98, 1047-1048.

78. Gaines,G.L., J.Phys.Chem., (1979) 83, 3088-3091.

79. Bock,C.R., Connor,J.A., Gutierrez,A.R., Meyer,T.J., and Witten,D.G., (1979) 101, 4815-4824.

80. Kalyanasundaram,K., Kiwi,J., and Gratzel,M., Helv.Chim.Acta (1978) 61, 2720-2730.

81. Darwent,J.R., Kalyanasundaram,K., J.Chem.Soc.Faraday Trans.2 (1981) 77, 373-382.

82. Mandel,K. and Hoffman,M.Z., J.Phys.Chem. (1984) 88, 5632-5639.

83. Ebbesen,T.W. and Ohgushi,M., Photochem.Photobiol. (1983) 38, 251-252.

84. Prasad,D.R., Mandel,K., and Hoffman,M.Z., Coor.Chem.Rev. (1985) 64, 175-190.

85. Jones,G. and Malba,V., J.Organ.Chem. (1985) 50, 5776-5782.

86. Kimura,M. and Doi,s., J.Chem.Soc.Dalton Trans. (1983) ??, 37.

87. Photogeneration of Hydrogen, Harriman,A. and West,M.A., Eds. Academic Prass: New York, 1982.

88. Chan,S.F., Chou,M., Matsubara,T., and Sutin,N., J.Amer.Chem.Soc. (1981) 103, 369-378.

89. Xu,J. and Porter,G.B., Can.J.Chem. (1982) 60, 2856-2858.

90. Turro,N., Modern Molecular Photochemistry, Chap.9, Benjamin/Cumming Publish Co., Menlo Park, CA. 1978.

91. Nagle,J.K., Bernstein,J.S., Young,R.C., and Meyer,T.J., Inorg.Chem. (1981) 20, 1760-1763.

92. Curtis,J.C., Bernstein,J.S., and Meyer,T.J., Inorg.Chem. (1985) 24, 385-397.

93. Fendler,J., J.Phys.Chem. (1985) 89, 2730-2740.

94. Gerischer,H., Pure Appl.Chem. (1980) 52, 2649-2667.

95. Gratzel,M., Acc.Chem.Res. (1981) 14, 376-384.

96. Calvin,M., Photochem.Photobiol. (1983) 37, 349-360.

97. Witten,D.G., Russell,J.C., and Schmel,R.H., Tetrohedron, (1982) 38,2455-2487.

98. Inorganic Reactions in Organized Media, ACS Symposium Series No. ??, American Chemical Society, 1982.

99. Kitamura,N. and Tazuke S., Pure Appl.Chem. (1984) 56, 1269-1280.

100. Qayle,W.H. and Lunsford,J.K., Inorg.Chem. (1981) 20, 97-103.

101. Alkaitis,S.A., Beck,G., and Gratzel.M., J.Amer.Chem.Soc. (1975) 97, 5723-5729.

102. Infelta,P.P., Gratzel.M., and Thomas,J.K., J.Phys.Chem. (1974) 78, 1906-1913.

104. Infelta,P.P. and Gratzel,M., J.Amer.Chem.Soc. (1980) 108, 1479-1483.

105. Fox,M.A., Acc.Chem.Res. (1983) 16, 314-326.

106. Ford,W.E., Otvos,J.W., and Calvin,M., Nature (London) (1978), 274, 507-508.

107. Lehn,J.M., Science, 277, 849-856.

108. Gershfelt,N.L., Annu.Rev.Phys.Chem. (1976) 27, 346-368.

109. Kuhn,H.,Mobius,D., Angew.Chem.Int.Ed.Engl. (1971) 10, 620-637.

110. Wheeler,J. and Thomas,J.K., J.Phys.Chem. (1982) 86, 4540-4544.

111. Kajiwara,T., Hasimoto,K., Kawai,T, and Sakata,T, J.Phys.Chem. (1982) 86, 4518-4522.

112. Baxendale,J.H. and Rodgers,M.A., Chem.Phys.Lett. (1980) 72, 424-426.

113. Lachish,U, Ottolenghi,M. and Rabani,J., J.Amer.Chem.Soc. (1977) 99, 8062-8063.

114. Furlong,D.N., Aust.J.Chem. (1982) 35, 911-917.

115. Thorton,A.T. and Laurence,G.S., J.Chem.Soc. Chem.Commun. (1978) 408-409.

116. Kurimura,Y., Katzumata,K., Bull.Chem.Soc.Jpn. (1982) 55,

2560-2563.

117. Krenske,D., Abdo,S., Van Damme,H., Cruz,M., and Fripiat,J.J., J.Phys.Chem. (1980) 84, 2447-2457.

118. Abdo,S., Canesson,P., Cruz,M., Fripiat,J.J., and Van Damme,H., J.Phys. Chem. (1981) 85, 797-809

119. Ghosh,P.K. and Bard,A.J., J.Phys.Chem. (1984) 88, 5519-5526.

120. Milosavijevic,B.H. and Thomas,J.K., J.Phys.Chem. (1983) 87, 616-621.

121. Milosavijevic,B.H. and Thomas,J.K., Macromolecules, (1984) 17, 2244-2248.

122. Milosavijevic,B.H. and Thomas,J.K., J.Chem.Soc.Faraday Trans.1, (1985) 81, 735-744.

123. Milosavijevic,B.H. and Thomas,J.K., J.Phys.Chem. (1985) 89, 1830-1835.

124. Szentirmay,M.N., Prieto,N.E., and Martin,C.R., J.Phys.Chem. (1985) 89, 3017-3023.

125. Gaudiello,J.G., Ghosh,P.K., and Bard,A.J., J.Amer.Chem.Soc.(1985) 107, 3027-3032.

126. Furlong,N.D., Tricot,Y.M., Swift,J.D., and Sasse,W., Aust.J.Chem. (1984) 37, 703-711.

127. Lee,L.Y., Hurst,J.K., Politi,M., Kurihara,K., and Fendler,J.H., J.Amer.Chem.Soc. (1983) 105, 370-373.

128. Tunneli,M.S. and Fendler,J.H., J.Amer,Chem.Soc. (1981) 103, 2507-2513.

129. Willner,I., Otors,J.W., and Calvin,M., J.Amer.Chem.Soc. (1981) 103, 3203-3205.

130. Willner,I., Degani,Y., J.Amer.Chem.Soc. (1983) 105, 6228-6233.

131. Schoonheydt,R.A., DePauw,P., Vliers,D., and DE Schrijver,F.C., J.Phys.Chem. (1984) 88, 5113-5118.

132. Ege,D., Ghosh,P.K., White,J.R., Eqney,J.F., and Bard,A.J., J.Amer.Chem.Soc. (1985) 107, 5644-5652.

133. Nakamura,T. and Thomas,J.K., Langmuir,(1985) 1. 568-573.

134. De Laguardia,R.A. and Thomas,J.K., J.Phys.Chem. (1983) 87, 990-998; 3550-3557.

135. Habti,A., Keravis,D., Levitz,P., and Van Damme,H., J.Chem.Soc. Faraday Trans.2, (1984) 80, 67-83.

136. Kalyanasundaram,K. and Gratzel,M., Chemistry and Physics of Solid Surfaces, Vol.5, Ed. Vanselow,R., Spring Verlag, Berlin, 1984.

137. Moser,J. and Gratzel,M., J.Amer.Chem.Soc. (1983) 105, 6547-6555.

138. Kuezynski,J.P. and Thomas,J.K., J.Phys.Chem. (1983) 87, 5498-5503.

139. Albery,W.J., Barlett,P.N., Wilde,C.P., and Darwent,J.R., J.Amer.Chem.Soc. (1985) 107, 1854-1858.

140. Kaneto,M., Motoyoshi,J., and Yamada,A., Nature (London) (1980) 285, 468-470.

141. Kaneto,M., and Motoyoshi,J., Phoyochem.Photobiol. (1981) 33, 793-798.

142. Nozik,A.J., Ann.Rev.Phys.Chem. (1978) 29, 189-222.

143. Rossetti,R.,Beck,S.M., and Brus,L.E., J.Amer.Chem.Soc. (1984) 106, 980-984.

144. Chandrasekaran,K. and Thomas,J.K., J.Chem.Soc.Faraday Trans.1, (1984) 80, 1163-1172.

145. Clark,W.D.K. and Sutin,N., J.Amer.Chem.Soc. (1977) 99, 4676.

146. Spitler,M.T. and Calvin,M., J.Chem.Phys. (1977) 66, 4294-4299.

147. Borgarello,E., Kiwi,J., Pelizetti,E., Visca,M., and Gratzel,M., Nature, (1981) 289,158.

148. Duoghong,D., Borgarello,E., and Gratzel,M., J.Amer.Chem. Soc. (1981) 103, 4685-4693.

149. Borgarello,E., Kiwi,J., Gratzel,M., Pelizetti,E, Visca,M., J.Amer.Chem.Soc. (1982) 104, 2996-3002.

150. Houlding,V.H. and Gratzel,M., J.Amer.Chem.Soc. (1983) 105, 5695-5699.

151. Furlong,D.N.,Wells,D., and Sasse,W.H.F., J.Phys.Chem. (1986) 90, 1107-1115.

152. Brown,G.T., Darwent,J.R., and Fletcher,P.D.I., J.Amer.Chem.Soc. (1985) 107, 6446-6451.

153. Tricot,Y.M., Emeren,A., and Fendler,J.H., J.Phys.Chem.

(1986) 90, 0000.

154. Fan,F.R.F., Liu,H.Y., and Bard,A.J., J.Phys.Chem. (1985) 89, 4418-4420.

155. Krishnan,M., White,J.R., Fox,M.A., and Bard,A.J., J.Amer.Chem.Soc. (1983) 105, 7002-7003.

156. Mau,A., Huang,H., Kakuta,C.B., and Bard,A.J., J.Amer.Chem.Soc. (1984) 106, 6537-6542.

157. Kennelly,T. and Gafney,H.D., Inorg.Nucl.Chem. (1881) 43, 2988-2993.

158. Wolfgang,S. and Gafney,H.D., J.Phys.Chem, (1983) 87, 5395-5401.

159. Meisel,D., Matheson,M.S., Mulac,W.A., and Rabani,J., J.Phys.Chem. (1977) 81,1449-1455.

160. Kennelly,T., Gafney,H.D., and Braun,M., J.Amer.Chem.Soc. (1985), 107, 4431-4440.

161. Mulazzani,Q.G., Emmi,S., Fuochi,P.G., Hoffman,M.Z., and Veturi,M., J.Amer.Chem.Soc. (1978) 100, 981-983.

162. Palmer,R.A. and Piper,T.S., Inorg.Chem. (1965) 5, 861-869.

163. Klassen,D.M. and Crosby,G.A., J.Chem.Phys. (1968) 48, 1853-1860.

164. a) Smay,G.L., Non-Cryst. Solids, (1980) 38-39, 559-563. b) Pink,H.,Tritinger,L., Vite,L., Jpn.Appl.Phys. (1980) 19, 513-520.

165. Vogel, A.I., Quantitative Inorganic Analysis, 3rd Ed., Wiley: New York, 1961.

166. Gafney,H.D., Kennelly,T, and Gellis,P., unpublished results.

167. Kennelly,T., Ph.D. Thesis, City University of New York, 1980.

168. Dimitrijevic,N.M., Savic,D., Micic,O.I., and Nozik,A.J., J.Phys.Chem. (1984) 88, 4278-4283.

169. Demas,J.N.,Crosby,G.A., J.Phys.Chem. (1971) 75, 991-1024.

170. Norberg,M.E., J.Amer.Ceram.Soc. (1944) 27, 299-

171. Hair,M.L., Chapman,I.D., J.Amer.Ceram.Soc. (1966) 49, 651.

172. Sidorov,A.N., Opt.Spectr.USSR English Translation, (1960), 8, 424.

173. Hockey,J.A., Chem.Ind. (London) (1965) 57.

174. Davydov,V.Y., Kisekev,A.V., and Zhurvlev,L.T., Trans.Faraday Soc. (1964) 60, 2254-

175. Stanton,J.H., Maatman,R.W., Colloid Sci. (1963) 18, 132

176. Arland,S., Grenthe,I., and Noren,B., Acta Chem.Scand. (1960) 14, 1059

177. Elmer,T.H., J.Amer.Ceram.Soc. (1970), 53, 171-

178. Thomas,T.R., "Rough Surfaces", Longman: London, 1982.

179. Mandelbrot,B.B., "TheFractal Geometry of Nature", Freeman: San Francisco, 1982.

180. Avnir,D., Farin,D., and Pfeifer,P., Nature (London) (1984) 308, 761-763.

181. Pfeifer,P., and Avnir,D., J.Chem.Phys. (1983) 79,3558-3565; 3566-3573.

182. Avnir,D., Pfeifer,P., Nouv.J.Chim. (1983) 7, 71-73.

183. Farin,D., Volpert,A., and Avnir,D., J.Amer.Chem.Soc. (1985) 107, 3368-3370.

184. Farin,D., Peleg,S., Yavin,D., and Avnir,D., Langmuir (1985) 1, 399-407.

185. Even,U., Rademan,K., Jortner,J., Manor,N., and Reisfeld.R. Phys.Rev.Lett. (1984) 52, 2164-2167.

186. Avnir,D., Proc. 2nd. Int.Conf. Unconvetional Photoactive Materials,(Cleveland,Sept. 1985), Scher,H., Ed. Plenum Press, 1986.

187. Iler,R.K., "The Chemistry of Silica", Wiley: New York, 1979. pp 660, 185.

188. ibid, pp 665-666.

189. Shi,W. and Gafney,H.D., unpublished results, 1985.

190. Reference 187, pp 664.

191. Avnir,D., Levy,D., and Reisfeld,R., J.Phys.Chem. (1984) 88, 5956-5959.

192. Nakashima,N. and Phillipps,D., Chem.Phys.Lett. (1983)

97, 337-341.

193. Simon,R., Ph.D. Thesis, City University of New York, 1983.

194. Furlong,D.N., Aust.J.Chem. (1982) 35, 911-917.

195. a) Sacconi,L., Dicuss. Faraday Soc. (1949) 7, 173-179. b) Burstall, F.H.,Davies, G.R.,and Wells, R.A.,ibid, 179-183.

196. Douglas,B., McDaniel,D., and Alexander,J.J., "Inorganic Chemistry", 2nd Ed., Wiley: New York, 1983; Chapter 9.

197. Caspar,J.V., Westmoreland,T.D., Allen,G.H., Bradley,P.G., Meyer,T.J., and Woodruff,W.H., J.Amer. Chem.Soc. (1984) 106, 3492-3500.

198. Turro,N., private communications, 1985.

199. Warshel,A., Ann.Biophys.Bioeng. (1977) 60, 273-300.

200. Herzber,G., "Molecular Spectra and Molecular Structure", Van Norstrand: New York; Vol.1, Chapter 4.

201. Klafter,B., Blumen,A., J.Chem.Phys. (1984) 80, 875-882.

202. Van Damme,H. and Fripiadt,J.J., J.Chem.Phys. (1985) 82, 2785-2789.

203. a) Frank,R. and Rau,H., J.Phys.Chem. (1983) 5181-5184. b) Bolletta,F., Maestri,M., Moggi,L., and Balzani,V., J.Phys.Chem. (1974) 78, 1374-1377.

204. Inokuti,M. and Hirayama,F., J.Chem.Phys. (1965) 43, 1978-1989.

205. Wong,P.K., Photochem.Photobiol. (1974) 19, 391-406.

206. Guarr,T., Mcguire,M., Strauch,S., McLendon,G.,J.Amer. Chem.Soc.(1983) 105, 616-618; J.Phys.Chem. (1983) 87, 3579-3581.

207. McLendon,G., Guarr,T., McGuire,M., Simolo,K.,Strauch,S., and Taylor,K., Coor.Chem.Rev. (1985) 64, 113-124.